Chapter 4

Engineering the First Coordination Sphere of Tris-thiolate Sites in *De Novo* Designed Peptides by D-amino acid ligands to Perturb the Metal Coordination Structures

Background

The previous chapter has illustrated how the incorporation of D-Leu in the second coordination sphere is structurally capable of indirectly perturbing the steric environments of the metal center. With this approach, I showed how steric modification could provide a high degree of control on Cd(II) structures in designed 3SCC constructs. Following the exploration of metal-peptide interactions in the TRI system, one might raise the question of how the metal structure would change if the modified stereochemistry were applied directly into the metal ligand itself. In this chapter, two ligands of interest (D-Cys and D-Pen) are used to understand the direct effect of chirality toward the metal center. The first ligand, D-Cys, was used to prepare **TRI**L16$_D$C. Matzepetakis *et al*. showed that **TRI**L16C, with the substitution of L-Cys at the sixteenth position, gives a mixture of 3- and 4-coordinate Cd(II) species.[1] The crystal structure analyses in Chapter 2 demonstrated that a high degree of thiol rotation of the L-Cys is required in order to accept the metal into the binding site. This shift of the sulfur plane from the apo-coordination causes a larger interlayer space between the twelfth and sixteenth positions which is believed to open a small cavity for an exogenous water to access occasionally the hydrophobic core and bind to the metal 60% of the time. Herein, it is hypothesized that the reorientation caused by substituting D-Cys would alter the thiol plane reorientation, which would change the environment of the metal

structure. First, I will discuss the spectroscopic characterization of Cd(**TRI**L16$_D$C)$_3^-$ to provide evidence for the Cd(II)-peptide behavior in solution. Second, a combination of apo-(**CS**L16$_D$C)$_3$ and Zn(II)-bound (**CS**L16$_D$C)$_3$ crystal structures are discussed to determine the level of *predisposition* and *preorganization* of the cysteine sulfur atoms prior to metal binding. Due to the lack of a metallated Cd(II) structure with D-Cys, the Zn(II)-bound (**CS**L16$_D$C)$_3$ will be used as a model of a possible Cd(II) D-Cys environment in order to clarify the spectroscopic observations.

Given the success of incorporating L-Pen into the 3SCC peptide, Zastrow *et al*. demonstrated that [Hg(II)]$_S$[Zn(II)(H$_2$O/OH$^-$)]$_N$(**CS**L9PenL23H)$_3^{n+}$ binds Hg(II) in a trigonal structure.[2] The fact that the orientation of D-Pen ligands in the absence of Hg(II) illustrated from the published apo-(**CS**L16$_D$Pen)$_3$ crystal structure is completely different from that seen for the L-Pen ligands [apo-(**CS**L16Pen)$_3$], it was hypothesized that the inverted chirality of D-Pen might sequester Hg(II) into a different coordination environment and, possibly, in a different location within the 3SCC construct. In this section, the structural data for Hg(II)(**CS**L16$_D$Pen)$_3^-$ will be reported and compared to a trigonal Hg(II) structure obtained from [Hg(II)]$_S$[Zn(II)(H$_2$O/OH$^-$)]$_N$(**CS**L9PenL23H)$_3^{n+}$. Lastly, I will also discuss the steric effect of D-Pen derivative compared to D-Cys and propose potential Hg(II) binding modes that may exist with D-Cys ligands. These comparison studies will allow deeper understanding of the inherent structural differences based on the change in chirality of penicillamine and cysteine toward different coordination modes of Hg(II) that can open up new vistas for metalloprotein design.

Experimental Section

Materials: Lists of chemicals used for peptide synthesis and characterizations were noted in Chapter 2.

Peptide synthesis and purification: The **TRI**L16$_D$C and **CS**L16$_D$C peptides (sequences as given in **Table 4-1**) were synthesized and purified based on the methods stated in Chapter 2.

Physical Characterization: All CD, UV/VIS, ^{113}Cd NMR, ^{199}Hg NMR and ^{111m}Cd PAC spectroscopic characterizations for the **TRI**L16$_D$C peptide are described in the experimental section of Chapter 3.

Crystallizations: All peptides were crystallized by sitting drop vapor diffusion experiments at 20 ^{o}C with drops containing equal volumes of peptide (0.75 μL) and precipitant (0.75 μL) solutions. The peptide solution of apo-**(CS**L16$_D$C)$_3$ was prepared from 20 mg/mL apo-

Table 4-1. Peptide sequences

Peptides		**a b c d e f g** 2	**a b c d e f g** 9 12	**a b c d e f g** 16 19	**a b c d e f g** 23	**a b c d e f g** 30
TRI	Ac-G	LKALEEK	LKALEEK	LKALEEK	LKALEEK	G-NH_2
TRIL16C	Ac-G	LKALEEK	LKALEEK	**C**KALEEK	LKALEEK	G-NH_2
TRIL16$_D$C	Ac-G	LKALEEK	LKALEEK	$_D$**C**KALEEK	LKALEEK	G-NH_2
Coil-Ser (**CS**)	Ac-E	WEALEKK	LAALESK	LQALEKK	LEALEHG	-NH_2
CSL16C	Ac-E	WEALEKK	LAALESK	**C**QALEKK	LEALEHG	-NH_2
CSL16$_D$C	Ac-E	WEALEKK	LAALESK	$_D$**C**QALEKK	LEALEHG	-NH_2
CSL16Pen	Ac-E	WEALEKK	LAALESK	**Pen**QALEKK	LEALEHG	-NH_2
CSL16$_D$Pen	Ac-E	WEALEKK	LAALESK	$_D$**Pen**QALEKK	LEALEHG	-NH_2
CSL9PenL23H	Ac-E	WEALEKK	**C**AALESK	LQALEKK	**H**EALEHG	-NH_2

Bold and underlined residues indicate substitutions.
C-and N-termini are capped by Ac and NH_2 groups, respectively.

CSL16$_D$C, 15 mM $Zn(OAc)_2$ and 0.5 mM Tris buffer pH 8.5. The precipitant solution to grow apo-(**CS**L16$_D$C)$_3$ crystals contain 20% (w/v) PEG-8000 and HEPES pH 7.5. The metallated Zn(II) structure was prepared from 13.2 mg/mL **CS**L16$_D$C peptide, 0.92 eq of $HgCl_2$ per 3SCC peptide, 15 mM $Zn(OAc)_2$ and 0.5 mM Tris buffer pH 8.5. The well solution contains 40% (v/v), Cacodylate pH 6.5 and 5% (w/v) PEG-800. The crystals of Hg(II)($_D$Pen)$_2$(H$_D$Pen) were grown from a peptide solution (20 mg/mL **CS**L16$_D$Pen peptide, 15 mM $Zn(OAc)_2$ and 0.5 mM Tris buffer pH 8.5) and a precipitant solution (0.1 M Tris pH 7.0 and 30% (w/v) PEG-2000MME). Crystals were cryoprotected in a mother liquor containing 20% glycerol prior to supercooling in liquid N_2 for data collection.

Data collection and refinement: Data were collected at the Advanced Photon Source of the Argonne National Laboratory on the LS-CAT Beamline 21-ID-F and 21-ID-D, equipped with a Mar 225 CCD and a Mar 300 CCD detectors, respectively. All data were collected with a 1 oscillation then processed and scaled with HKL2000[3]. All structures presented in this chapter were solved by molecular replacement using Molrep[4] in the CCP4 suite of programs[5–7], then underwent iterative rounds of electron density fitting and refining in Coot[8] and Buster 2.11.2 program[9], respectively. The validity of the models were verified using the MolProbity software.[10] The Crystallography Data Collection and Refinement Statistics of the obtained crystal structures are shown in **Table 4-2**.

The apo-(**CS**L16$_D$C)$_3$ was diffracted to 1.69 Å resolution in the $P2_12_12_1$ (#19) space group containing one three stranded coiled coil per asymmetric unit with a Matthew's coefficient of 3.76 corresponding to 67.31% solvent content. The structure was solved using the apo-(**CS**L16C)$_3$ obtained from Chapter 2 as a search model in MolRep. After the first round of rigid body refinement, the D-Cys residue was built at the twelfth position using the difference density present in F_o-F_c map contour at 3σ. The apo-(**CS**L16$_D$C)$_3$ structure was refined to 1.69 Å ($R_{working}$ = 20.1%, R_{free} = 21.1 %). All side chains of all structures are present within allowed regions of the Ramachandran plot.

The same strategy was implemented to solve the metallated Zn(II)Cl(**CS**L16$_D$C)$_3^{2-}$ structure which diffracted to 1.92 Å resolution in the C2 (#5) space group. The Matthew's coefficient appears to be 2.10 corresponding to 41.39% solvent content. The published apo-(**CS**L16Pen)$_3$ (PDB code: 3H5F)[11] was used as a starting model by mutating Pen at the sixteenth position to L-Cys. The D-Cys was replaced the L-Cys after the first round of rigid body refinement

Table 4-2: Crystallography Data Collection and Refinement Statistics

Peptide	apo-(**CS**L16$_D$C)$_3$	Zn(II)Cl(**CS**L16$_D$C)$_3^{2-}$	Hg(II)($_D$Pen)$_2$(H$_D$Pen)
Data Collection			
SpaceGroup	$P2_12_12_1$	C2	C2
Unit Cell a, b, c (Å)	32.327, 67.517, 69.034	76.119, 28.977, 43.917	77.925, 29.746, 44.484
Wavelength (Å)	0.97872	0.97872	0.97856
Resolution (Å)[1]	1.69(1.72-1.69)	1.92 (1.95-1.92)	1.43 (1.46-1.43)
Rsym (%)[2]	7.6 (44.4)	6.0 (20.7)	5.5 (35.8)
<I/sI>[3]	>50 (2)	>50 (2)	>50 (2)
Completeness (%)[4]	99.9 (100)	96.7 (84.9)	99.4 (100)
Redundancy	7.1 (7.2)	7.4 (7.0)	10.2 (10.5)
Refinement			
Resolution (Å)	1.69	1.92	1.43
R-Factor (%)[5]	20.1	19.5	21.0
Rfree (%)[6]	21.1	22.8	22.6
Protein atoms	691	642	737
Metal ions	4 Zn(II) on surface	1 Zn(II) in the interior 5 Zn(II) on surface	1 Hg(II) 3 Zn(II) on surface
Water Molecules	88	34	33
Unique Reflections	17505	6288	16369
R.m.s.d.[7]			
Bonds	0.010	0.010	0.010
Angles	1.14	1.08	1.38
MolProbity Score[8]	1.31	1.48	1.53
Clash Score[8]	3.95	4.60	4.88

[1]Statistics for highest resolution bin of reflections in parentheses.

[2]$R_{sym} = \Sigma_h\Sigma_j | I_{hj} - \langle I_h \rangle | / \Sigma_h\Sigma_j I_{hj}$, where I_{hj} is the intensity of observation j of reflection h and $\langle I_h \rangle$ is the mean intensity for multiply recorded reflections.

[3]Intensity signal-to-noise ratio.

[4]Completeness of the unique diffraction data.

[5]R-factor = $\Sigma_h | IF_oI - IF_cI | / \Sigma_h|F_o|$, where F_o and F_c are the observed and calculated structure factor amplitudes for reflection h.

[6]R_{free} is calculated against a 10% random sampling of the reflections that were removed before structure refinement.

[7]Root mean square deviation of bond lengths and bond angles.

[8]Chen et al. (2010) MolProbity: all-atom structure validation for macromolecular crystallography. Acta Crystallographica D66:12-21.

as guided from the F_O-F_C difference density. The structure was refined to 1.92 Å with the final $R_{working}$ of 19.5% and R_{free} of 22.8 %.

The Hg(II)-bound (**CS**L16$_D$Pen)$_3$ structure which is defined as Hg(II)($_D$Pen)$_2$(H_DPen) was solved using the published apo-(**CS**L16$_D$Pen)$_3$[11] as a search model. The peptide contains one three stranded coiled coil per asymmetric unit with a Matthew's coefficient of 2.26 corresponding to 45.66% solvent content. Electron difference density maps (F_O-F_C) contoured at 3σ showed one possible metal site at the sixteenth (16Cys) position corresponding to a Hg(II) and three possible metal sites on the packing interface corresponding to Zn(II) ions. These positions were confirmed by solving the structure by single anomalous dispersion (SAD) using AutoSol in Phenix.[12–15] The structure was refined to 1.43 Å with final $R_{working}$ of 21.0% and R_{free} of 22.60 %.

Results

Physical characterization

Circular Dichromism Spectroscopy (CD)

Two large, negative ellipticity bands at 208 and 222 nm, corresponding to the alpha helix and coiled coil, respectively, were observed at pH 8.5 for both apo-(**TRI**L16$_D$C)$_3$ and Cd(II)(**TRI**L16$_D$C)$_3^-$. The molar ellipticity values at 222 nm were used to determine the helical coiled coil percentage of formation which correspond to 85.9±2.5% folded for the non-metallated peptide and 85.1±3.6% folded for the metallated peptides Representative spectra are shown in **Figure 4-1**.

Guanidinium Chloride Denaturation Titration

Using CD spectroscopy, the signal at 222 nm was monitored to evaluate the percent folded of the peptide at pH 8.5 upon the increase of Guanidinium Chloride (GuaHCl) denaturant. The titration curves reveal that the apo-peptide has a half denaturation point of 1.14 M and $\Delta G_{folding}$ of 1.37 kcal mol^{-1}, while the half denaturation increases to 1.97 M when Cd(II) is presence in the system with 1:1 ratio of Cd(II) to 3SCC (**Figure 4-2**). Moreover, the stability of the Cd(II)(**TRI**L16$_D$C)$_3^-$ is also indicated by a higher $\Delta G_{folding}$ (3.45 kcal mole^{-1}).

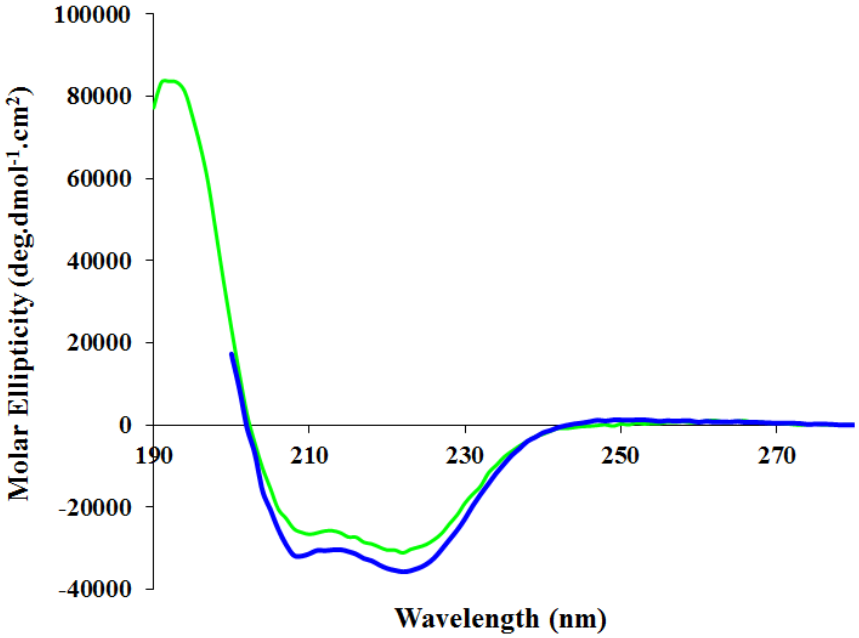

Figure 4-1. Far UV circular dichroism spectra of the apo-diastereopeptide and metalated-diastereopeptide monitored by CD. The negative double well feature at 208 and 222 nm reveals the α-helical coiled coil structure. The green and blue lines represent the spectra of apo-(**TRI**L16$_D$C)$_3$ and Cd(II)-(**TRI**L16$_D$C)$_3^-$ (1 eq. of Cd(II) per 3SCC), respectively, at micromolar concentration of monomer. The spectra were recorded at pH 8.5 and ambient temperature.

UV/VIS metal binding titrations

A Cd(II) binding titration was performed by adding small aliquots of $Cd(NO_3)_2$ to the peptide solution at pH 8.5. When Cd(II) was added, the signals at 231 nm, indicating LMCT of Cd(II) to three thiols, increased. As shown in **Figure 4-3**, the titration curve levels off at one equivalent of Cd(II) per trimer yielding a final extinction coefficient of 21,600 $M^{-1}cm^{-1}$.

^{113}Cd Nuclear Magnetic Resonance

A single resonance was observed in the ^{113}Cd NMR spectrum of (**TRI**$L16_DC)_3$ recorded at pH 8.5 in the presence of one equivalent of $^{113}Cd(NO_3)_2$, with a chemical shift of 646 ppm. The resulting data is presented in **Figure 4-4**.

^{199}Hg Nuclear Magnetic Resonance

The spectrum recorded for a (**TRI**$L16_DC)_3$ solution at pH 8.5 in the presence of one equivalent of $^{199}Hg(NO_3)_2$ results in a single peak with a chemical shift of -136 ppm (**Figure 4-5**).

^{111m}Cd Perturbed Angular Correlation Spectroscopy

The Fourier transform of ^{111m}Cd and the **TRI**$L16_DC$ peptide monomer in a 1:12 ratio at pH 8.6, 1 °C shows a clear NQI at $\omega_o = 0.316$ rad/ns ($\eta = 0.17$) corresponding to a 100% CdS_3O species (**Figure 4-6**).

Structural characterization

The results of the following crystallographic evidence (χ1 dihedral angles, atomic distances, interlayer distances, M-S distances, etc.) are referred to **Tables 4-3** and **4-4**.

First coordination sphere at the sixteenth position

*apo-(**CS**L16$_D$C)$_3$*

In the apo-$(CSL16_DC)_3$, all D-Cys residues display two alternative conformations as shown in **Figure 4-7**. The D-configuration causes the C_β carbons to point down toward the C-termini, while the S_γ atoms are oriented upward toward the other end. In chain A, both rotamers are directed to the center of the core, while chains B and C have their rotamers oriented toward the helical interface. The thiol sulfur atom orientations for all major rotamers along with the S_γ to S_γ

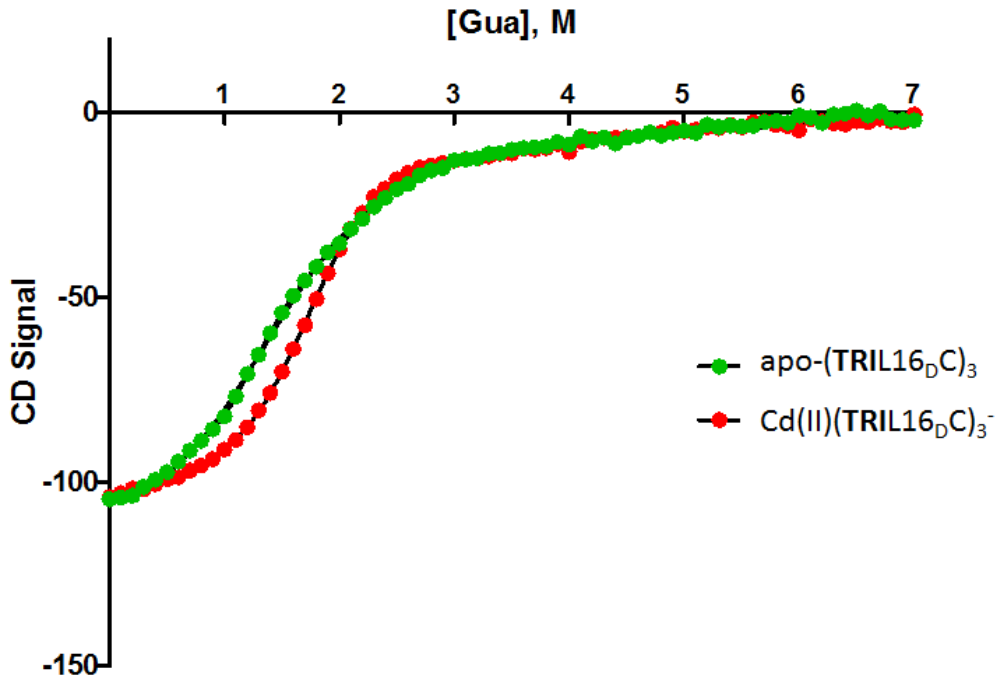

Figure 4-2. GuaHCl denaturation titration curves for apo-(TRIL16$_D$C)$_3$ (green) and Cd(II)-(TRIL16$_D$C)$_3^-$ (red). The titration curves of the peptides at pH 8.5 were plotted as mean residue ellipticity at 222 nm versus GuaHCl concentration.

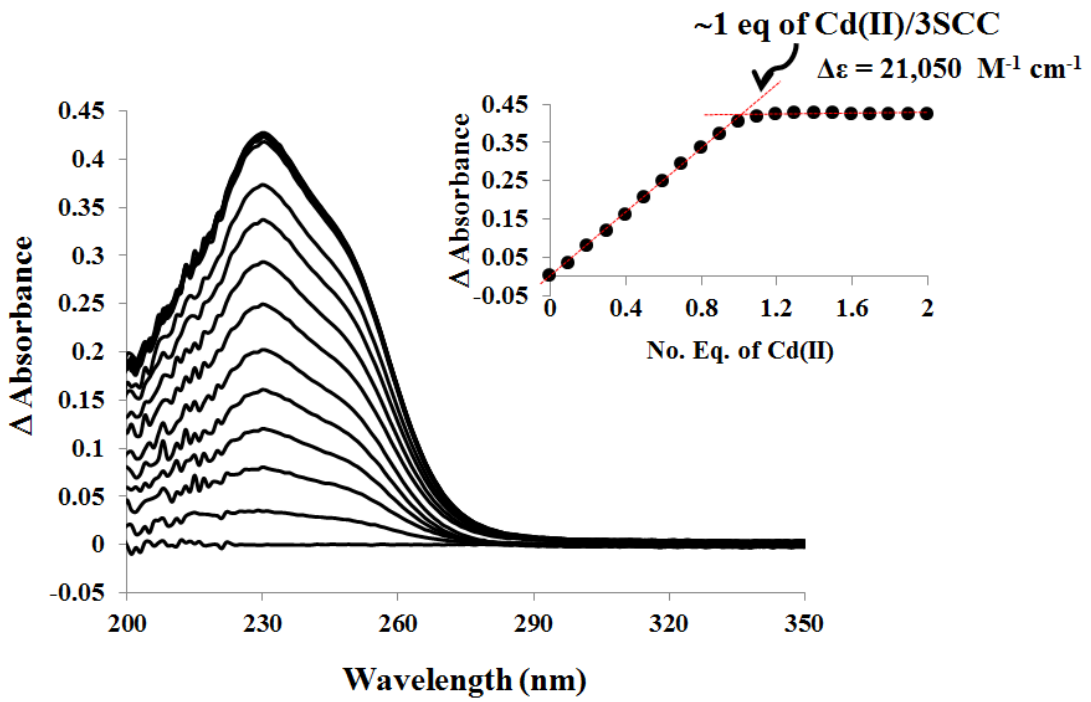

Figure 4-3. UV/VIS Cd(II) binding titrations. UV/VIS titration of Cd(II) into a solution of **TRI**L16$_D$C at pH 8.5. The data were plotted as ΔAbsorbance (M^{-1} cm^{-1}) vs wavelength (nm). The inset to each titration profile shows the titration curve plotted as Δε at λ_{max} vs equivalents of Cd(II) added.

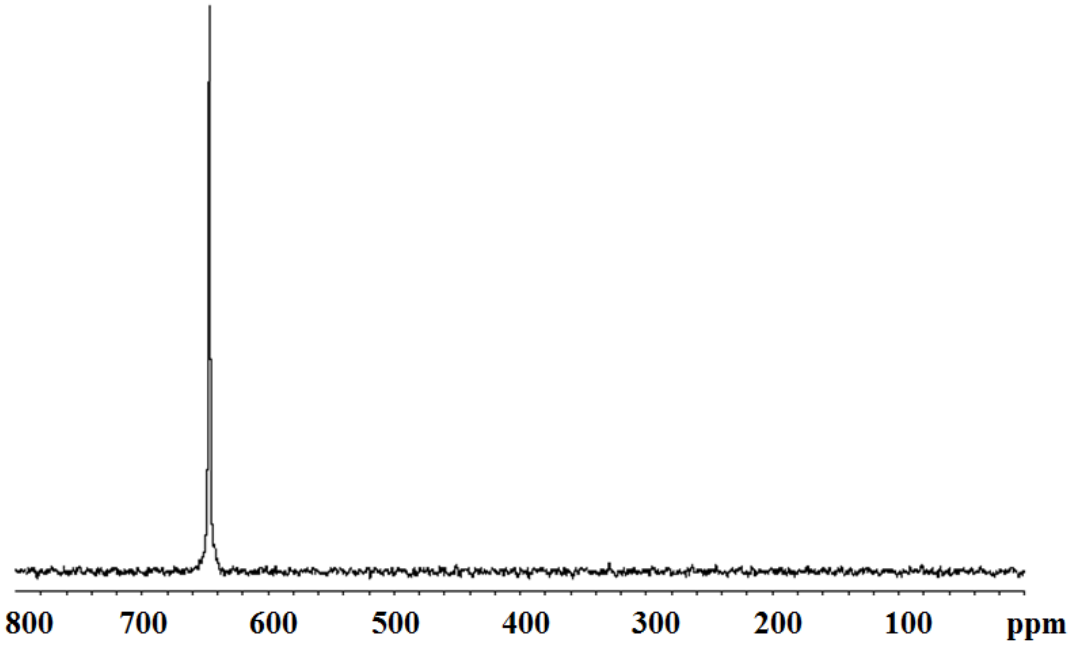

Figure 4-4. ^{113}Cd NMR of Cd(TRIL16C$_D$C)$_3^-$. The spectrum was recorded at pH 8.5.

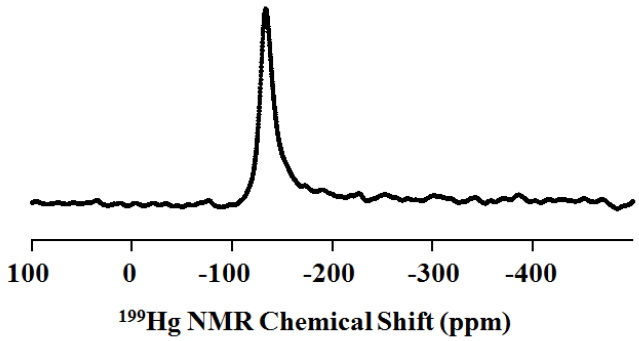

Figure 4-5. ^{199}Hg NMR spectrum of a solution containing Cd(II)(TRIL16C$_D$C)$_3^-$ at pH 8.5.

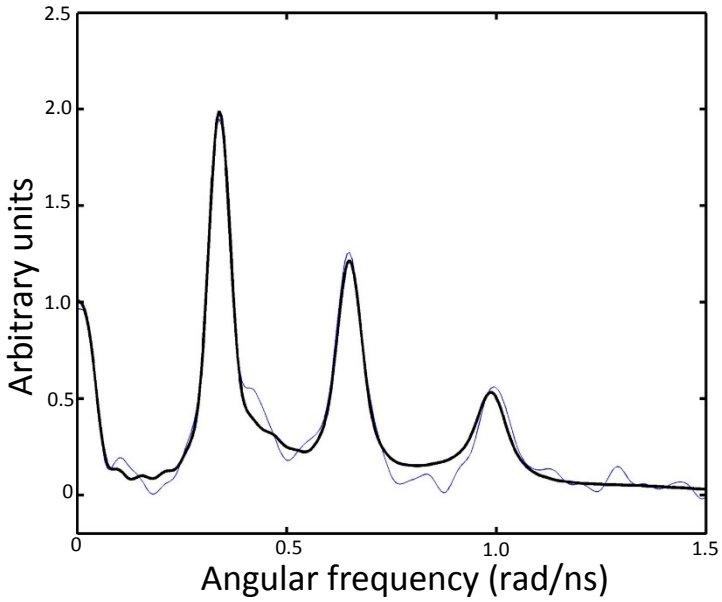

Figure 4-6. ^{199m}Hg PAC spectra of Cd(II)(TRIL16C$_D$C)$_3^-$. Shown is the Fourier transform of **Cd(II)-(TRIL16C$_D$C)$_3^-$** (the thin line gives the experimental data, and the bold faced line gives the Fourier transform of the fit). The data was collected and fitted by Prof. Lars Hemmingsen, University of Copenhagen.

Table 4-3: Crystallographic evidence observed from the crystal structures

Peptide structures	apo-(**CS**L16C)$_3$ (Chapter 2)	apo-(**CS**L16$_D$C)$_3$	Zn(II)Cl(**CS**L16$_D$C)$_3^{2-}$
rotamers at the sixteenth position	(L-Cys)	(D-Cys)	(D-Cys)
χ_1 (interior rotamers) for chain A, B, C [a]	-71.47°, -67.24°,-70.87°	84.93°, 38.18°, 51.40°	51.11°, 12.12°, 44.96°
S_γ -S_γ distance[b] (Å)	3.29 (average)	3.43(average)	3.64(average)
χ_1 (exterior rotamers)for chain A, B, C	174.45°(A) ,176.96°(C)	41.78°, 171.09°, 158.20°	112.05°(A), 138.57°(C)
S_γ -S_γ distance[c] (Å)	5.36 (average)	3.99(average)	3.70(average)
Metal site			
M-S bond length (Å)	-	-	2.13(average), Zn(II)-S 2.43, Zn(II)-Cl
S-M-S angle(average)	-	-	119.07°
Distance of metal from to the bound Cys plane[d] (Å)	-	-	+0.24
12Leu rotamers			
χ_1 [e]			
: chain A	-81.68°	-152.80°$_{(conA)}$, -61.76°$_{(conB)}$	149.23°
: chain B	-75.68°	-146.50°$_{(conA)}$, -124.09°$_{(conB)}$	-89.02°
: chain C	-171.24°	-173.26°	-101.78°
Distance between the Leu layer to the interior sulfur plane[f] (Å)	5.08	6.02	6.17
19Leu rotamers			
χ_1 [e]			
: chain A	-78.93°	-177.52°	-178.56°
: chain B	-65.99°	-54.64°	-69.01°
: chain C	-62.92°	-55.08°	-60.49°

[a] χ_1 of Cys residue is determined from the dihedral angle of N-C_α-C_β-S_γ; [b] Distance determined between S_γ atoms of the interior Cys conformers; [c] Distance determined between S_γ atoms of the exterior Cys conformers.; [d] Plus sign (+) indicates the metal is situated above the bound Cys plane. Minus (-) indicates the metal is situated below the bound Cys plane.; [e] χ_1 of Leu residue is determined from the dihedral angle of N-C_α-C_β-C_γ and [f] Distance determined between the interior C_δ (Leu) layer and the inner S_γ (Cys) layer.

Table 4-4: Crystallographic evidence observed from the crystal structures

Peptide structures	apo-(**CS**L16Pen)$_3$ (PDB code: 3H5F)	apo-(**CS**L16$_D$Pen)$_3$ (PDB code: 3H5G)	[Hg(II)]$_S$[Zn(II)(H$_2$O/OH$^-$)]$_N$ (**CS**L9PenL23H)$_3^{n+}$ (PDB code : 3PBJ)	Hg(II)($_D$Pen)$_2$(H_DPen)
rotamers at the metal site	(L-Pen)	(D-Pen)	(L-Pen)	(D-Pen)
χ_1(interior rotamers) for chain A, B, C [a]	-49.85^o (average)	166.66^o,	-50.23^o (average)	154.65^o, 54.00^o, 160.07^o
S_γ -S_γ distance[b] (Å)	3.71	165.78^o,165.89^o	3.84 (average)	6.82 (average)
χ_1 (exterior rotamers)	72.96^o	6.59 (average)	-	178.96^o, -178.35^o, 58.93^o
S_γ -S_γ distance[c] (Å)	8.36	-	-	4.89 (average)
		-		
Metal site				
M-S bond length (Å)	-	-	2.21, Hg(II)-S(average)	2.31, Hg(II)-S(major rotamer of chain A) 2.36, Hg(II)-S(minor rotamer of chain C)
S-M-S angle(average)	-	-	119.92^o (average)	170.01^o, S-Hg(II)-S
Distance of metal from to the bound Cys plane[d] (Å)	-	-	-0.06	-
Leu(above) rotamers	(12Leu)	(12Leu)	(5Leu)	(12Leu)
χ_1 (chain A, B, C)[e]	-82.66^o,-79.23^o,-104.59^o	-128.41^o,-80.90^o, -65.88^o	-174.14^o,-179.20^o,-172.74^o	-94.24^o, -72.75^o,-76.61^o
Leu(below) rotamers	(19Leu)	(19Leu)	(12Leu)	(19Leu)
χ_1 (chain A, B, C)[e]	-128.41^o, -80.90^o, -65.88^o	-175.56^o,-79.25^o,-63.21^o	-128.41^o, -80.90^o, -65.88^o	-170.79^o, -76.69^o, -59.82^o

[a] χ_1 of Cys residue is determined from the dihedral angle of N-C_α-C_β-S_γ; [b] Distance determined between S_γ atoms of the interior Cys conformers; [c] Distance determined between S_γ atoms of the exterior Cys conformers.; [d] Plus sign (+) indicates the metal is situated above the bound Cys plane. Minus (-) indicates the metal is situated below the bound Cys plane.; [e]χ_1 of Leu residue is determined from the dihedral angle of N-C_α-C_β-C_γ and [f] Distance determined between the interior C_δ (Leu) layer and the inner S_γ (Cys) layer.

distances are shown in **Figure 4-7**,**a** and all minor rotamers in **Figure 4-7**,**b**.

*Zn(II)Cl(**CS**L16$_D$C)$_3^{2-}$*

Interestingly, all of the D-Cys rotamers present in the metallated Zn(II)-bound structure are directed toward the helical interface. As demonstrated in **Figure 4-8**, only chain B has a thiol ligand present as a single rotamer, while the other two chains display two alternate conformations where the major conformer of each chain points oppositely to the other side of the helical interface from the minor conformer. A Zn(II) ion forms a 4-coordinate structure at the center of the sixteenth position with three sulfur ligands and a chloride ion bound (**Figure 4-9**). The Zn(II)-S bond lengths are 2.19 Å (major Cys, chain A), 2.08 Å (chain B) and 2.13 Å (major Cys, chain C) and the Zn(II)-Cl distance is 2.43 Å.

*Hg(II)-$_D$Pen$_2$ in the 3SCC formed by (**CS**L16$_D$Pen)$_3$*

Each D-Pen residue in the Hg(II)($_D$Pen)$_2$(H_DPen) structure shows two alternative conformations (**Figure 4-10**). Both conformers of chain A are directed outward to the helical interface, while the ligands of the remaining chains have one conformer inward and the other outward. A Hg(II) ion is present as a linear Hg(II)S_2 complex using two D-Pen thiols from the minor D-Pen conformers of chain A and C with Hg(II)-S bond distances of 2.31 and 2.35 Å, respectively (**Figure 4-11**).

<u>*Second coordination sphere: Leu layers*</u>

*apo-(**CS**L16$_D$C)$_3$*

The orientation of Leu residues at the twelfth position is relatively more inward at the core of structure compared to the residues at the nineteenth position, shown in **Figure 4-12**. In the twelfth position, two alternate conformations are present in chain A and B, while chain C displays only a single rotamer. In the lower position, every chain has a single conformation.

*Zn(II)Cl(**CS**L16$_D$C)$_3^{2-}$*

The hydrophobic packing is observed in the Zn(II)(**CS**L16$_D$C)$_3^-$ structure (**Figure 4-13**) where the orientation of Leu residues at both of the twelfth and nineteenth positions are relatively oriented at the core of structure.

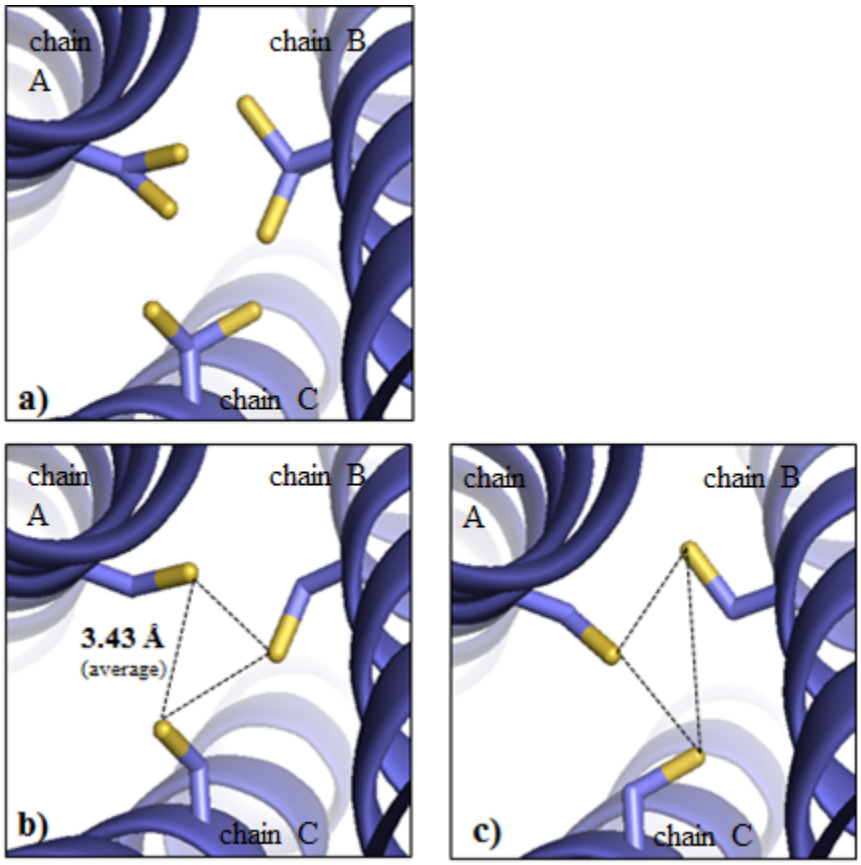

Figure 4-7. PyMOL representation showing the orientations of D-Cys side chains in the sixteenth layer of apo-(CSL16$_D$C)$_3$. The Cys side chains are shown as blue sticks with the thiol groups labeled in yellow. a) Top-down view from the N-termini represents the major and minor conformers of Cys residues. b) Top-down view of the major conformers. c) Top-down view of the minor conformers.

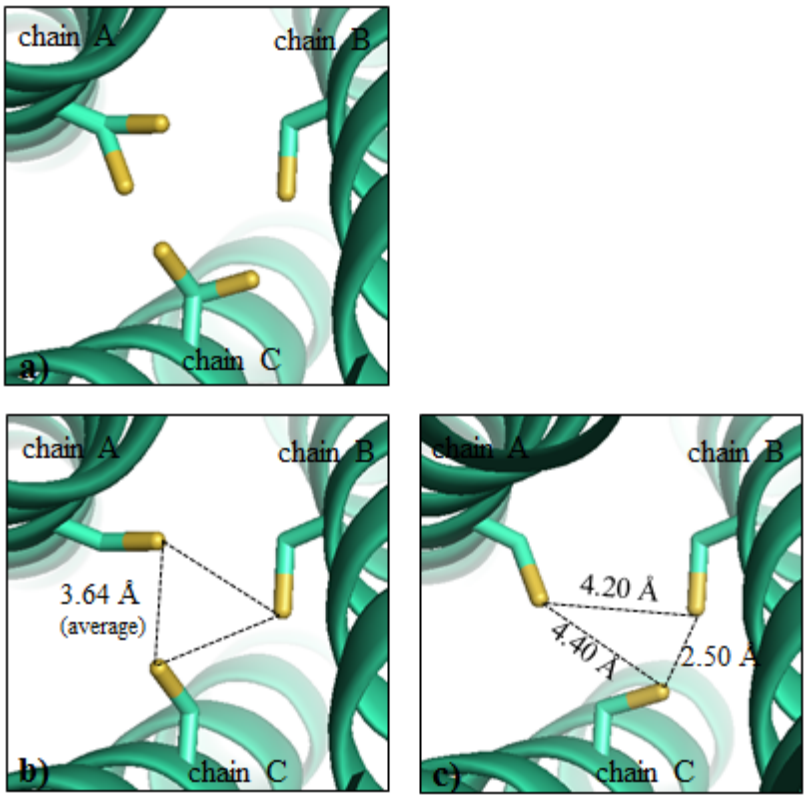

Figure 4-8. Ribbon diagrams of the Zn(II)Cl(CSL16$_D$C)$_3^{2-}$ showing the orientation of D-Cys side chains. Main chain atoms are shown as green ribbon and the D-Cys side chains as green sticks with the thiol groups being labeled as yellow. Top-down view from the N-termini showing the exclusive orientations of a) all conformers, b) major conformers and c) minor conformers. The Zn(II) ion and the chloride ligand are omitted for clarity.

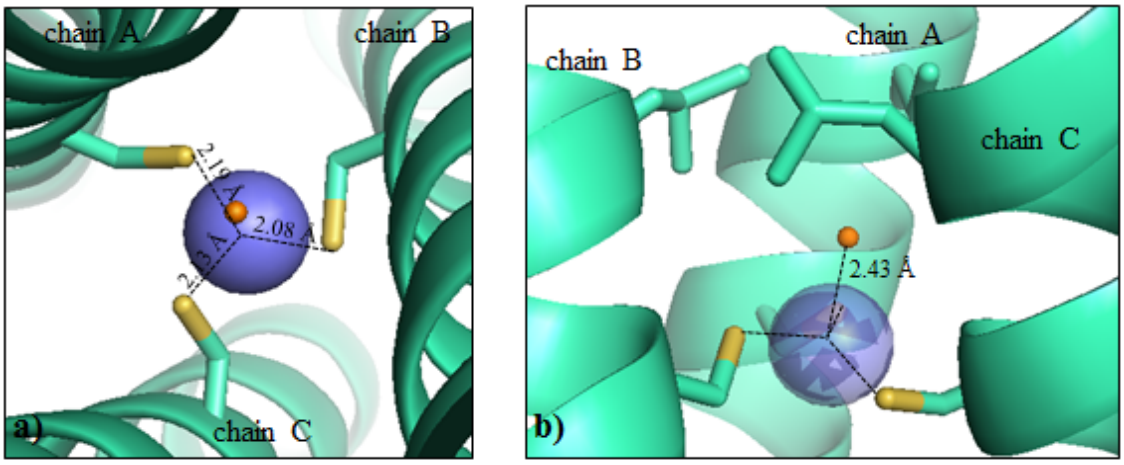

Figure 4-9. PyMOL visualization of the 4-coordinate Zn(II)(DCys)$_3$(Cl)$^{2-}$. a) Top down view from the N-termini and b) side view of the Zn(II) binding site. Main chain helices are shown as green ribbons, D-Cys side chains in the sixteenth position are present as sticks (sulfur = yellow). The Zn(II) ion is shown as a blue sphere and the coordinated chloride is represented as an orange small sphere.

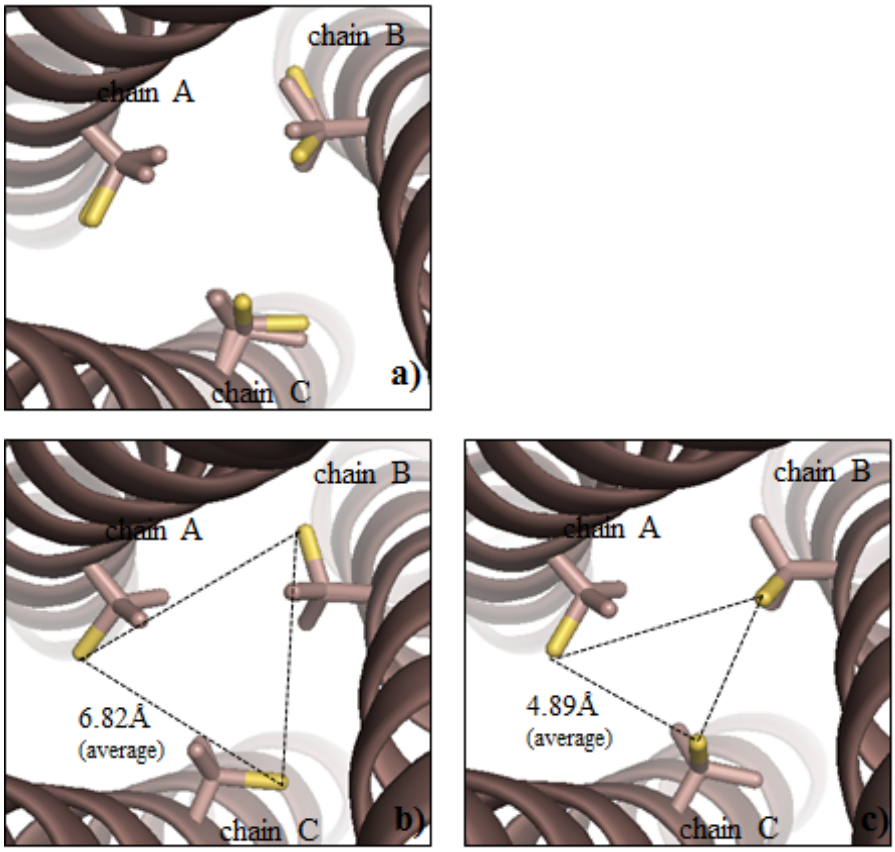

Figure 4-10. D-Pen side chain arrangements in the sixteenth position of the Hg(II)($_D$Pen)$_2$(H_DPen). The D-Pen side chains are shown as brown sticks in which the thiol groups are labeled in bright yellow. Shown from a top-down view of the structure are a) both alternate conformers of D-Pen residues, b) combination of conformers that point to the helical interface and c) combination of the minor conformers. The Hg(II) ion is omitted for clarity.

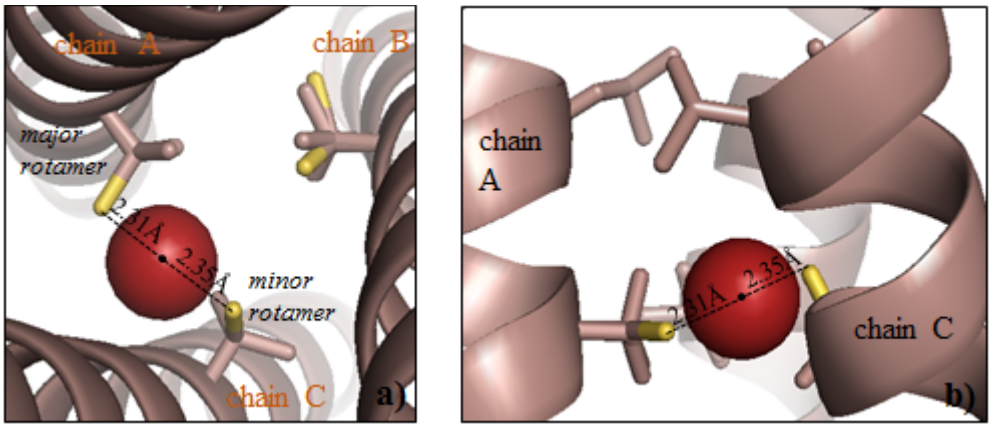

Figure 4-11. PyMOL visualization of the linear Hg(II)($_D$Pen)$_2$ complex formed in the Hg(II)($_D$Pen)$_2$($_H$$_D$Pen) structure. a) Top down view from the N-termini and b) side view of the binding site. Main chain atoms are shown as ribbon diagrams in brown, 12Leu and 16D-Pen side chains are present as sticks (sulfur = yellow). The Hg(II) ion is shown as a red sphere.

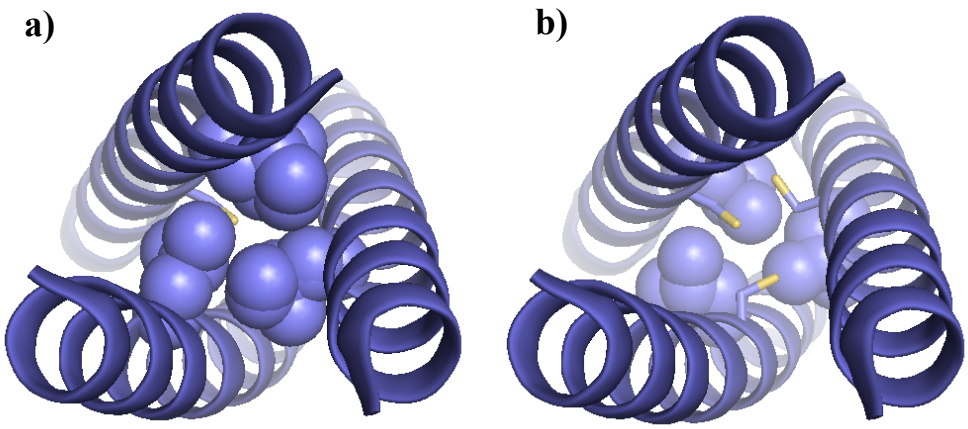

Figure 4-12. PyMOL representation of the hydrophobic packing around the 16Cys layer of apo-(CSL16$_D$C)$_3$. The packing of Leu residues is shown as spheres from the top down view of a) the twelfth layer and b) the nineteenth layer. The D-Cys side chains are shown as sticks where sulfur atoms are colored yellow.

Hg(II)($_D$Pen)$_2$(H_DPen)

The same trend of hydrophobic packing around the metal site is observed in this structure as shown in **Figure 4-14**.

Discussion

Physical characterization of Cd(II)(TRIL16$_D$C)$_3^-$

In the previous chapter, I described how D-Leu side chains that are placed in the second coordination sphere perturb the hydrophobic environment around the metal binding site, resulting in different Cd(II) coordination number and geometry. In this chapter, I focus on using alternative chirality intrinsic to the metal binding side chain to perturb the first coordination sphere of a bound ion using D-Cys in the construct (**TRI**L16$_D$C)$_3$.

While numerous studies of TRI family peptides have demonstrated that they form stable, well structured aggregates, it was unknown whether the incorporation of a D-amino acid residue into an α-helix that forms a 3SCC would perturb significantly the folding free energy or structure of the system. Previous studies with D-Pen substitution suggested that a small decrease in ΔG_{fold} would occur and that a well-folded 3SCC with minor perturbation to the helical backbone resulted.[11] Similarly, the modifications of the leucine layer above or below the cysteine layer described in Chapter 3 were well tolerated, although again with a decrease in ΔG_{fold}. The α-helical structure of (**TRI**L16$_D$C)$_3$ was determined by CD spectroscopy. The D-Cys residue at the sixteenth position does not appear to perturb the α-helical coiled coil significantly as evidenced by the two large negative ellipticity bands at 208 and 222 nm shown in **Figure** 4-**1**. According to the signal at 222 nm which is reflective of the coiled coil formation, the percent helicity of the apo-peptide is 85.9±2.5%, and it is 85.1±3.6% when the Cd(II) is present in the bundle with a 1:1 Cd(II):trimeric peptide ratio. Obviously, Cd(II) does not improve the overall folding of the peptide, which already was substantial, while in case of the L-analogue **TRI**L16C the addition of Cd(II) into the system was found to increase the percent helicity to fully 100%.[16] This improvement could be a preliminary indication that Cd(II) might prefer to interact with L-Cys to D-Cys rotamers because the metal incorporation into the binding site can induce a high percentage of coiled coil formation. The CD spectroscopy can directly probe the binding environment of metal-ligand clusters following the LMCT signal in the near UV region of the spectrum around 230-260 nm. It is assumed that differences in chirality of the metal ligand between L-Cys and D-Cys would lead

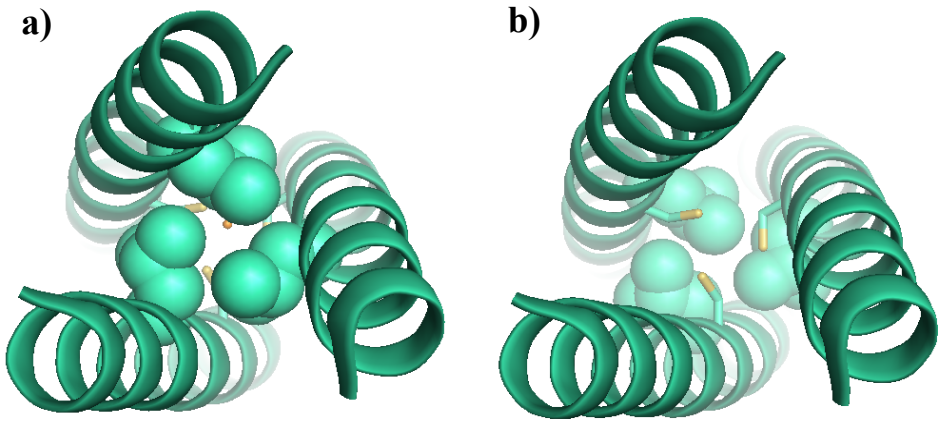

Figure 4-13. Packing of the hydrophobic residues around the 16D-Cys site of metallated Zn(II)Cl(CSL16$_D$C)$_3^{2-}$. Shown from a top down view of the N-termini, representing Leu residues as spheres of a) the twelfth and b) the nineteenth positions. The D-Cys side chains are shown as sticks where sulfur atoms are colored yellow. The other amino acid side chains have been omitted for clarity.

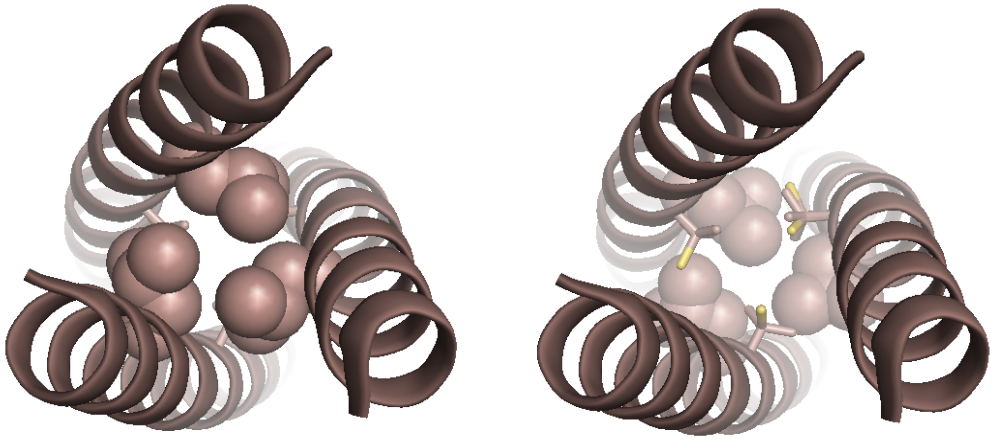

Figure 4-14. PyMOL representation of the hydrophobic packing around the sixteenth position of the Hg(II)(DPen)$_2$(HDPen). Leu residues are shown as spheres from the top down view of the packing in a) the twelfth position and b) the nineteenth position. The D-Pen side chains are shown as sticks where sulfur atoms are colored yellow.

to different CD signals. This proposal is confirmed as the presence of Cd(II) causes different spectra from the apo-form of the peptide and, more important, different CD signals are seen when comparing Cd(II)(**TRI**L16C)$_3^-$ and Cd(II)(**TRI**L16$_D$C)$_3^-$. The difference CD signal between the metal region determined from Cd(II)(**TRI**L16$_D$C)$_3^-$ and the apo-(**TRI**L16$_D$C)$_3$ is shown in **Figure 4-15**. The spectrum shows a maximum negative ellipticity at 252 nm and a maximum positive ellipticity band at 231 nm reflective of metal-peptide interaction. While D- and L-Cys residues have opposite orientations of the thiol atoms, one would hypothesize that the different chirality may cause an inverted spectrum within the binding region. However, based on a comparison between **TRI**L16$_D$C obtained from these studies and **TRI**L16C collected by Dr. Anna Peacock (data is not shown), the inverted spectra are not observed. **TRI**L16C also shows a positive ellipticity at 231 nm but the negative ellipticity shifts to 274 nm (**Figure 4-16**). The similarity of the characteristic LMCT at 231 nm suggests that the metal binding of both engineered sites occur from Cd(II) to three sulfurs; however, the difference values in longer wavelength region may reflects different environments of the first coordination sphere due to the different orientations of sulfurs and species of the metal complexes. As expected, the destabilization of the coiled coil system is pronounced when the opposite enantiomer of Cys is incorporated. The apo-(**TRI**L16$_D$C)$_3$ has a half denaturation point of 1.14 M (ΔG = 1.37 kcal mol^{-1}) obtained from the Gua denaturation titration at pH 8.5 (**Figure 4-2**), while it is 2.0 M (ΔG = 5.93 kcal mol^{-1}) for the apo-(**TRI**L16C)$_3$ peptide (data not shown, acquired by Manolis Matzapetakis) and 3.8 M (ΔG = 7.8 kcal mol^{-1}) for the native (**TRI**)$_3$ peptide.[17] It is obvious from these results that a mutation of L-Cys for Leu destabilizes the peptide and the effect is worse when the D-configuration of the Cys residue is additionally included. The apo-(**TRI**L16$_D$C)$_3$ would appear, based on spectroscopy, to be poorly coiled compared to its counterpart. In the presence of Cd(II) these two metallated-peptides behave with a similar trend in which Cd(II) enhances the folding free energy and the midpoint of titration from the unmetallated protein forms of the respective peptide. This observation indicates that at the pH 8.5, where the thiolates are formed, the addition of Cd(II) would stabilize the folding by preferentially binding into the tris-thiolate binding site. This neutralization of negative charge helps improve the tolerance of the coiled coils against the increase of denaturant. However, Cd(II)(**TRI**L16$_D$C)$_3^-$ still showed decreased resistance to Gua-induced denaturation (T_M= 1.97 M, ΔG = 3.44 kcal mol^{-1}, data obtained at pH 8.5) compared to Cd(II)(**TRI**L16C)$_3^-$ (T_M=3.3 M, ΔG = 8.01 kcal mol^{-1}, data not shown).[18] This evidence, again, emphasizes that the change in chirality

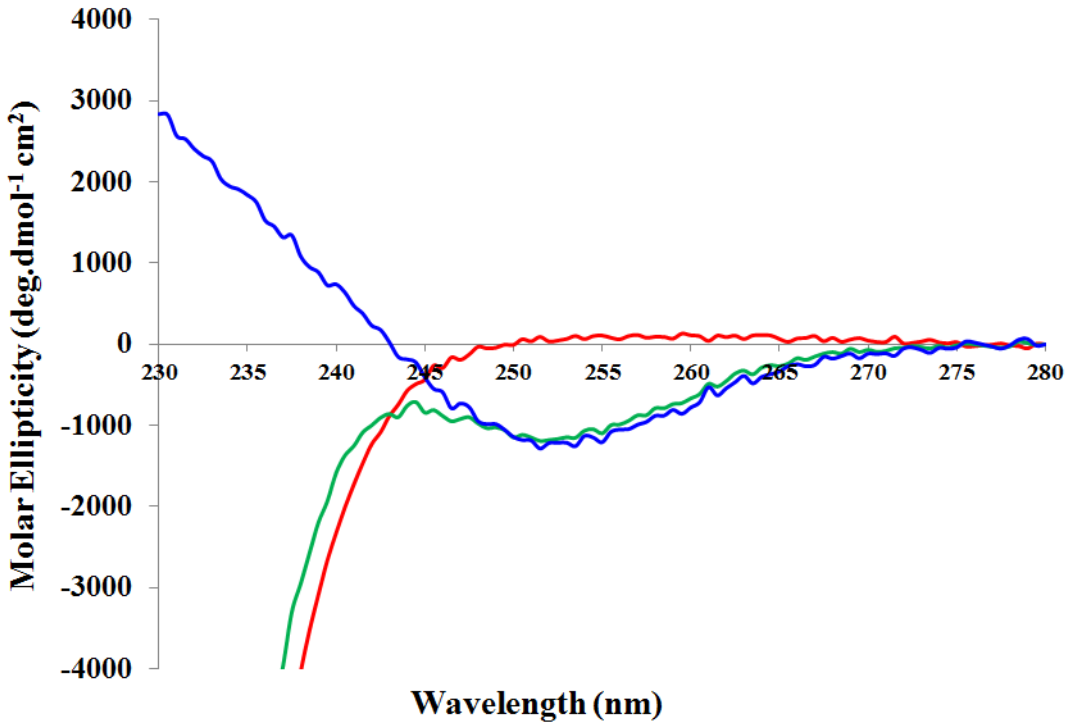

Figure 4-15. Difference CD spectra for Cd(II)(TRIL16$_D$C)$_3^-$ (blue) in the far UV circular dichroism region. Shown as red and green lines are the CD spectra for apo-(**TRI**L16$_D$C)$_3$ and Cd(II)(**TRI**L16$_D$C)$_3^-$. The difference between these apo- and metallated peptides is shown as the blue line.

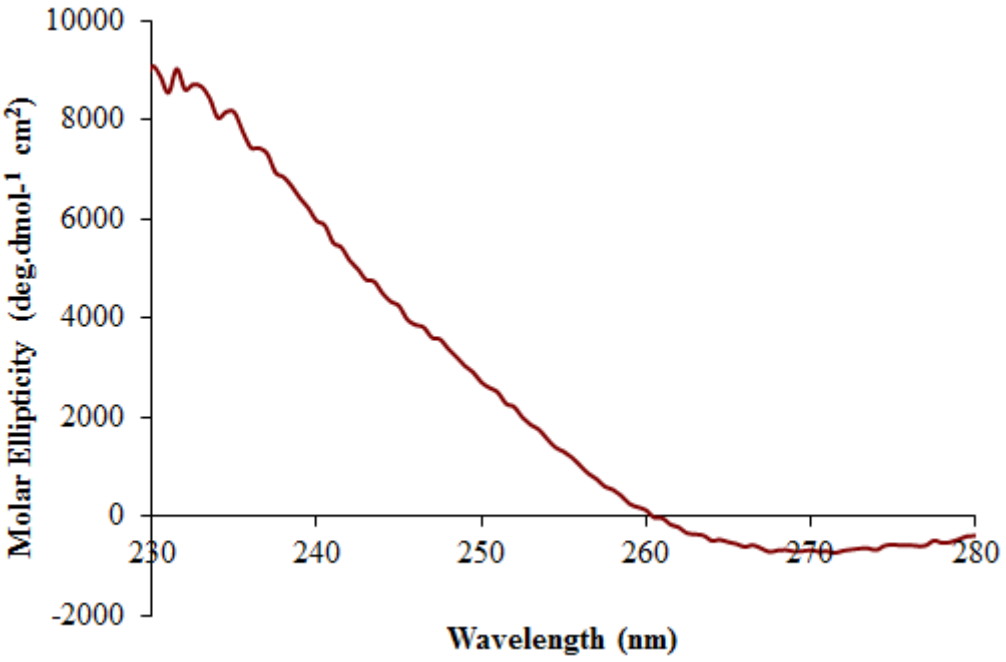

Figure 4-16. Difference CD spectra for Cd(II)(TRIL16C)$_3^-$ in the far UV circular dichroism region. Data was collected by Dr. Anna Peacock.

causes a more detrimental effect by D-Cys on the stability to the **TRI**-family series rather than L-Cys.

Although D-Cys substitution destabilizes the 3SCC to some extent, the increase in the UV-Vis LMCT bands upon Cd(II)-binding demonstrates that the peptide is still able to sequester the metal into the sulfur containing site (**Figure 4-3**). The titration curve centering at 231 nm confirms the formation of the Cd(II)-peptide interaction with 1:1 of Cd(II):trimer ratio ($\Delta\varepsilon$ of 21,050 M^{-1} cm^{-1}). While for Cd(II)(**TRI**L16C)$_3^-$, the maximum of the LMCT transition occurs at 232 nm with $\Delta\varepsilon$ of 22,600 M^{-1} cm^{-1}.[1] Based on the trend for L-Cys variants from the previous chapter, it was noted that Cd(II)(**TRI**L12$_D$L16C)$_3^-$ with a pure Cd(II)S_3^- has the highest extinction coefficient ($\Delta\varepsilon$ of 23,600 M^{-1} cm^{-1}) among all peptides, a 100% Cd(II)S_3O obtained from Cd(II)(**TRI**L12AL16C)$_3^-$ has $\Delta\varepsilon$ of 21,200 M^{-1} cm^{-1} while the mixture between Cd(II)S_3O^- and Cd(II)$S_3O_2^-$ from Cd(II)(**TRI**L2WL16CL19$_D$L)$_3^-$ lowers to 19,900 M^{-1} cm^{-1}.[19,20] The high percentage of Cd(II)$S_3O_2^-$ observed in Cd(II)(**GRAND-CS**L12$_D$L16CL19$_D$L)$_3^-$ shows the lowest $\Delta\varepsilon$ of 17,550 M^{-1} cm^{-1}. Following this trend, the value of the extinction coefficient obtained from Cd(II)(**TRI**L16$_D$C)$_3^-$ is close to Cd(II)(**TRI**L12AL16C)$_3^-$ (λ_{max} = 231 nm). The similarity of the extinction coe-efficients between these two peptides hints that the geometry of Cd(II)-peptide complex in both peptides may be similar; however, UV-Vis spectroscopy is not sufficiently sensitive to assign the Cd(II) geometries confidently. Moreover, the trend in extinction coefficients derived for L-Cys may not apply for a D-Cys binding site.

To characterize the Cd(II)-peptide interactions further, the coordination number and geometry of Cd(II)(**TRI**L16$_D$C)$_3^-$ was evaluated using the complementary techniques of ^{113}Cd NMR and ^{111m}Cd PAC. In **Figure 4-4**, the resulting ^{113}Cd NMR chemical shift of 646 nm confirms the interaction of Cd(II) to three thiolate residues. If the linear relationship of ^{113}Cd NMR chemical shifts and the percentage of Cd(II) species determined from the L-Cys peptides (*a* site) in Iranzo *et al*.[21] were applicable to D-Cys systems in order to extrapolate and predict the percentage contributions of Cd(II)S_3O^- and Cd(II)S_3^- species, the value of 646 ppm would be indicative of 60% CdS_3 and 40% Cd(II)S_3O^-. This ratio would be inverted from that observed for Cd(II)(**TRI**L16C)$_3^-$ (δ = 625 ppm) where the high coordination number Cd(II) structure is predominant.[1] However, as previously mentioned, a correlation derived for an L-Cys system may not be applicable for D-Cys Cd(II) sites. Examination of the ^{111m}Cd PAC reveals a clean spectrum with an angular frequency of 0.316 rad/ns (**Figure 4-6**), characteristic of a Cd(II)S_3O^- complex.

Given this apparent discrepancy, one must ask which spectroscopic technique would give the most reliable prediction for this system. The ^{113}Cd NMR chemical shifts are highly sensitive to the LMCT in this system as described by Ramsey.[22–27] Because this LMCT is directly related to the energy and orientation of the p orbitals of the cysteine, one can imagine that a change in chirality could change the overlap of p orbitals and the extent of charge transfer which would impact the observed chemical shifts. In contrast, PAC probes the electric field gradient around the Cd nucleus, which is defined by the sulfur atom positions, but not the intrinsic chirality of the metal center. Based on the PAC data, it is likely that the CdS_3 may not even exist in Cd(II)(**TRI**L16$_D$C)$_3^-$. Based on these results, it appears that changing the chirality of the Cys dramatically alters the coordination preference of Cd(II) within a 3SCC scaffold. To my knowledge, this is the first observation of coordination number control of a metal site in a protein based on the simple expedient of changing first coordination sphere chirality and illustrates a significant advance for metalloprotein design.

The discussion above demonstrates that altering the chirality of the metal ligands influences the coordination chemistry of the metal; however, these data do not provide a basis for understanding how the modified center changes structurally. To address this important issue, I have completed crystal structures of these peptides with bound metals as described below.

Structural Characterizations

Different orientations between D-Cys and L-Cys in the non-metallated form

The crystal structure of apo-(**TRI**L16$_D$C)$_3$ is first described to evaluate the ligand conformation prior to metal complexation. **Figure 4-7** shows the different orientations observed for D-Cys residues in the apo-(**TRI**L16$_D$C)$_3$, with each helix displaying two conformations. The atomic positions are asymmetric due to the lack of a crystallographically imposed threefold axis in the $P2_12_12_1$ space group. Only chain A has both conformers directed to the core of structure, while the other two chains point both of their rotamers rather closely to the helical interface (corresponding to one rotamer to the right and the other to the left.). The combination of the major rotamers for each chain (A 60%, B 70%, C 60%) is illustrated in **Figure 4-7**,**b** and the minor rotamers (A 40%, C 40%) in **Figure 4-7**,**c**. The combination containing all major rotamers, though distorted, looks more *preorganized* for metal binding than the minor conformers. Examining the combination of major conformers yields an average $S\gamma$-$S\gamma$ separation of 3.43 Å, while the similar

average is 3.99 Å for minor combination with only one thiol directed to the core and the others facing the helical interface. The D-configuration shows its effect when the 16D-Cys layer of apo-(**TRI**L16$_D$C)$_3$ is overlaid onto the 16L-Cys layer of apo-(**TRI**L16C)$_3$ as shown in **Figure 4-17**. In all cases with D-Cys conformations, the Cβ carbon of each residue points downward to the C-termini and Sγ atom is positioned upward to the top part of the structure, while for L-Cys residues two orientations are be observed depending on the directions of thiols. For the case of the major rotamers of L-Cys, the thiols point at the core with both Cβ and Sγ atoms pointing toward the N-termini. The minor L-Cys residues (chain A and C) have Cβ and Sγ directions oppositely oriented from D-Cys. Regardless of the L-Cys residue conformation, the positions of the corresponding D-Cys thiols are lower in space. This is a consequence of the torsional angle deviation of Cβ associated with the D-chirality. To evaluate the altered configuration effect further, the overlays of D-Cys and L-Cys isomers for major and minor conformers were determined. The studies suggest that the major rotamer combination for both chiralities seem to have the possibility of providing a degree of ligand pre-organization. This effect appears to be greater than for their minor arrangements, because with the minor conformers these orientations are slightly more inward toward the core. However, as illustrated in **Figure 4-17**,**c** the D-Cys ligand complexation looks rather more distorted than L-Cys. This is mainly because the directions of D-Cys thiols are not as highly regular as the L-configuration. This observation can be confirmed by the wide range of positive χ_1 values (see **Table 4-3**), which indicates that these side chains point quite differently through space In contrast, the thiols of L-Cys are more symmetric and highly *preorganized* as suggested by a small range among their values. The average Sγ-Sγ of L-Cys(major) pocket (3.29 Å) is also smaller than D-Cys. Moreover, the distortion also causes the Sγ plane formed by D-Cys (major) to be inclined and approximately 0.90-1.10 Å (**Figure 4-17**,**d**) lower with respect to the plane formed by the L-Cys (major).

It appears that the lowering of the sulfur plane toward the C-termini observed in the apo-(**TRI**L16$_D$C)$_3$ structure could be crucial for metal complexation as it may result in a more open interlayer spacing between the 12Leu and 16D-Cys layers. Subsequently, the increased space may have an impact on water access to the metal site. This could explain why Cd(II)(**TRI**L16$_D$C)$_3^-$ forms 100% Cd(II)S$_3$O$^-$ while the L-Cys isomer generates a 60:40 mixture of Cd(II)S$_3$O$^-$:Cd(II)S$_3^-$

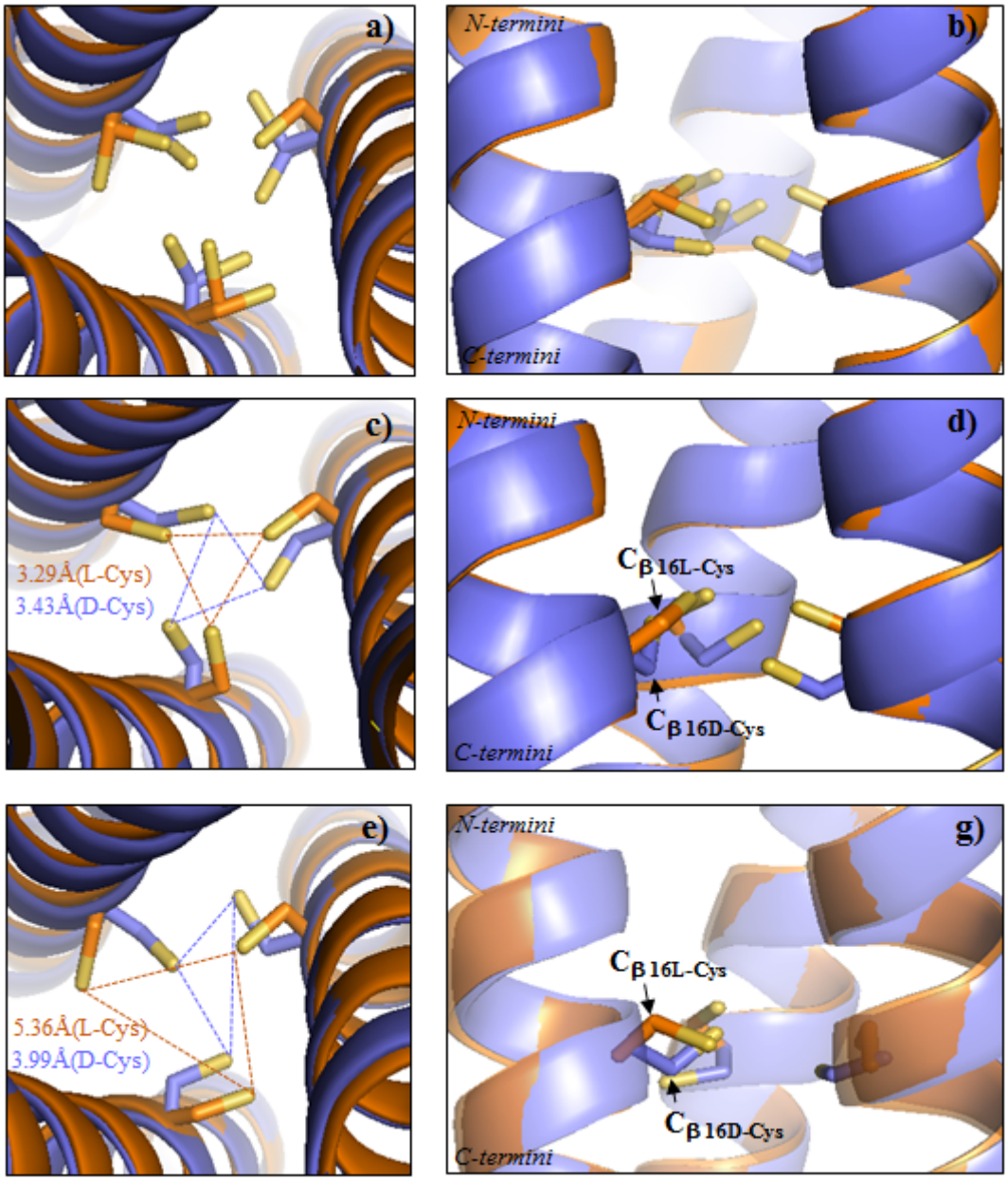

Figure 4-17. Overlays of apo-(CSL16$_D$C)$_3$ and apo-(CSL16C)$_3$ showing the differences in the side chain orientations. Left and Right columns represent the top down and side views, respectively. Shown in a) and b) are the overall binding sites, c) and d) the combination of major conformers, and e) and g) the combination of the minor conformers. Main atoms of apo-(**CS**L16$_D$C)$_3$ are shown in blue and apo-(**CS**L16C)$_3$ in orange. Side chains at the sixteenth position are present as sticks with the thiol groups labeled in yellow.

To determine the space available above the metal site, the packing of Leu residues at the twelfth position of apo-(**CS**L16$_D$C)$_3$ was overlaid onto the apo-(**CS**L16C)$_3$ in **Figure 4-18**. It is seen that the packing of both structures is very similar, indicating that lowering the plane of thiols observed in apo-(**CS**L16$_D$C)$_3$ will yield a larger space above the metal site compared to apo-(**CS**L16C)$_3$. The distances determined from the separation of these two layers confirms this conclusion (6.12 versus 5.08 Å for apo-(**CS**L16$_D$C)$_3$ and apo-(**CS**L16C)$_3$, respectively). One should remember that it was shown in Chapter 3 that a similar shift of ~1 Å between the sulfur mean plane and the Cδ of the leucine plane was sufficient to convert a mixture of Cd(II)S_3^- and Cd(II)S_3O^- in **TRI**L16C to a fully three coordinate Cd(II)S_3^- complex in **TRI**L12$_D$LL16C. These observations demonstrate that the Cβ deviation of D-Cys not only causes an opposite orientation of thiol atom from the L-analogue, but it subsequently leads to a shift of metal plane which perturbs the hydrophobic environment and may lead to a change in the coordination number and dynamic properties of the metal site. However, to investigate if the resulting space has a potential to influence Cd(II)S_3O^- formation, the metallated form of the peptide needs to be further analyzed.

The effect of chirality upon metal binding

To generate a crystal structure of Cd(II)(**CS**L16$_D$C)$_3^-$, many crystal growth conditions with attempted which varied salts and precipitants; however, while crystals were obtained from these wells, none of the collected data shows evidence of Cd(II) in the binding site. The absence of this metal in the 16D-Cys site could be that Cd(II) might not have a strong binding affinity toward D-Cys ligands, but spectroscopic studies have been completed with Cd(II) bound to the protein using stoichiometric metal to peptide ratios. Another possibility is that Cd(II) has a lower affinity for this site than Zn(II) or that the relative affinity of Cd(II) is sufficiently low to be unable to complete with the large excess of Zn(II) used during the crystallization conditions. In fact, a structure that has Zn(II) located in the 16D-Cys site has been obtained. The binding site displays a distorted Zn(II)(D-Cys)$_3Cl^{2-}$ pseudo-tetrahedral geometry, which may reveal a possible model for 4-coordinate Cd(II)S_3O^-. The active site is shown in **Figure 4-9**. Zn(II) (at an occupancy of 60%) is found at the center of three D-Cys residues that are donated by each of the three helices. The D-Cys ligand conformations of each chain are shown in **Figure 4-8**. Apparently, both chain A and C show two alternate conformers with a contribution of 60% to 40% of major to minor rotamers, while chain B contains a single rotamer with 60% occupancy indicating that there are some other

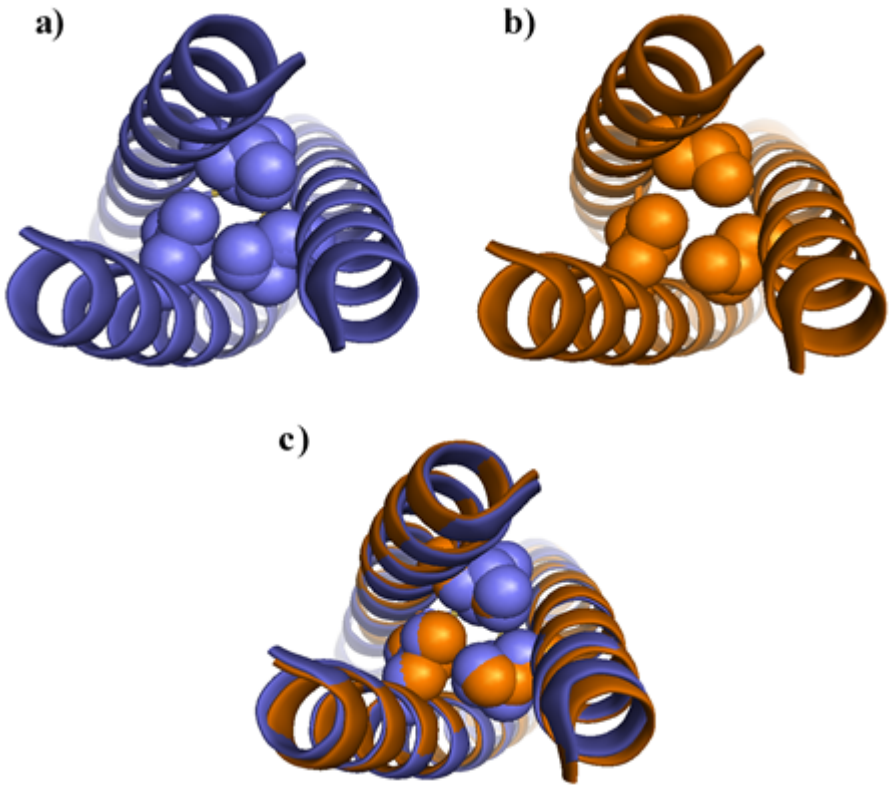

Figure 4-18. Comparison of the hydrophobic packing at the twelfth position between apo-(CSL16$_D$C)$_3$ and apo-(CSL16C)$_3$. The figure is shown from a top down view of the N-termini representing the packing in a) apo-(**CS**L16$_D$C)$_3$, b) apo-(**CS**L16C)$_3$ and c) an alignment between the two structures. Main atoms of apo-(**GRAND-CS**L16$_D$C)$_3$ are shown in blue and apo-(**CS**L16C)$_3$ in orange. Side chains at the sixteenth position are present as sticks with the thiol groups labeled in yellow.

highly dynamic orientations of this particular ligand in chain B that could not be detected during the refinements because of the ambiguous electron density. In chain A, only the major conformer ($\chi_1 = 46.37^o$) is thought to be binding a ligand with a Zn(II)-S distance of 2.19 Å, while the distance extends to 2.33 Å for the minor conformer ($\chi_1 = 112.50^o$), which is too long to be appropriate four a 4-coordinate Zn(II)-S bond. The second ligand is from chain B (χ_1 of 66.16^o) at a Zn(II)-S bond length of 2.08Å. The third ligand comes from the major conformer (χ_1 of 54.04^o) with the metal to this sulfur distance of 2.13 Å. In fact, chain C also shows another minor contribution at a distance of 2.65 Å from Zn(II) with χ_1 of 138.57^o. The fourth ligand of this site is a chloride ion at 2.43 Å from the Zn(II). Moreover, the metal is close to the D-Cys sulfur plane, with a 0.24 Å out-of-plane distance above the metal site. The chloride ligand is not located on the helical axis, therefore, the average S-Zn(II)-S and S-Zn(II)-O angles are not close to the ideal tetrahedral angle of 109.5^o. However, the presence of the chloride ligand on the top part of the structure is significant as it fills the space above the 12Leu and 16D-Cys layers.

Before applying this knowledge to model the 4-coordinate Cd(II) structure, it is useful to assess how different chiral ligands behave prior to and upon metal binding. For L-Cys, as previously described in Chapter 2, the apo-coordination (major conformer, apo-(**CS**L16C)$_3$) is predisposed for 4-coordinate Zn(II) metal binding, Zn(II)(**GRAND-CS**L12AL16C)$_3^-$ (**Figure 4-19**, top panels). In order to complex Zn(II) in a 4-coordinate structure, the sulfur atoms need to rotate significantly (by 80^o) from pointing up toward the N-termini to being directed to the side and outward toward the helical interface. An overlay of the major D-Cys rotamers between apo-(**CS**L16$_D$C)$_3$ and Zn(II)Cl(**CS**L16$_D$C)$_3^{2-}$ structures strongly suggests that the behavior of D-Cys upon metal binding is different from L-Cys. **Figure 4-19** (bottom panels) illustrates that no significant change is observed between the apo- and metallated D-Cys structures. The overall ligand arrangements are similar both prior and after binding. It is observed that the rotations of chain A (major) and B occur within 10 degrees (χ_1 changing from 40.94^o to 51.62^o for chain A, and from 38.18^o to 45.07^o for chain B). Chain C is found to have the highest rotation upon metal binding, but still the rotation happens only with a 40 degree perturbation, changing from 51.58^o to 12.17^o. The direction of the metallated chain C is directed more outward to the helical interface. As a result, the overall sulfur average S_γ-S_γ slightly increases to 3.64 Å in order to put Zn(II) in with appropriate Zn(II)-S distances (average S_γ-S_γ separation of L-Cys pocket, 3.29 Å). These

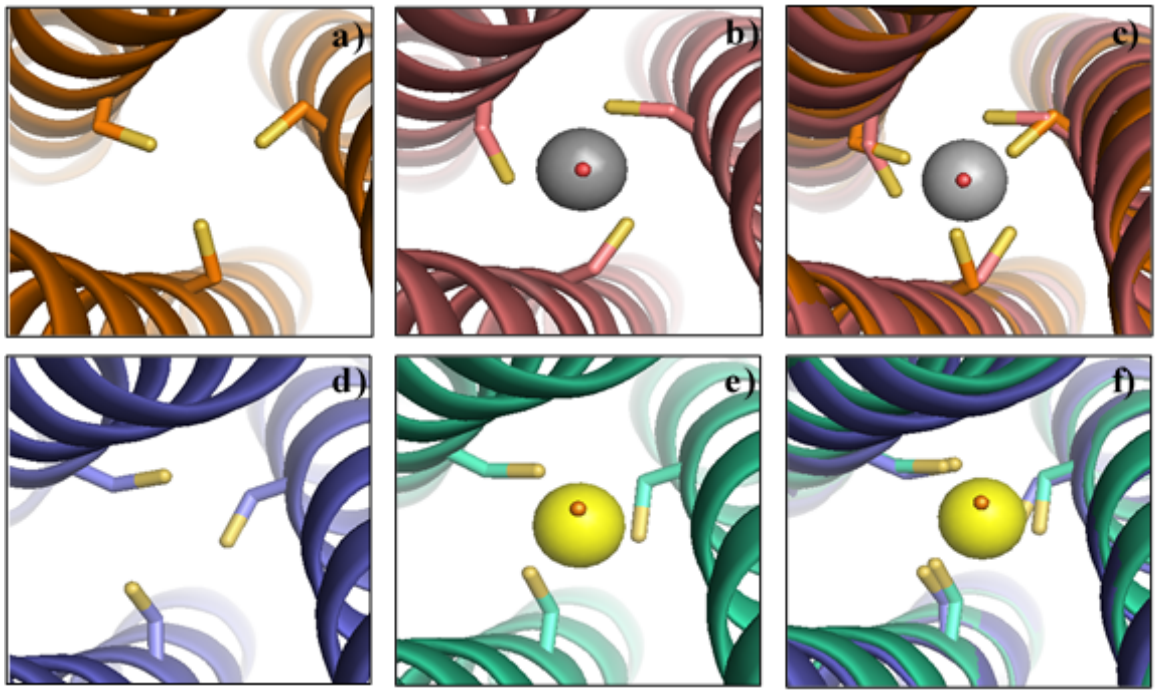

Figure 4-19. Comparison of the ligand organization (L-Cys versus D-Cys) upon Zn(II) binding. Top panels: Top down view from the N-termini representing the 16Cys side chain orientations a) in the absence of Zn(II) [apo-(**CS**L16C)$_3$] and b) upon binding to Zn(II) [Zn(II)(**GRAND-CS**L12AL16C)$_3^-$]. The alignment of a) and b) addresses the level of *predisposition* of the L-Cys ligands toward metal binding. **Bottom panels:** The arrangements of D-Cys side chains. Represented are d) the apo-coordination from apo-(**CS**L16$_D$C)$_3$, e) the metallated Zn(II)-(**CS**L16$_D$C)$_3$ and f) an overlay of d) and e) illustrating the high degree of *preorganization* of D-Cys ligands toward the Zn(II) binding. Main chain atoms are shown as ribbon diagrams. The metal ligands are present as sticks (sulfur = yellow). The Zn(II) ion in the metallated Zn(II)Cl(**CS**L16$_D$C)$_3^{2-}$ and Zn(II)(**GRAND-CS**L12AL16C)$_3^-$ are grey and yellow. The coordinated water is red and chloride is orange.

parameters reveal that in the absence of Zn(II), the S_γ-thiol arrangement of D-Cys is *preorganized* for the binding of a tetrahedral or pseudo-tetrahedral cation. This observation is in marked contrast to L-Cys binding sites which are predisposed, but not *preorganized*, for tetrahedral structures, but are *preorganized* for the binding of trigonal pyramidal molecules.

To evaluate the effect of chirality ligands on the metal coordination sphere more deeply, the binding site of Zn(II)Cl(**CS**L16$_D$C)$_3^{2-}$ is overlaid on Zn(II)(**GRAND-CS**L12AL16C)$_3^-$ as shown in **Figure 4-20**. The thiol orientations of metallated D-Cys versus L-Cys, point outward to the helical interface, but are at the same time directed through space in opposite directions. The reorientation of D-Cys results in different χ_1 dihedral angles of the metal ligands. The χ_1 in metallated L-Cys is -146.96°, whereas the values become positive in the D-configuration (51.62°, 45.07°, 12.17° for chain A, B and C, respectively). Because the D-Cys ligands are preorganized, there is no significant rotation of thiols upon binding. As a consequence, the directions of C_β and S_γ atoms in metallated D-Cys ligands are unchanged and that of the C_β-S_γ bond of D-Cys residues still points upward. This observation, however, is in contrast to the metallated L-Cys ligands of the Zn(II)(**GRAND-CS**L12AL16C)$_3^-$, where all C_β-S_γ bonds point down to the end of the helices. The side view of the alignment clearly affirms that the positions of β-carbons of all three D-Cys residues are direct downward to the C-termini and lower than the β-carbons of L-Cys. The differences in height between C_β atoms of D-Cys and L-Cys are 1.90, 1.60 and 1.40 Å for chain A, B and C, respectively.

Due to the high irregularity of the D-Cys positions, the alignment of the two structures reveals that the D-Cys layer is not perpendicular to the helical axis and is inclined, with one side of the plane higher and the other side is lower with respect to the L-Cys plane (which is perfectly perpendicular to the helical axis due to the R32 space group). It is difficult to determine whether this conformational change is a consequence of the D-Cys substitution or a crystallographic artifact. One explanation for why the L-Cys site is not distorted is because in general GRAND-CoilSer peptides crystallize in the R32 space group, while the CoilSer peptides are often found in C2, which does not impose a crystallographic threefold axis. Alternatively, the distortion could arise due to the intrinsic properties of the D-configuration itself, with the different space groups reflecting the basic differences in structures. It is interesting to note that neither the apo- or

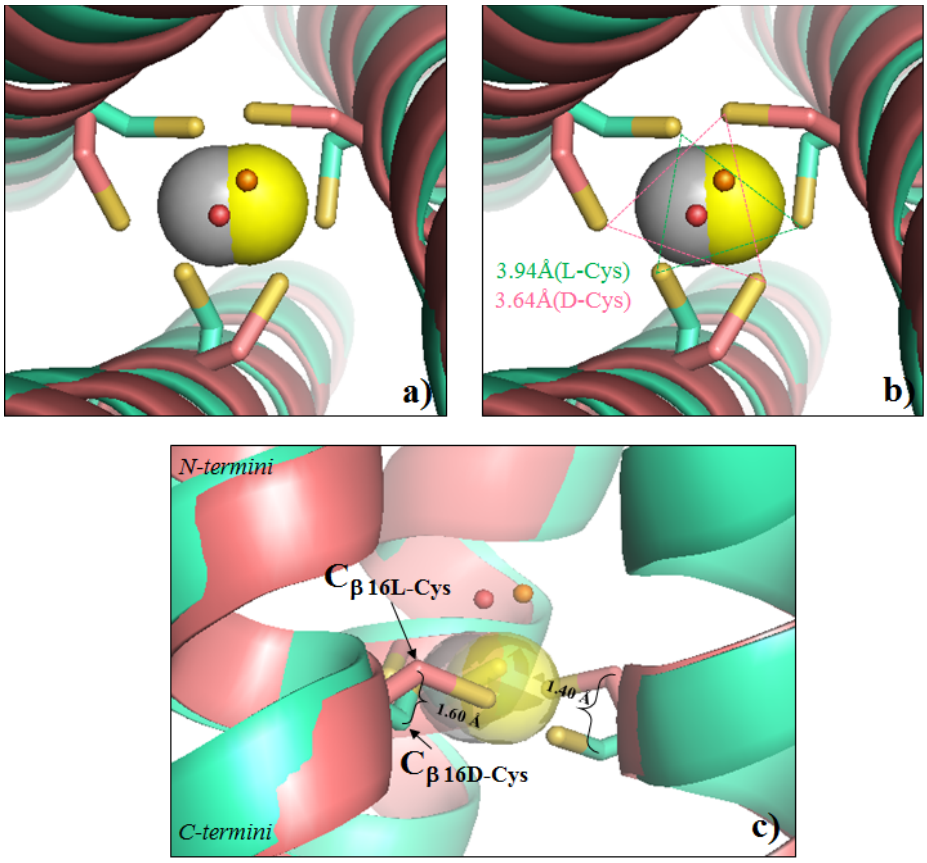

Figure 4-20. Overlays comparing the 4-coordinate Zn(II) structures obtained with apo-(CSL16$_D$C)$_3$ and Zn(II)Cl(CSL16$_D$C)$_3^{2-}$. In a) and b) representing a top down view from the N-termini and c) a side view of the binding sites. Main atoms of apo-(**CS**L16$_D$C)$_3$ are colored in green and Zn(II)Cl(**CS**L16$_D$C)$_3^{2-}$ in red. The metal ligands are present as sticks (sulfur = yellow). The Zn(II) ion in the metallated Zn(II)Cl(**CS**L16$_D$C)$_3^{2-}$ and Zn(II)(**GRAND-CS**L12AL16C)$_3^{-}$ are grey and yellow. The coordinated water is red and chloride is orange.

Zn(II) D-Cys structures I have obtained have had a crystallographically imposed three fold axis, which may indicate that this distorted cysteine plane is real.

In addition, the site pocket of D-Cys (average $S\gamma$-$S\gamma$ separation of 3.64 Å) appears to be relatively smaller than L-Cys ($S\gamma$-$S\gamma$ separation of 3.94 Å). The overlay (**Figure 4-20**,**b**) of the top down view reveals that the Zn(II) centers of both structures are at the same height but located within 0.70 Å distance from each other. The Zn(II) ion of the Zn(II)Cl(**CS**L16$_D$C)$_3^{2-}$ structure is distorted toward chain B and C, while it is in the center of Zn(II)(**GRAND-CS**L12AL16C)$_3^-$ 3SCC. It is interesting that regardless of D-Cys or L-Cys substitution, both of the Zn(II) ions are not positioned far outside the thiol plane. In Zn(II)Cl(**CS**L16$_D$C)$_3^{2-}$, the metal is located at a distance of 0.29 Å above the D-Cys layer, while a shorter distance is observed in the Zn(II)(**GRAND-CS**L12AL16C)$_3^-$ structure (0.08 Å). This causes the average S-Zn(II)-S angle of both structures to be distorted from the perfect tetrahedral values. For Zn(II)(**GRAND-CS**L12AL16C)$_3^-$, it was primarily assumed that the observed S-Zn(II)-S angle of 119.84^o is due to the crystallographic restraint of the R32 space group (The angle is not at an exact 120^o because the Zn(II) ion is slightly out of the thiol plane as previously mentioned). However, it is rather surprising that even the Zn(II)Cl(**CS**L16$_D$C)$_3^{2-}$ peptide, which is crystallized in $P2_12_12_1$ space group, also has similar values for the related angles (100.27^o ,136.31^o and 120.65^o). Thus, the average of the angle is 119.07^o, a value that is close to the requirement for a trigonal planar geometry. The fact that the first coordination sphere of these Zn(II) sites has a fourth ligand on top of the structure with appropriate metal-ligand distances, suggests that both polyhedra are highly distorted 4-coordinate Zn(II) systems. They may be best described as trigonally compressed tetrahedra. The fourth ligand of these two structures are different in which it is a chloride ligand for Zn(II)Cl(**CS**L16$_D$C)$_3^{2-}$ with a Zn(II)-Cl distance of 2.43 Å, while it is a water molecule at a distance of 2.17 Å away from the Zn(II) center of Zn(II)(**GRAND-CS**L12AL16C)$_3^-$. The top down view overlay in **Figure 4-20**,**a** shows that the fourth ligands between the two Zn(II) structures are not aligned. This orientation occurs because the two Zn(II) ions are not at the same position in space. Moreover, the chloride ligand itself is highly distorted in the Zn(II)(**CS**L16$_D$C)$_3^-$ structure with S-Zn(II)-Cl angles of 66.30^o (chain A), 120.90^o (chain B) and 94.60^o (chain C). Its position deviates from the center of the 3SCC and is situated quite close to the edge of the binding site between chains A and chain B. Additionally, the side view in **Figure 4-20**,**c** confirms that the

height of the chloride ion in the Zn(II)Cl(**CS**L16$_D$C)$_3^{2-}$ is higher than the water ligand in Zn(II)(**GRAND-CS**L12AL16C)$_3^-$, which is consistent with the longer Zn(II)-Cl bond.

Applying the 4-coordinate Zn(II)Cl(CSL16$_D$C)$_3^{2-}$ to model CdS$_3$O structure

As the original purpose of the Zn(II)(**GRAND-CS**L12AL16C)$_3^-$ structure was to understand the effect of steric modification of the twelfth position to allow for more water access, the second coordination sphere of the 4-coordinate Zn(II) structures that exist in Zn(II)Cl(**CS**L16$_D$C)$_3^{2-}$ and Zn(II)(**GRAND-CS**L12AL16C)$_3^-$ are not directly comparable. However, given that the fourth ligand to Zn(II) in Zn(II)Cl(**CS**L16$_D$C)$_3^{2-}$ is chloride, which is present at 100% occupancy, it is clear that the hydrophobic pocket defined by leucines at the twelfth position above the D-Cys layer is sufficient to accommodate large exogenous ligands bound to the metal. Even though the occupancy of the Zn(II) center is found to be only 60%, the existence of chloride at all time can occur because the ion can weakly form H-bonds with protonated D-Cys side chains (minor rotamers) of chain A and chain C. Moreover, chloride is stabilized through Van De Waal interactions with the carbonyl oxygen of the 12Leu peptide backbone when the metal ion is not bound. The fact that chloride and zinc(II) can co-exist in Zn(II)Cl(**CS**L16$_D$C)$_3^{2-}$ demonstrates that the altered position for the Zn(II) in this diastereopeptide generates a sufficiently large pocket, even with leucines in the 12 position, to allow access of large, neutral or anionic exogenous ligands. This knowledge can then be applied to explain why a pure Cd(II)S$_3$O$^-$ in Cd(II)(**CS**L16$_D$C)$_3^-$ can be exclusively formed while the Cd(II)(**CS**L16C)$_3^-$ system displays a mixture of Cd(II)S$_3$O$^-$ and Cd(II)S$_3^-$.

I propose a model of Cd(II)S$_3$O$^-$ (**Figure 4-21**) based on the Cd(II)-S and Cd(II)-O bond distances determined from the EXAFS results for the 4-coordinate Cd(II) complex. As the metal-to-sulfur distance of Cd(II) is longer than Zn(II), the bound D-Cys rotamers are modeled by rotating the ligands slightly farther out toward the helical interface. Using this approach, it is found that the rotations not only causes the thiol plane to drop down to a distance of 0.50 Å with respect to the Zn(II) position, but also increases the average S_γ-S_γ separation from 3.64 to 4.15 Å. The χ_1 dihedral angles of the modeled structure are 34.36°, -2.63° and 31.19° for chains A, B and C, respectively, with the S-Zn(II)-S angles being 125.01°, 102.61° and 90.00°. Even though the average of these angles is closer to an ideal angle for a tetrahedral structure (105.87°), the large range of values among the three angles suggest that the site is likely quite distorted. As previously

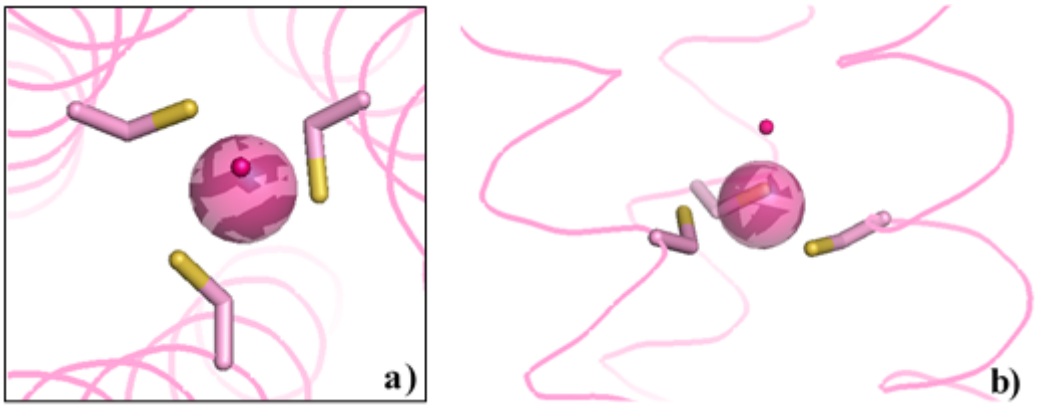

Figure 4-21. Model of $Cd(II)S_3O^-$ using the $Zn(II)Cl(CSL16_DC)_3^{2-}$ crystal structure. a) Top down view from the N-termini and b) side view of the binding site. Cd(II) is modeled as a pink sphere. D-Cys side chains are shown as sticks where sulfurs are labeled in yellow. The modeled water is in red. Backbones of the helices are shown as lines.

mentioned, the distortion could result from the low symmetry crystal packing that does not have a threefold symmetry between the three helices or, more likely, that the D-Cys ligands tend to generate a relatively distorted pseudo-tetrahedral structure. If this conclusion is true, the shift in the sulfur plane toward the C-termini in the modeled Cd(II) structure also supports the idea that the hydrophobic region between 12Leu and 16D-Cys could be expanded to 6.62 Å which is longer than the related distance determined from the actual Zn(II)Cl(**CS**L16$_D$C)$_3^{2-}$ (6.17Å) and apo(**CS**L16$_D$C)$_3$ (6.12 Å) aggregates.

To test my hypotheses regarding the impact of ligand chirality on the Cd(II) structures, the Cd(S$_{D\text{-}Cys}$)$_3$O$^-$ structure was modeled from Zn(II)Cl(**CS**L16$_D$C)$_3^{2-}$. Shown in **Figure 4-22**, this new model is overlaid onto the Cd(II)(S$_{L\text{-}Cys}$)$_3$O$^-$ model previously obtained from Zn(II)(**GRAND-CS**L12AL16C)$_3^-$ in *Section III* chapter 2. A reasonable bond length and S-metal-S angle can be achieved when the χ_1 dihedral angle of L-Cys is -150.62^o with the metal positioned at a distance of 0.22 Å above the metal plane. Due to the Cβ-Sγ bond rotation of 16D-Cys, that allows the thiols to position lower toward C-termini, the overlay clearly suggests the thiol plane of 16D-Cys of Cd(II)(S$_{D\text{-}Cys}$)$_3$O$^-$ structure should be lower than Cd(II)(S$_{L\text{-}Cys}$)$_3$O$^-$. The calculated separation of the two planes is 0.62 Å. If the twelfth position of both structures were to be Leu residues, the shift of thiol planes toward the C-termini can cause the space above the 16D-Cys to be larger than the 16L-Cys plane. Moreover, the model suggests that the metal position in Cd(II)(S$_{D\text{-}Cys}$)$_3$O$^-$ is also lower than the one in Cd(II)(S$_{L\text{-}Cys}$)$_3$O$^-$. As a consequence, the water ligand of the Cd(II)(S$_{D\text{-}Cys}$)$_3$O$^-$ is situated significantly lower than the water ligand in Cd(II)(S$_{L\text{-}Cys}$)$_3$O$^-$ with respect to the N-termini. It can be concluded from these studies that the additional space above the 16D-Cys and the lower position of water that occurs because the metal has shifted significantly within the 3SCC, which would allow less steric repulsion for an exogenous ligand. The effect is of a comparable magnitude, but in the opposite direction (meaning to allow more space), to the relative shifts of the 12 layer/sulfur layer with the D-Leu and L-Pen structures described in the previous chapter which excluded water from the first coordination sphere. Thus, it is likely that the water may be favorably housed in the space above the 16D-Cys layer as compared to 16L-Cys where the water location is relatively close to the twelfth position, causing more possibility of steric clashing.

The physical and structural analyses of the series of peptides that contain D-Cys as the metal ligand has proved that the alternative chirality of cysteine exhibits distinct features within a 3SCC that may be exploited to differentiate metal binding in the two sites. First, the D-Cys layer

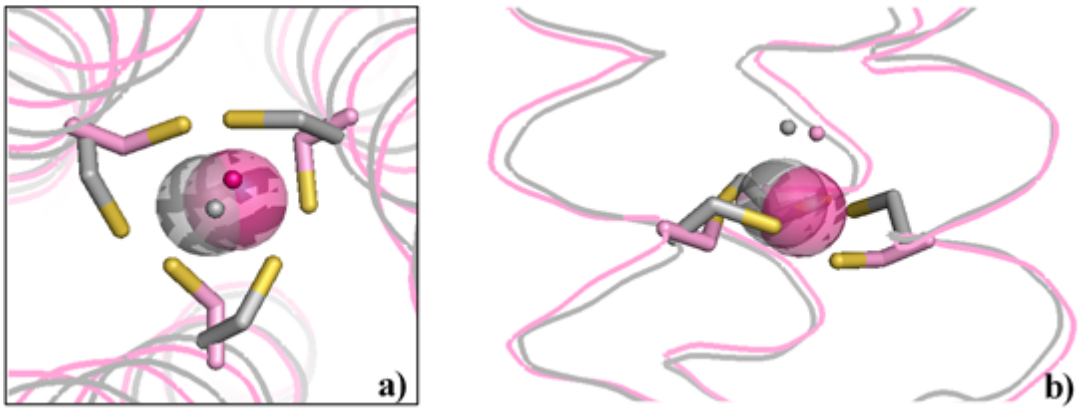

Figure 4-22. Overlays of modeled Cd(II)($S_{L\text{-}Cys}$)$_3$O$^-$ and Cd(II)($S_{D\text{-}Cys}$)$_3$O$^-$ sites based on different chirality of metal ligands. The pink model represents a possible binding site from D-Cys ligands [modeled from the Zn(II)Cl(**CS**L16$_D$C)$_3^{2-}$ structure], while the grey model shows a possible L-Cys orientation to generate a 4-coordinate Cd(II) structure [modeled from the Zn(II)(**GRAND-CS**L12AL16C)$_3^-$]. Main chain atoms are shown as lines, metal ligands as sticks, metal centers as spheres, waters as small spheres.

is *preorganized* for binding 4-coordinate metals whereas L-Cys layers are *preorganized* for trigonal pyramidal structures. Second, the D-Cys leads to a more distorted apo- and metallated structure than the corresponding L-Cys containing 3SCC. Third, D-Cys allows metal binding at a position further from the leucine layer in the twelfth position, which ultimately affords a 100% $Cd(II)S_3O^-$ chromophore which can only be achieved with L-Cys 3SCCs when additional space is made in the hydrophobic later above the metal site. The results of this work have prompted addressing another interesting question in protein design: Will alternative chirality of bulky derivatives such as found with the Pen ligand also influence protein coordination chemistry? In the next section, I will present the structural characterization of a linear $Hg(II)(_DPen)_2(H_DPen)$ which answers this question.

Structural evidence of Hg(II)-binding to a tri-thiolato D-Pen site

a) First Coordination Sphere at the sixteenth position

The fact that Hg(II) can bind L-Pen ligands into a trigonal $Hg(_LPen)_3^-$ structure at pH 8.5 was confirmed by spectroscopic characterization in solution (^{199}Hg NMR and UV/Vis) and a crystal structure of $[Hg(II)]_S[Zn(II)(H_2O/OH^-)]_N(\mathbf{CS}L9PenL23H)_3^{n+}$.[2] I now address how the change of the ligand chirality to D-Pen influences Hg(II) binding. Peacock *et al*. demonstrated that the orientation of D-Pen side chains in the apo-$(\mathbf{CS}L16_DPen)_3$ is directed to the opposite direction of the major conformers of L-Pen ligands in the apo-$(\mathbf{CS}L16_LPen)_3$.[11] These differences are shown in **Figure 4-23**. All three D-Pen ligands are directed outward to the helical interface causing a large separation of 6.59 Å between adjacent thiols, while the L-Pen ligands point inward toward the helical core with an average Sγ-Sγ separation of 3.71 Å. Moreover, the orientation of D-Pen was also opposite from the metallated L-Pen structure where all the thiols are sterically restricted toward the core similar to the apo-coordination (Sγ-Sγ separation of 3.84 Å). Unsurprisingly, the completely different orientation of D-Pen ligands in the 3SCC binding site leads the protein to bind Hg(II) in a different mode at the same pH condition. As shown in **Figure 4-11**, a lower coordination number occurs as a linear $Hg(II)(_DPen)_2(H_DPen)$ complex is formed. Due to the orientation of D-Pen ligands that point outward to the helical interface, the position of Hg(II) ion is subsequently located on the edge of the 3SCC coordinating to two ligands, one each from chain A and chain C with Hg(II)-S distances of 2.31 and 2.35 Å, respectively. To investigate

more fully the behavior of D-Pen ligands in metal coordination, **Figure 4-24**,**c** shows an overlay representing a comparison between apo- and metallated-(**CS**L16$_D$Pen)$_3$. In the presence of Hg(II), the arrangement of D-Pen ligands is different than in the apo-form. D-Pen ligands in the metallated structure display two conformations (**Figure 4-10**), whereas only a single rotamer is present in the apo-(**CS**L16$_D$Pen)$_3$ (**Figure 4-24**,**b**). In chain A, both of the conformations have the thiols oriented to one face of the helical interface and the γ-methylene groups directed oppositely to the other side. While the first conformer directs the Cβ-Sγ bond toward the C-terminal region (χ_1 of 178.96°), the related bond of the second conformer points slightly upward to the N-termini (χ_1 of 154.65°) which allows the thiol to reach a reasonable Hg(II)-S distance (2.31 Å). The overlay of the two structures reveals that the orientation of the thiol in the apo-structure is in between the two conformers observed in the metallated structure, suggesting that the presence of Hg(II) induces the thiol to rotate upward around the Cβ-Sγ bond and when Hg(II) is absent this bond can rotate further down by 25° toward the C-termini. It is obvious that this ligand in Hg(II)($_D$Pen)$_2$(H_DPen) complex does not require a significant thiol rotation from the apo-orientation to bind to Hg(II); however, the second ligand from chain C must move significantly. In chain C, the major chain C conformer (χ_1 of 160.07°) points the thiol to the outer face (between chain A and C) (**Figure 4-10**) and resembles the orientation observed in the apo-(**CS**L16$_D$Pen)$_3$ (χ_1 of 164.89°) (**Figure 4-23**,**b**). This thiol position is definitely too far from the Hg(II) atom (4.25 Å), therefore, in order to bind to Hg(II) a rotation of 100° by the Cβ-Sγ bond is required to coordinate the metal. However, the second rotamer of chain C has a χ_1 dihedral angle of 58.93°, which is perfect to bind a Hg(II)-S distance of 2.35 Å. For this linear Hg(II) complex, the separation between the two bound Sγ thiols is 4.64 Å. The low occupancy (15%) of Hg(II) that is observed from the experiment implies a low affinity of D-Pen toward the metal center. The rotation of the thiol in D-Pen must be difficult because of the steric clashes caused by the additional γ-methylene groups around the β-carbon; however, the thermodynamically stable Hg(II)-dithiolato bonds are thought to be sufficient enough to overcome the energy penalty that results from these contacts. Furthermore, the unbound rotamers of chain B behave similarly to chain C where two alternative conformers are present. The first rotamer (χ_1 of -178.35°) is oriented outward to the helical interface and the other is directed in the opposite direction (χ_1 of 54.00°) facing toward chain C at a distance of 4.80 Å from the unbound rotamer

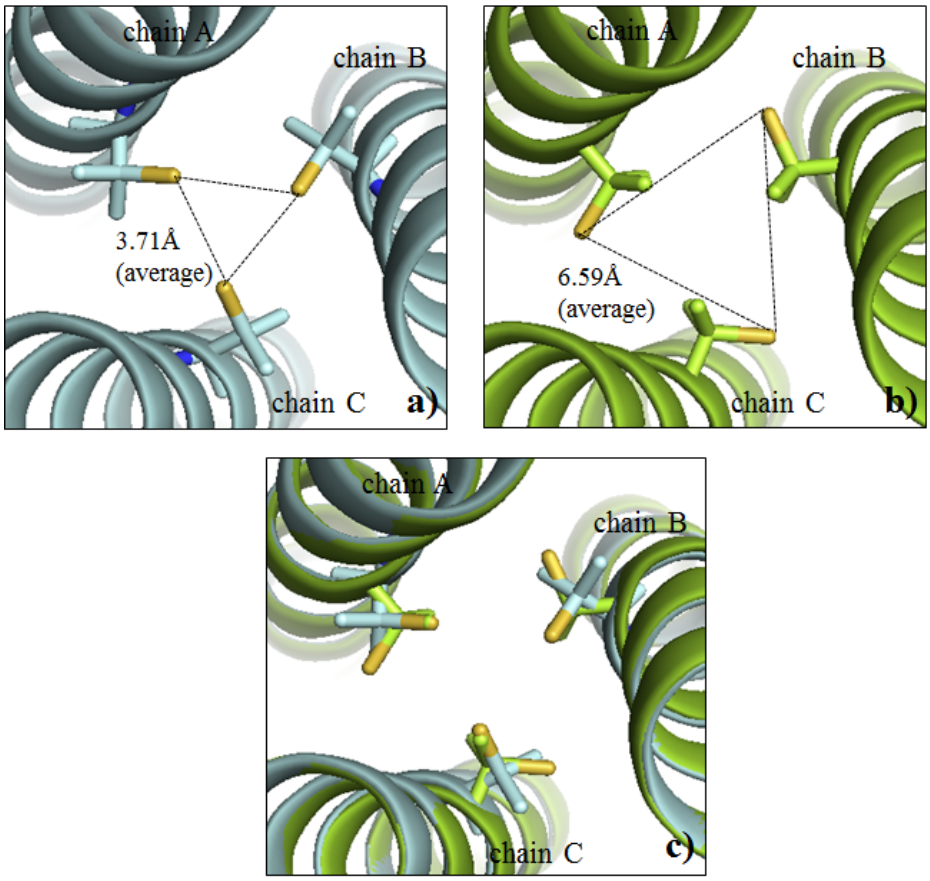

Figure 4-23. Difference in ligand orientations between L-Pen versus D-Pen in the absence of metal. The view in a) represents the combination of major rotamers of L-Pen from the apo-(**CS**L16Pen)$_3$ (PDB code: 3H5F)[11] and b) D-Pen ligands from the apo-(**CS**L16$_D$Pen)$_3$ (PDB code: 3H5G)[11]. Diagram c) shows an overlay between L-Pen and D-Pen ligands. The main chain atoms are shown as ribbon diagrams. Residues at the sixteenth position are shown as sticks in which the thiol groups are labeled in yellow.

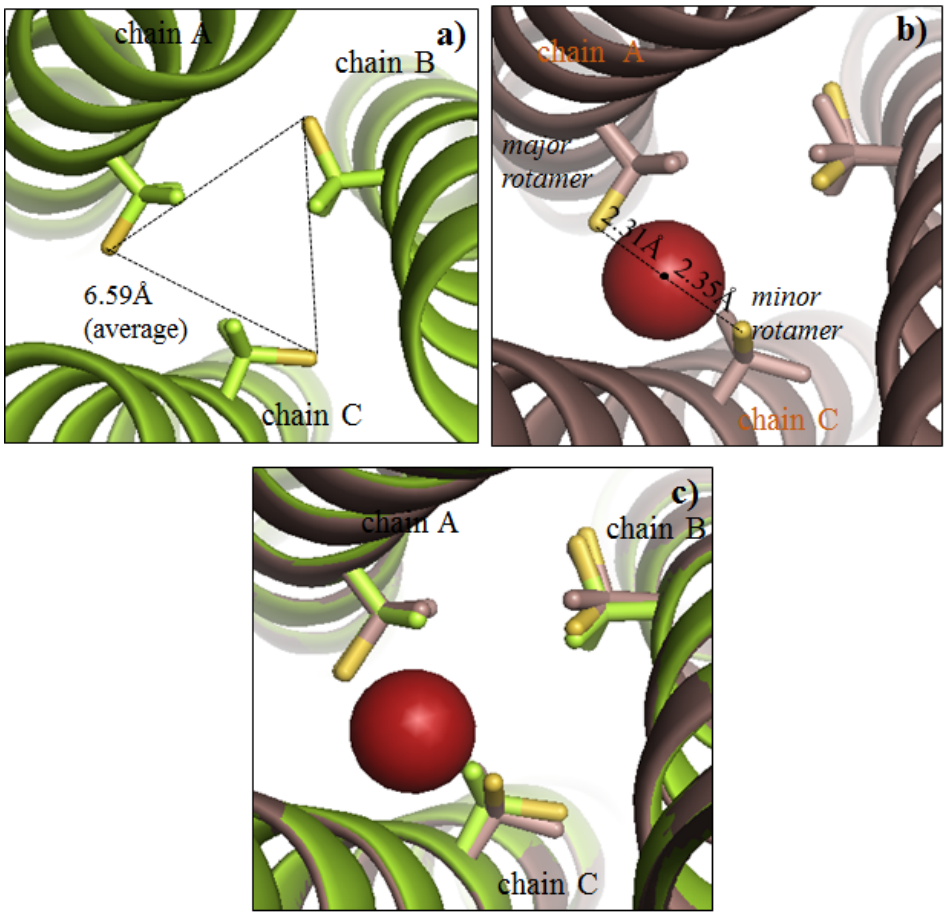

Figure 4-24. Ribbon diagrams representing D-Pen ligand orientations prior and upon binding to Hg(II). Shown from the top down view, a) D-Pen ligand orientation from apo-(**CS**L16$_{D}$Pen)$_3$ (PDB code: 3H5G)[11], b) rearrangement of D-Pen when Hg(II) is present, and c) an overlay between apo- and metallated structures. Main chain atoms of the helices are shown as ribbons, D-Pen as sticks and Hg(II) as a red sphere.

of chain C. It could be that these particular conformations could generate a second linear Hg(II) complex along the helical interface of these respective chains, but the results of the refinements revealed that the observed electron density fit far better to a water molecule, instead with distances of 2.07 and 2.78 Å from chain B and chain C, respectively. This water is observed to form a H-bonding network between the thiols and a nearby water stabilizing the D-Pen conformations. Therefore, when the linear Hg(II) is formed within the binding site the rotamers in chain C can move freely through space and do not contribute to the binding because the thiol positions from both conformers are too long to interact with Hg(II).

b) Second Coordination Sphere around the Metal Layer

The overlay of the Leu layers around the sixteenth position was analyzed in order to evaluate the behavior of hydrophobic packing between the non-metallated and metallated-(**CS**L16$_D$Pen)$_3$. At the twelfth position, the Leu residues are oriented in almost similar manners as confirmed by their similar dihedral angles. This indicates that the hydrophobic packing above the metal layer is very similar between the two structures as shown in **Figure 4-25**. The same behavior is also observed at the nineteenth position below the metal binding site where the packing of the Leu residues remains unchanged (**Figure 4-26**). These crystallographic results suggest that the binding of Hg(II) does not perturb the internal hydrophobic packing of the helical coiled coil which could possibly be due to the location of the linear Hg(II) complex that is observed on the edge of the binding site rather than internally anchored within the core of the structure. The position of Hg(II) is situated at distances quite far from the closet δ-carbon atoms of Leu residues from above and below layers. It is separated from the $C_{\delta 2}$ atom of 12Leu (chain C) at 4.37 Å and from the $C_{\delta 1}$ atom of 19Leu (chain C) at 5.02 Å. Moreover, the fact that Hg(II) is present at a very low occupancy in the crystal structure implies that the intensity of electron density from the heavy atom may not be sufficient to have a strong repulsion toward the hydrophobic environments around the metal site. However, the presence of a trigonal Hg(II)($_L$Pen)$_3^-$ located right at the center of the metal plane was shown in *Section III* chapter 2 to change the hydrophobic packing above the metal site upon binding.

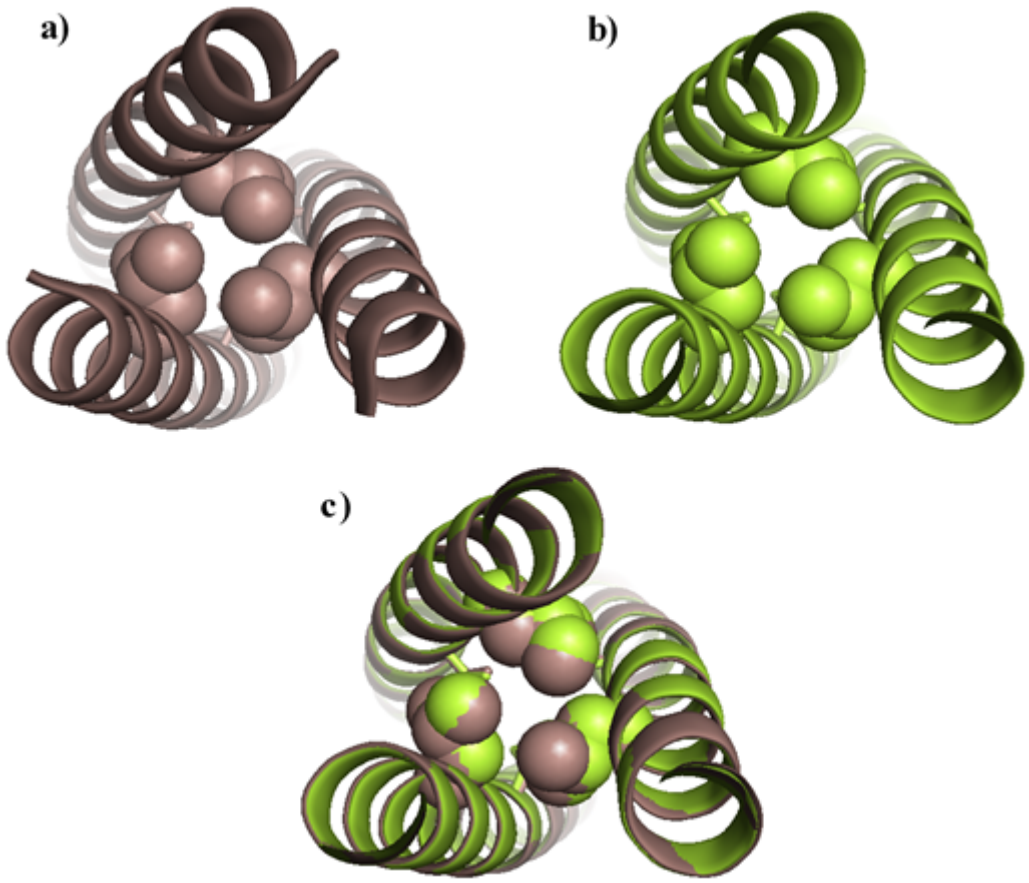

Figure 4-25. Hydrophobic packing of Leu residues at the twelfth position comparing the apo-(CSL16$_D$Pen)$_3$ and metallated Hg(II)($_D$Pen)$_2$(H$_D$Pen) structures. A top down view from the N-termini is shown, representing the 12Leu layer of a) apo-(**CS**L16$_D$Pen)$_3$, b) Hg(II)($_D$Pen)$_2$(H$_D$Pen) and c) an overlay between the two structures. Main chain atoms of the helices are shown as ribbons, Leu at the twelfth position as spheres and D-Pen at the sixteenth position as sticks. The Hg(II) ion in the metallated structure is omitted for clarity.

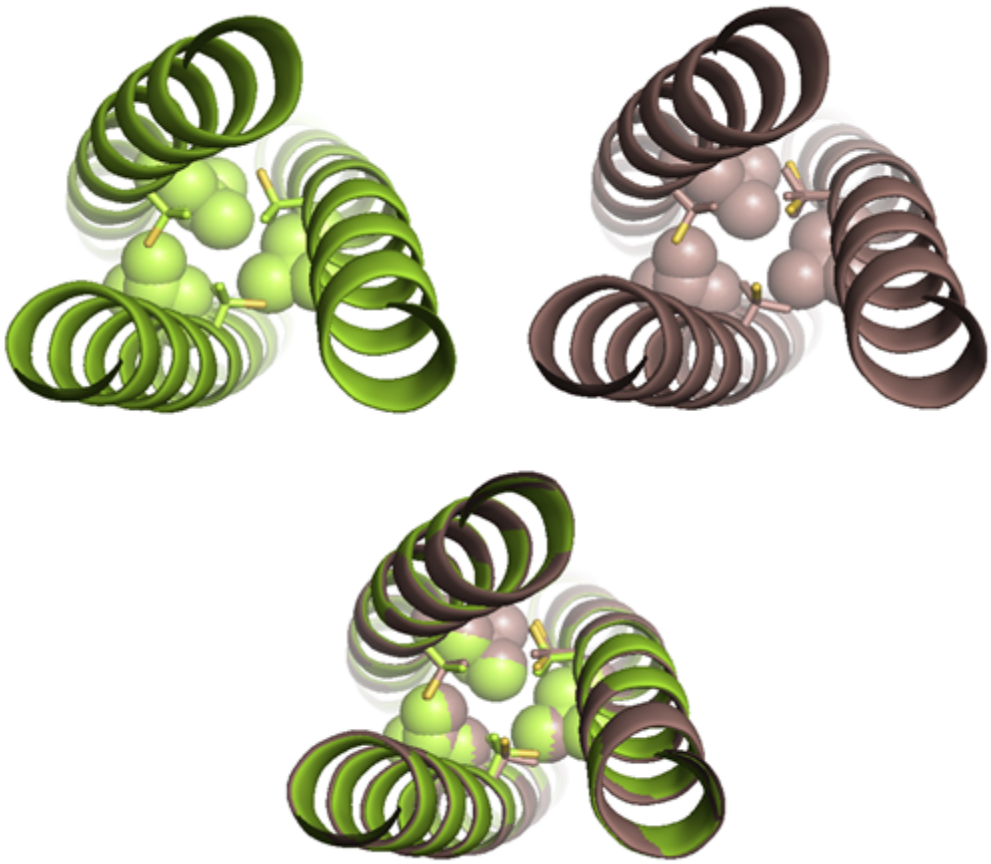

Figure 4-26. Hydrophobic packing of the Leu residues at the nineteenth position comparing the apo-(CSL16$_D$Pen)$_3$ and Hg(II)($_D$Pen)$_2$(H$_D$Pen). A top down view from the N-termini is shown, representing the 19Leu layer of a) apo-(**CS**L16$_D$Pen)$_3$, b) Hg(II)($_D$Pen)$_2$(H$_D$Pen) and c) an overlay between the two structures. Main chain atoms of the helices are shown as ribbons, Leu at the nineteenth position as spheres and D-Pen at the sixteenth position as sticks. The Hg(II) ion in the metallated structure is omitted for clarity.

The Effect of Chirality between D-Pen versus L-Pen ligands toward Hg(II) structures

Due to the alteration of chirality and steric restriction described, the Hg(II) complex prepared using D-Pen ligands within the 3SCC environment is not located deeply within the hydrophobic core of the 16D-Pen layer. The use of two out of the three D-Pen ligands for coordination does not affect the overall protein scaffold as the construct remains a well folded 3SCC. This strongly suggests that the linear S-Hg-S binding mode in the $Hg(II)(_{D}Pen)_2(H_{D}Pen)$ does not drastically perturb the native folding of the designed peptide by causing the peptide aggregation states to change from 3SCC to 2SCC. This result reflects that a thermodynamically preferred Hg(II) coordination geometry can be prepared by D-Pen ligands within a preferred aggregation state of the designed peptide. This is interesting because when the ligand chirality is altered to the normal L-Pen, Zastrow *et al*. revealed that the inward orientation of three thiols can enforce an unusual coordination number of $Hg(II)S_3^-$ anchored within the hydrophobic environment of 3SCC. [2] **Figure 4-27** confirms that the linear Hg(II) is obviously located on one edge of the sulfur layer, while the trigonal Hg(II) sits internally in the core center. The difference in Hg(II) positions is reasoned to depend on the thiol orientations of the coordinating ligands. The chemical configuration of L-Pen ligand causes the thiol directed at the core of the helices, while keeping the γ-methyl groups in an opposite direction and (outward to the helical interface). This arrangement makes a reasonable trigonal plane that subsequently facilitates a trigonal Hg(II) formation with an average Hg(II)-S bond length of 2.23 Å and an average separation between two thiols of 3.84 Å. However, the linear Hg(II) center in D-Pen construct is directed to the edge of the binding site because one of the coordinating ligands (chain A) points the thiol at the helical interface while pointing the γ-carbons inside. This orientation is completely opposite to the L-Pen of the respective chain. The other coordinating thiol (chain C) is observed to reorient toward the core where one of the γ-carbons is also at the core and the other points to the helical interface. Though both of the Cβ-Sγ bonds (chain C) of two Hg(II) structures are inward, their positions are separated by 100°. The L-Pen can point both of the γ-carbons completely to the helical interface. The thiol separation between thiols from chain A and chain C at distance of 3.7 Å. In contrast, it is found that the linear structure requires a larger separation of these two thiols (4.66 Å) in order to make reasonable Hg(II)-S distances of 2.31 and 2.35 Å. These distances correspond to the Hg(II)-S bond length of a di-thiolato Hg(II) complexes in small molecule studies.[28–30]

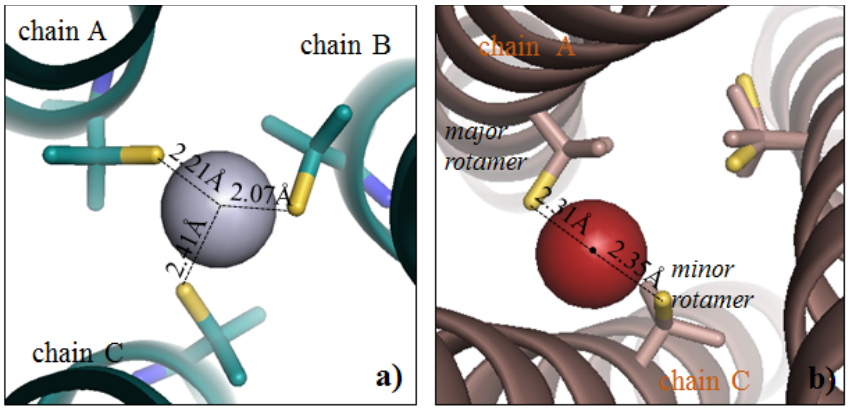

Figure 4-27. PyMOL visualization representing different locations and different geometries of the bound Hg(II) center prepared from L-Pen versus D-Pen ligands obtained at pH 8.5. Figures are a) a trigonal thiolate site, $Hg(II)(_{L}Pen)_3$ in the published structure $[Hg(II)]_S[Zn(II)(H_2O/OH^-)]_N(\mathbf{CS}L9PenL23H)_3^{n+}$ (PDB code: 3PBJ)[2] and b) a linear $Hg(II)(_{D}Pen)_2(H_{D}Pen)$. Main chain atoms of the helices are shown as ribbons, D-Pen at the sixteenth position as sticks. The trigonal Hg(II) is grey and the linear Hg(II) is red.

Even though the di-thiolato Hg(II)S_2 complex is a preferred geometry of Hg(II)[28–30], the fact that there is only a 15% occupancy of the metal is indicative of weak Hg(II) binding with the D-Pen ligands. This is potentially because the Hg(II)($_D$Pen)$_2$(H_DPen) structure requires one D-Pen ligand to reorient from its preferred ligand geometry (from directing the thiol outward to pointing inward). As penicillmine also has γ-methylene groups around Cβ-carbon, the rotation of all these atoms requires a significant reorganization energy and entropic penalty in order to achieve the final geometry. The complex is eventually formed because of the enthalpic gain upon forming a thermodynamically stable Hg(II)S_2 center.. The crystallographic results suggest from a comparison of the apo-(**CS**L16$_D$Pen)$_3$ and metallated structures that only the coordinating rotamer in chain A seems to be *preorganized* and influences the location of Hg(II) binding, while the second coordinating ligand (chain C) is predisposed and requires a significant rotation upon complex formation (**Figure 4-24**,**c**). On the other hand, the trigonal Hg(II)S_3^- prepared with the L-Pen ligands in [Hg(II)]$_S$[Zn(II)(H_2O/OH^-)]$_N$(**CS**L9PenL23H)$_3^{n+}$ was shown to have a higher occupancy for the Hg(II) center, reflective of the slightly stronger Hg(II) affinity compared to the linear structure. The strong Hg(II) affinity may, in part, be a consequence of the *preorganized* tris-thiolate metal environment that the L-configuration of penicillamine ligands adopts (**Figure 4-28**). Thus, when Hg(II) comes to the site it does not require a significant adjustment of the L-Pen ligands in order to be accommodated within the sulfur binding plane. Although a trigonal planar geometry is not the geometrical preference for Hg(II), the L-Pen ligands 100% restricted upon metal binding indicating that these are preferred conformations of L-Pen.

In summary, it is obvious that changing the chirality of the penicillamine ligands impacts the resultant metal structures. The geometries of ligands prior to metal complexation can influence the geometry of the metal center. By using the L-configuration at higher pH, a preformed tris-thiolate environment can enforce a higher coordination number of Hg(II) within the hydrophobic core. On the other hand, the reorientation of D-Pen ligands is partially predisposed to form Hg(II) into a preferred linear fashion.

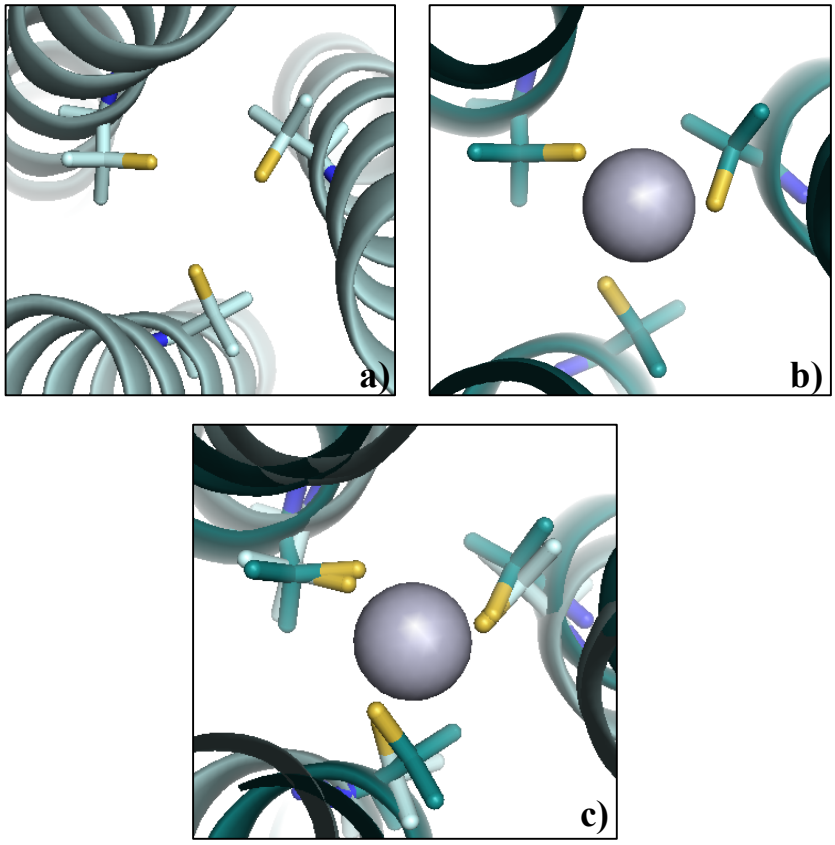

Figure 4-28. Ribbon diagrams representing L-Pen ligand organizations prior to and upon binding Hg(II). Shown from the top down view, a) L-Pen ligand orientation from apo-(**CS**L16Pen)$_3$ (PDB code: 3H5F)[11], b) arrangements of L-Pen in the trigonal Hg(II) structure of [Hg(II)]$_S$[Zn(II)(H_2O/OH_2)]$_N$(**CS**L9PenL23H)$_3^{n+}$ crystal structure (PDB code: 3PBJ)[2], and c) an overlay between apo- and metallated structures. Main atoms of the helices are shown as ribbons, L-Pen as sticks and Hg(II) as a grey sphere.

Impact of D-Configurations Using Different Ligand Compositions

a) A comparison of D-Cys and D-Pen Ligands

As discussed in *Section III* of chapter 2, the inclusion of γ-methyl groups causes a restricted C_β-S bond rotation of the L-Pen ligand within the 3SCC environment due to increased steric hindrance. In contrast, the less sterically encumbered L-Cys side chain rotates around the β-carbon at ease. The restricted rotation allows L-Pen to sequester metals in different geometries than observed with L-Cys. Based on these observations, it is interesting to see how metal coordination changes when the D-configuration is applied to Pen and Cys ligands and how these might alter the metal structures. To answer these questions, the apo-(**CS**L16$_D$C)$_3$ is overlaid onto the apo-(**CS**L16$_D$Pen)$_3$. The combination of three major D-Cys rotamers clearly shows that the ligands are oriented more inward to the helical core compared to D-Pen where the ligands are directed to the outer face (**Figure 4-29**). The wide open layout of the D-Pen ligands causes this binding pocket (average S_γ-S_γ of 6.59 Å) to be almost two times larger than D-Cys (average S_γ-S_γ of 3.43 Å). This supports the idea that D-Cys ligands have a greater potential to bind a pseudo-tetrahedral metal within the hydrophobic cavity (e.g. Zn(II)Cl(**CS**L16$_D$C)$_3^{2-}$), whereas a linear metal complex is formed at the helical interface of the D-Pen metal layer (e.g. Hg(II)($_D$Pen)$_2$(H_DPen)). Moreover, in solution studies Peacock *et al*. reported that **TRI**L16$_D$Pen results in a ^{113}Cd NMR chemical shift of 557 ppm in the presence of Cd(II).[11] This upfield shift was proposed to represent Cd(II) binding that might occur at the helical surface as either $CdSO_3$ or CdS_2O_2 complexes when the thiols are pointing out due to the D-chirality.[11] The proposed Cd(II) structures are illustrated in **Figure 4-30**. Based on the knowledge of Hg(II) binding to the D-Pen ligands, the previous proposal is further supported with the possibility that the Cd(II) is bound to two sulfur atoms, which places the metal at the helical interface where two water molecules might easily bind. On the other hand, **TRI**L16$_D$C peptide turns out to exhibit a larger downfield chemical shift of 646 ppm while retaining a 100% Cd(II)S_3O^- structure based on PAC spectra. These observations and comparison to the 4-coordinate Zn(II) structure are reflective of a tris-thiolate environment (**Figure 4-6**). This supports the previous assumption that D-Cys adopts a more interior orientation of metal ligands. However, the crystal structure of apo-(**CS**L16$_D$C)$_3$ also reveals alternative conformations of each D-Cys ligand in which the orientations of these minor contributions in chain B and chain C points the thiols far out to the helical interface to almost the same extent seen with D-Pen. Though the combination of minor D-Cys rotamers does not seem to prepare a well-ordered tris-thiolate metal

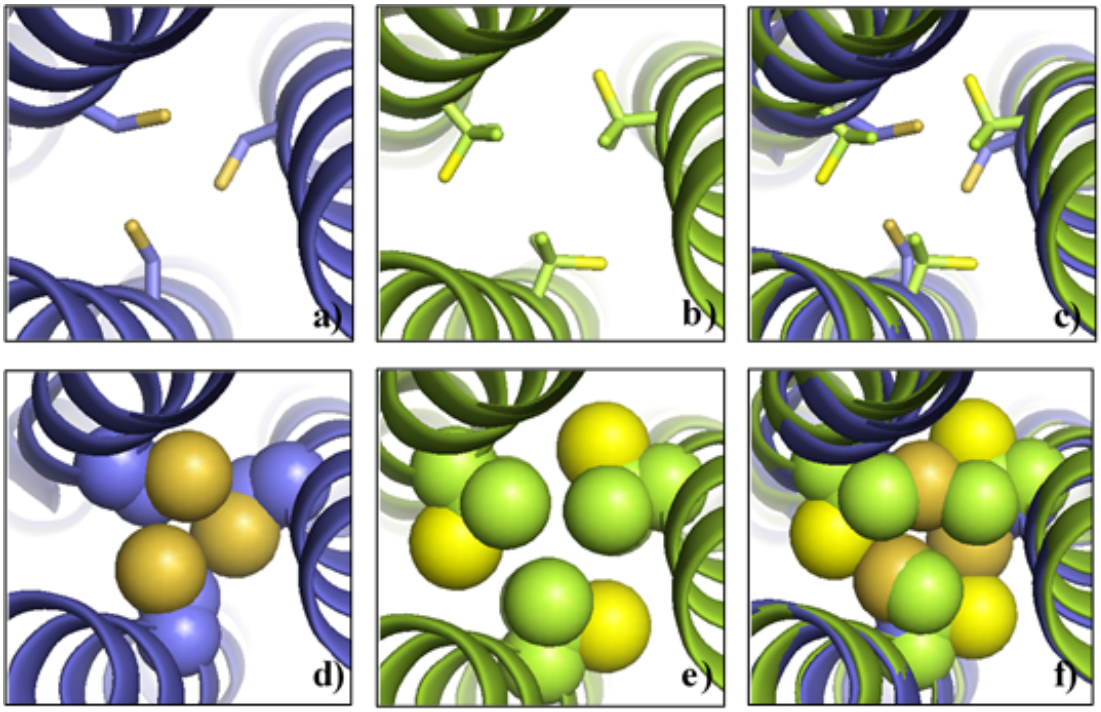

Figure 4-29. PyMOL representation illustrating the metal ligand orientation between D-Cys and D-Pen in the absence of metal. D-Cys ligands are shown in a) and d). D-Pen ligands are present in b) and e). The overlay between the two binding sites are in c) and f). The top panels represent the ligands as sticks, while spheres are used to represent the packing of the corresponding ligands from the top. Main chain atoms of the peptides are shown as ribbons.

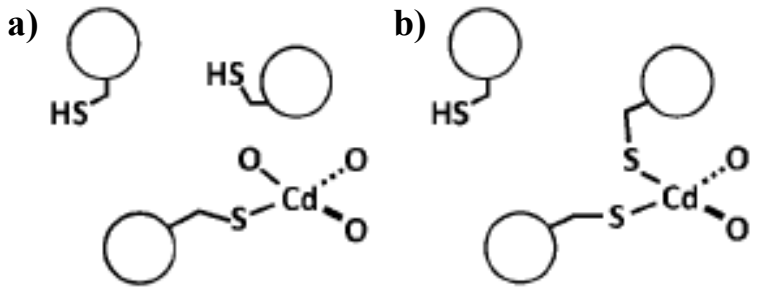

Figure 4-30. ChemDraw representation of two possible modes for Cd(II) binding to D-Pen ligands at the helical interface of 3SCC: a) $CdSO_3$ and b) CdS_2O_2 (This would require reorientation of one D-Pen to achieve the binding.) This figure was taken from Peacock *et al*.[11]

binding (**Figure 4-7**,**c**), the flexibility of ligand orientations indicates that even when the configuration of cysteine components is reversed the ligand can still easily rotate. The three D-Pen ligands contain only a single conformer in the apo-structure, emphasizing the role of the bulky methyl groups of penicillamine ligands in causing a steric restriction to steer the direction of thiols within the binding site. Both Pen isomers appear to restrict motion and limit the conformational space available to the thiol sidechains; however, when the D-configuration effect is added upon the penicillamine ligand, the D-Pen tends to have a greater potential to perturb a metal structure in the 3SCC environments. This combination of steric restriction and altered side chain rotamers leads to either linear Hg(II)S_2 or CdS_2O_2 structures rather than the previously observed Hg(II)S_3^-, Cd(II)S_3O^- and Cd(II)S_3^- chromophores. Interestingly, Zn(II) complexation seems less sensitive to the altered chirality as highly distorted structures are obtained for both isomers.

b) Prospective Hg(II) Binding Behaviors in a Tris-thiolate D-Cys Site

Nevertheless, the Hg(II) interactions with D-Cys ligands have not been structurally characterized, in this section the knowledge gained from the previous discussions will be used to propose possible Hg(II) structures that could be formed within a tris-thiolate D-Cys site. The analysis of the apo- and Zn(II)-bound (**CS**L16$_D$C)$_3$ structures confirms that the arrangement of three D-Cys major conformers are *preorganized* and suitable for binding Zn(II) into a 4-coordinate environment where the fourth ligand comes from a chloride ion. In order to bind a larger atom like Hg(II) in a trigonal structure, a significant reorientation of the D-cys ligands must be required. In the actual metallated Zn(II) structure, the two D-Cys thiols are at an average distance of 3.64 Å in which this binding plane can generate a reasonable Zn(II)-S bond length (average) of 2.13 Å. By using this structural information as a guide, the thiol orientation of D-Cys residues needs to be slightly rotate out to the helical interface in order to fit an ideal Hg(II)-S distance of 2.43 Å into this specific geometry. Upon modelling, the expansion of D-Cys to the outer face results in a slight shift of sulfur plane toward the N-termini. If the Hg(II) were to sit at the same position as Zn(II), the metal would be located at a distance of 0.5 Å below the plane. The model suggests that Hg(II) might also have to move slightly up toward the N-termini within this respective distance to achieve a reasonable S-Hg(II)-S angle. Based on the final model, Hg(II) fits nicely with an average angle 118.32^o close to a corresponding 120^o angle of a trigonal structure. The resulting S_γ-S_γ separation of 4.19 Å is also consistent with the related distances reported in Chapter 2 for the trigonal Hg(II)

complexes of $Hg(II)_SZn(II)_N$(**GRAND-CS**L16CL30H)$_3^+$ and $Hg(II)_S$(**GRAND-CS**L12A16C)$_3^-$. The proposed $Hg(II)S_3^-$ structure can be seen in **Figure 4-31** which may serve as a structural model to explain the observed ^{199}Hg NMR δ value of -136 ppm of Hg(II)(**TRI**L16C)$_3^-$ obtained at pH 8.5 (**Figure 4-5**). This chemical shift actually falls in a range of tris-thiolate Hg(II) complexes reported from Hg(II) substituted proteins.[31–34] These modeled structures suggest important insight into explaining possible Hg(II) interaction with D-Cys ligands; however, a future attempt on obtaining a crystal structure of a trigonal Hg(II) in 3SCC of (**CS**L16$_D$C)$_3$ is needed to provide a full structural explanation.

Conclusion

Not only can D-amino acids be incorporated in the second coordination sphere as described in the previous chapter to engineer indirectly the metal environment sterically, the altered stereochemistry can also be applied into the first coordination sphere to directly define the metal structures. By changing the chiral center of cysteines, the use of D-Cys in 3SCC shows to be able to shift Cd(II) structures from a mixture to a pure species. As structurally confirmed, the change in chirality causes D-Cys plane to be inclined and slightly lower toward the C-termini. The arrangement of the three thiols is *preorganized* and suitable for forming a 4-coordinate metal structure. When steric effect is added into the D-chirality ligand, the restricted rotation of D-Pen ligands also plays a major factor to control the ligand orientation in 3SCC which subsequently affects the metal coordination numbers. Structurally confirmed, Hg(II) binds with D-Pen ligands as a linear Hg(II) complex near the helical interface of the binding site, while the preferred orientation of L-Pen ligands can sequester Hg(II) as a trigonal complex within the hydrophobic core. The results of this work highlights that a change in the chirality of the coordinating ligand can not only drastically alter the coordination environment of the metal within a protein, but may change the physical location of the metal ion within the construct. All of these conclusions broaden the protein designer's toolbox to predictively develop defined coordination environments for structural and catalytic applications.

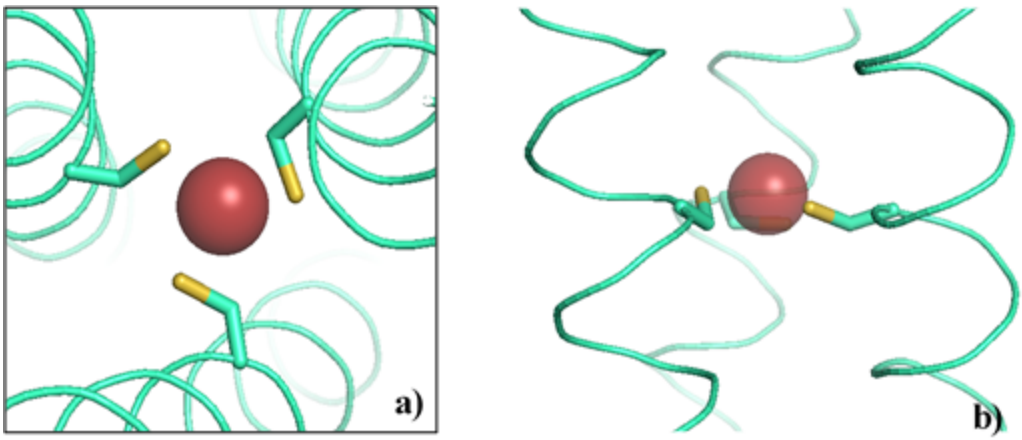

Figure 4-31. Model of a trigonal Hg(II) using the Zn(II)Cl(CSL16$_D$C)$_3^{2-}$ crystal structure. a) Top down view from the N-termini and b) side view of the binding site. Hg(II) is modeled as a red sphere. D-Cys side chains are shown as sticks where sulfurs are labeled in yellow. Backbones of the helices are shown as lines.

References

(1) Matzapetakis, M.; Farrer, B. T.; Weng, T.-C.; Hemmingsen, L.; Penner-Hahn, J. E.; Pecoraro, V. L. *J. Am. Chem. Soc.* **2002**, *124*, 8042–8054.

(2) Zastrow, M. L.; Peacock, A. F. A.; Stuckey, J. A.; Pecoraro, V. L. *Nat. Chem.* **2012**, *4*, 118–123.

(3) Otwinowski, Z.; Minor, W. *Methods Enzymol.* **1997**, *276*, 307-326.

(4) Vagin, A.; Teplyakov, A. *Acta Crystallogr., Sec D: Biol. Crystallogr.* **2010**, 22–27.

(5) Winn, M. D.; Ballard, C. C.; Cowtan, K. D.; Dodson, E. J.; Emsley, P.; Evans, P. R.; Keegan, R. M.; Krissinel, E. B.; Leslie, A. G. W.; McCoy, A.; McNicholas, S. J.; Murshudov, G. N.; Pannu, N. S.; Potterton, E. A.; Powell, H. R.; Read, R. J.; Vagin, A.; Wilson, K. S. *Acta Crystallogr. Sect. D Biol. Crystallogr.* **2011**, *67*, 235–242.

(6) Potterton, E.; Briggs, P.; Turkenburg, M.; Dodson, E. *Acta Crystallogr., Sec D: Biol. Crystallogr.* **2003**, *59*, 1131–1137.

(7) McCoy, A. J.; Grosse-Kunstleve, R. W.; Adams, P. D.; Winn, M. D.; Storoni, L. C.; Read, R. J. *J. Appl. Crystallogr.* **2007**, *40*, 658–674.

(8) Emsley, P.; Cowtan, K. *Acta Crystallogr., Sec D: Biol. Crystallogr.* **2004**, *60*, 2126-2132.

(9) Roversi, P.; Sharff, A.; Smart, O. S.; Vonrhein, C.; Womack, T.O. (**2011**). BUSTER version 2.11.2 Cambridge, United Kingdom: Global Phasing Ltd.

(10) Chen, V. B.; Arendall III, W. B.; Headd, J. J.; Keedy, D. A.; Immormino, R. M.; Kapral, G. J.; Murray, L. W.; Richardson, J. S.; Richardson, D.C. *Acta Crystallogr., Sec D: Biol. Crystallogr.* **2010***, 66*, 12-21.

(11) Peacock, A. F. A.; Stuckey, J. A.; Pecoraro, V. L. *Angew. Chem. Int. Ed. Engl.* **2009**, *48*, 7371–7374.

(12) Terwilliger, T. C.; Adams, P. D.;Read, R. J.; McCoy, A. J.; Moriarty, N. W.; Grosse-Kunstleve, R. W.; Afonine, P. V.; Zwart, P. H.; Hung, L. W. *Acta Crystallogr., Sec D: Biol. Crystallogr.* **2009**, *65*, 582-601.

(13) Grosse-Kunstleve, R.W; Adams, P.D. *Acta Cryst.* **2003**, *59*, 1966-1973.

(14) McCoy, A. J.; Grosse-Kunstleve, R. W.; Adams, P. D.; Winn, M. D.; Storoni, L. C.; Read, R. J. *J. Appl. Crystallogr.* **2007**, *40*, 658–674.

(15) Terwilliger, T. C. *Acta Crystallogr., Sec D: Biol. Crystallogr.* **2000**, *56*, 965-972.

(16) Dieckmann, G. R.; Mcrorie, D. K.; Tierney, D. L.; Utschig, L. M.; Singer, C. P.; O'Halloran,

T. V; Penner-hahn, J. E.; Degrado, W. F.; Pecoraro, V. L. *J. Am. Chem. Soc.* **1997**, *7863*, 6195–6196.

(17) Dieckmann, G. R.; McRorie, D. K.; Lear, J. D.; Sharp, K. a; DeGrado, W. F.; Pecoraro, V. L. *J. Mol. Biol.* **1998**, *280*, 897–912.

(18) Dieckmann, G. R. Ph.D. Dissertation, University of Michigan, 1995.

(19) Peacock, A. F. A.; Hemmingsen, L.; Pecoraro, V. L. *Proc. Natl. Acad. Sci. U. S. A.* **2008**, *105*, 16566–16571.

(20) Lee, K.-H.; Cabello, C.; Hemmingsen, L.; Marsh, E. N. G.; Pecoraro, V. L. *Angew. Chem. Int. Ed. Engl.* **2006**, *45*, 2864–2868.

(21) Hemmingsen, L.; Olsen, L.; Antony, J.; Sauer, S. P. *J. Biol. Inorg. Chem.* **2004**, *9*, 591–599.

(22) Ramsey, N.F. *Phys. Rev*. **1950**, *77*, 567.

(23) Ramsey, N.F. *Phys. Rev*. **1950**, *78*, 699-703.

(24) Ramsey, N.F. *Phys. Rev*. **1951**, *83*, 540-541.

(25) Ramsey, N.F. *Phys. Rev.* **1952**, *86*, 243-246.

(26) Ramsey, N.F. *Phys. Rev.* **1953**, *91*, 303-307.

(27) Ramsey, N.F. *Phys. Rev*. **1953**, *89*, 527.

(28) Skyllberg, U.; Bloom, P. R.; Qian, J.; Lin, C.-M.; Bleam, W. F. *Environ. Sci. Technol.* **2006**, *40*, 4174–4180.

(29) Kaupp, M.; Von Schnering, H. G. *Inorg. Chem.* **1994**, *33*, 2555–2564.

(30) Rulíšek, L.; Vondrášek, J. *J. Inorg. Biochem.* **1998**, *71*, 115–127.

(31) Natan, M. J.; Millikan, C. F.; Wright, J. G.; O' Halloran, T. V. *J. Am. Chem. Soc.* **1990**, *112*, 3255–3257.

(32) Blake, P.B.; Summers, M.F. *Adv. Inorg. Biochem*. **1994**, *10*, 201-228.

(33) Huffman, D.L.; Utschig, L.M.; O'Halloran, T.V. In *Metal Ions in Biological Systems*, Dekker, New York, **1997**, *34*, 503-527.

(34) Bebout, D.C.; Berry, S.M. *Struct. Bonding(Berlin)* **2006**, *120*, 81-105.

Chapter 5
Conclusions and Implications

De novo designed proteins provide a simplified scaffold allowing us to answer challenging questions that may be too complicated to address using a natural protein system, while maintaining the ability to correlate chemical observations directly with chemical structure on an atomic level in a fashion similar to small molecules.[1–4] In my studies, the *de novo* approach has been used to study heavy metal protein interactions by introducing a tris-thiolate rich site into the hydrophobic core of a 3SCC scaffold based on the **TRI**-family peptide sequence. Spectroscopic studies have shown that the engineered peptides are capable of direct binding to a variety of metals (Hg(II), Cd(II), Pb(II), As(III), Zn(II) and Bi(III)) in which the knowledge gained can be applied to investigate heavy metal interactions in the metalloregulatory systems.[5–12,2,13–26] Despite the success of spectroscopic experiments from solution studies, structural details of the metal structures are needed in order to provide a thorough understanding of how these tris-thiolate environments lead to each specific metal coordination mode based on their geometry preferences. Using the crystallographic **CoilSer**[27] and **GRAND-CoilSer** analogues, X-ray crystal structures of the designed peptides are obtained in this work to gain insight for the structural details of the engineered metal sites in order to pursue two main perspectives of research: native biological structure/function and protein design.

Biological Structure/Function perspective

Crystallographic descriptions of different ligand orientations that arise as a function of metal geometries were described in Chapter 2. These studies allow for deeper insight on how different metal geometrical preferences influence the ligand coordination to achieve target binding.

This knowledge is essential for understanding and predicting how metals are recognized selectively and with high affinity in the native metalloregulatory systems.

The metalloregulatory proteins MerR, PbrR, ArsR and CadC are important examples of native systems for which my work provides insight.[28–39] Very recently, an X-ray structure of MerR in the apo and metallated state has appeared.[32] While fully resolving the first coordination sphere environment of Hg(II) in this protein, the available structure is at relatively poor resolution (2.56 Å). The work of Dr.Melissa Zastrow was the first to characterize structurally a trigonal Hg(II) site derived from aqueous solution in a protein environment; however, the coordination geometry in that report was influenced by the nature of the coordinating ligand, penicillamine.[24] The structure of Hg(II) bound to cysteine reported in my thesis (**Figure 5-1**) bridges these two previous reports as it is at much higher resolution than the MerR structure and it uses cysteine, which does not have the germinal methyl substitution on the Cα of the side chain. It was shown that these methyl groups force the sulfur binding plane towards the N-termini of the 3SCC in order to accommodate the added steric bulk of the methyl groups. The cysteine structure provides a more natural placement of the Hg(II) within the cysteine plane.

Comparing the MerR (PDB code: 4UA1) and $Hg(II)_SZn(II)_N$(**GRAND-CS**L16CL30H)$_3^+$ structures, it is obvious that the protein environments around the two metal sites are completely different. MerR uses the loop region to bind to the metal, while the designed site is constructed into the helical coiled coil environment. Excitingly, both of the structures displays a trigonal binding site that has an Sγ-Sγ separation at similar distances, indicating that the size of the sulfur pockets are comparable (4.16 Å for the $Hg(II)_SZn(II)_N$(**GRAND-CS**L16CL30H)$_3^+$ and 4.24 Å from the native protein). As a result, the Hg(II)-S bond length in the designed structure (2.43 Å) is in excellent agreement with 2.44 Å in the MerR crystal structure. However, the Cys ligands of both structures point differently through space as shown in **Figure 5-2** indicating that the binding sites are not identical. The wide range of Cys torsion angles (-69.33º for Cys79, 173.45º for Cys 112 and 173.68º for Cys 127) observed in the native protein reflects the flexibility of the ligands located in the loop region, while in the designed protein the three Cys ligands are restrained into the threefold symmetric helical coiled coil environment with χ1 of -151.88º. Given the markedly different Cys torsion angles, the fact that the two divergent systems retain similar spectroscopic signatures is impressive.[5,11] These observations, combined with the structural information,

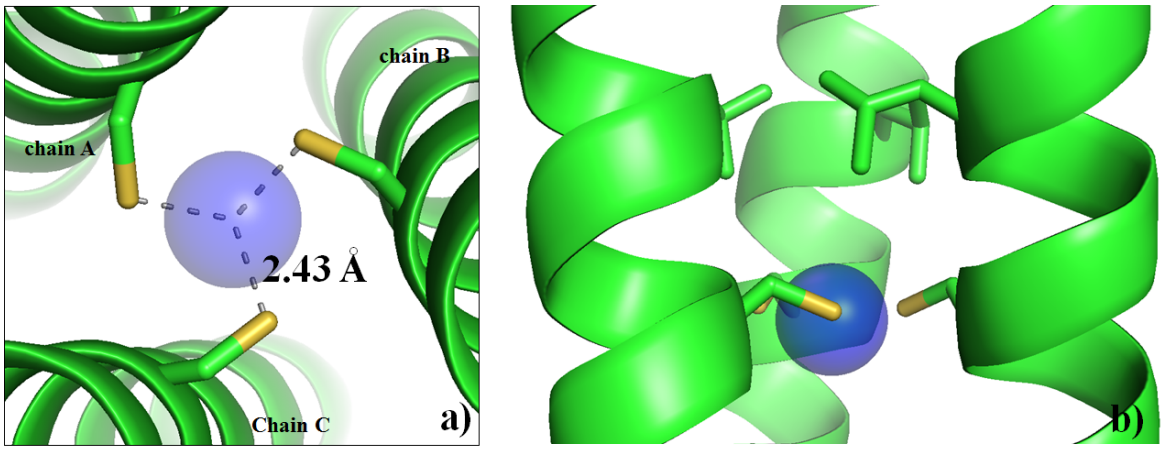

Figure 5-1. PyMOL visualization of the trigonal planar Hg(II)S_3^- in Hg(II)$_S$Zn(II)$_N$(GRAND-CSL16CL30H)$_3^+$ structure. Shown in a) top down and b) side view of the first coordination sphere of the binding site. c) and d) representing the uncoordinated water observed above the 16Cys plane. Main chain helices are shown as green ribbons, Cys side chains in the sixteenth position are in stick form (sulfur = yellow), Hg(II) ion is shown as a blue sphere and the uncoordinated water is represented as a red small sphere.

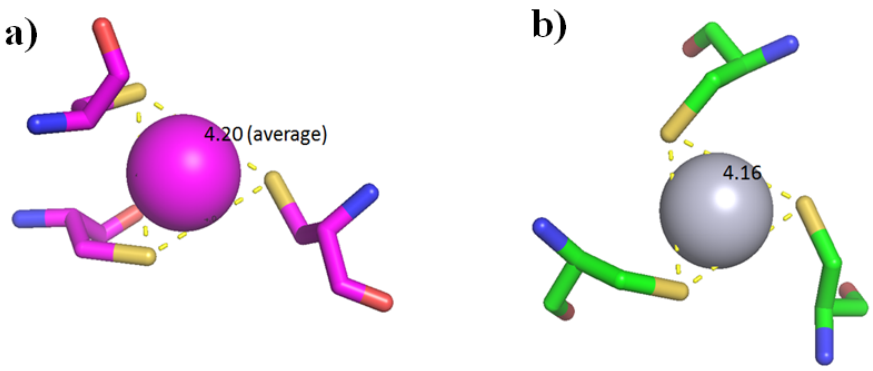

Figure 5-2. **PyMOL representation of the first coordination sphere of the Hg(II)S_3-sites in a) native MerR (PDB code: 4UA1) and b) $Hg(II)_SZn(II)_N$(GRAND-CSL16CL30H)$_3^+$.** The Cys residues in both structures are shown as sticks (sulfur=yellow, oxygen=red, nitrogen=blue, carbon in MerR=pink and carbon in $Hg(II)_SZn(II)_N$(**GRAND-CS**L16CL30H)$_3^+$=green). The Hg(II) ion in MerR is pink, while it is grey in $Hg(II)_SZn(II)_N$(**GRAND-CS**L16CL30H)$_3^+$ structure.

strongly highlight that specific protein secondary and tertiary structure as well as Cys ligand rotamers are not required to form the trigonal Hg(II) site.

PbrR is another member of the MerR family of metalloregulators.[26,40,41] In this case, an x-ray structure is not available. In at least one other Pb(II) protein structure, the metal bound to three sulfurs as a trigonal pyramid in a hemidirected, exo configuration.[42,43] For this reason, most models of Pb binding to proteins have adopted this geometry as the biologically relevant orientation of the metal.[44–48] My work shows that Pb(II) has a high affinity for the sulfur site and does bind in a trigonal pyramidal, hemi-directed fashion; however, there is a case that is represented by $Pb(II)_{S}Zn(II)_{N}$(**GRAND-CS**L16CL30H)$_3^+$ in **Figure 5-3** where the metal adopts an *endo* conformation with respect to the sulfur atoms. This conformation is not a consequence of the steric bulk of the adjacent leucine layers nor the large size of the Pb(II) atom, but instead is based on the pre-organization of the metal ligands. Thus, future computational models of Pb(II) bound systems should consider the *endo* conformer as a possible acceptable geometry. That Pb(II) and As(III) adopt the same structure, despite the difference in charge and in size, further illustrates the potential importance of this endo configuration in proteins. This will be especially true in helical systems that have similar torsion angle restrictions for cysteines. The metalloregulatory protein ArsR, a member of the SmtB family which differes from MerR, are helical and must bind As(III) in an irregular C-X-C sequence. Thus, it will be intriguing to see whether this protein generates its $As(III)S_3$ center in *endo* vs *exo* conformations.

CadC is also a member of the SmtB family.[36–38,49] There has been considerable discussion for this protein as to whether Cd(II) is bound as a $Cd(II)S_3^-$, $Cd(II)S_3O^-$ or $Cd(II)S_4^{2-}$ center.[37,49,50] My work has illustrated had structural modification to the second coordination sphere environment can control whether $Cd(II)S_3^-$ or $Cd(II)S_3O^-$ exist and, by modeling these centers using Hg(II) and Zn(II) structures allow us a far deeper understanding of Cd binding to proteins. A recent paper from the Pecoraro group using the a3D family of peptides has suggested that the chromophore in CadC is a mixture of $Cd(II)S_3O^-$ and $Cd(II)S_4^-$ geometries and that this mixture is critical to rapid CadC is a mixture of $Cd(II)S_3O^-$ and $Cd(II)S_4^-$ geometries and that this mixture is critical to rapid Cd(II) exchange, a feature which is essential for a metalloregulatory switch.[51] The structural data presented herein is consistent with this proposed model.

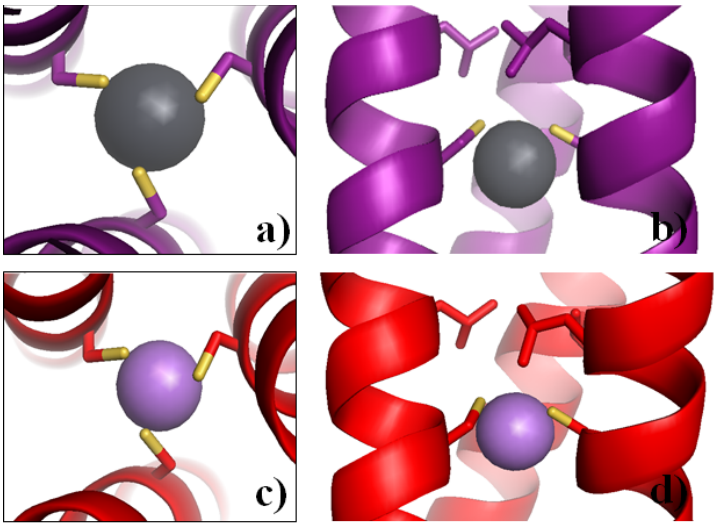

Figure 5-3. **PyMOL visualization of the trigonal pyramidal Pb(II)S_3^- and As(III)S_3 structures.** a) Top down view from the N-termini and b) side view of the Pb(II)S_3^- binding site in Hg(II)$_S$Zn(II)$_N$(**GRAND-CS**L16CL30H)$_3^+$. c) Top down and d) side views of the As(III)S_3 in As(III)(**CS**L9C)$_3$ (PDB code: 2JGO)[20]. Main chain atoms are shown as ribbon diagrams, 12Leu and 16Cys side chains in the sixteenth position are present as sticks (sulfur = bright yellow). The metal ion is shown as sphere.

Protein design perspective

Perhaps the most important and challenging question in *de novo* metalloprotein design is the ability to learn how the first and second sphere environments control metal coordination.[1,2] This is because coordination structure control helps define the metal-protein relationships that, as a consequence, can lead to the understandings of metalloprotein functions (e.g. structural, catalytic, and electron transfer properties). Given the success to mimic the structural biological-relevant sites found in metalloregulatory proteins, the geometrically threefold Cys-rich site in the 3SCC construct has proven to not only be able to enforce an uncommon, higher coordination number on a metal (e.g. $Hg(II)S_3^-$), but also to generate satisfactorily preferred geometries on metals (e.g. $Zn(II)S_3O$, $Pb(II)S_3^-$ and $As(III)S_3$) as shown in **Figure 5-4**. To extend the perspective of protein design, it would be the best to use this strategy to enforce a variety of coordination numbers onto a specific metal within the 3SCC scaffold. To serve this purpose, Cd(II) ion has been chosen to perform the studies. Cd(II) is beneficial as can accept a wide range of coordination numbers[52]; however, the most challenging task is to enforce the trigonal $Cd(II)S_3^-$ in an aqueous environment. This type of structure, though rare and unfavorable, is biological relevant to the Cd(II)-bound CmtR metalloregulatory protein.[39]If the structure can be prepared in our system, it will be a true test to prove that a lower coordination number of a metal can also be enforced within the simplified 3SCC environments. Moreover, the work of tris-thiolato Cd(II) interaction studies is unique as it also highlights the advantages of incorporation of non-coded amino acid ligands (especially D-amino acids in my dissertation project) to sterically modify the metal site environments.

Previously spectroscopic studies done by the Pecoraro group have shown that the $Cd(II)(\mathbf{TRI}L16C)_3^-$ design yielded a mixture of 3- and 4-coordination.[5] The steric removal above the metal site by a smaller Ala residue in $Cd(II)(\mathbf{TRI}L12AL16C)_3^-$ resulted in an exclusive $Cd(II)S_3O^-$ structure.[6,53] On the other hand, when the steric effect is added to the first coordination sphere by Pen ligand, a pure 3-coordinate $Cd(II)S_3^-$ center can be achieved in $Cd(II)(\mathbf{TRI}L16Pen)_3^-$.[53,54] It was observed that the only way to keep the Cys residue as the metal ligand and at the same time be able to form the 3-coordination is to enhance the steric hindrance above the metal site by reorienting the side chain of leucine at the twelfth position with D-configuration. As predicted, the water access to the $Cd(II)(\mathbf{TRI}L12_DLL16C)_3^-$ site is completely blocked, as 100% $Cd(II)S_3^-$ formation confirmed.[17] In these studies, the effect of D-amino acids has been further investigated in Chapter 3. D-Leu is now replaced at the nineteenth position to remove the steric environment

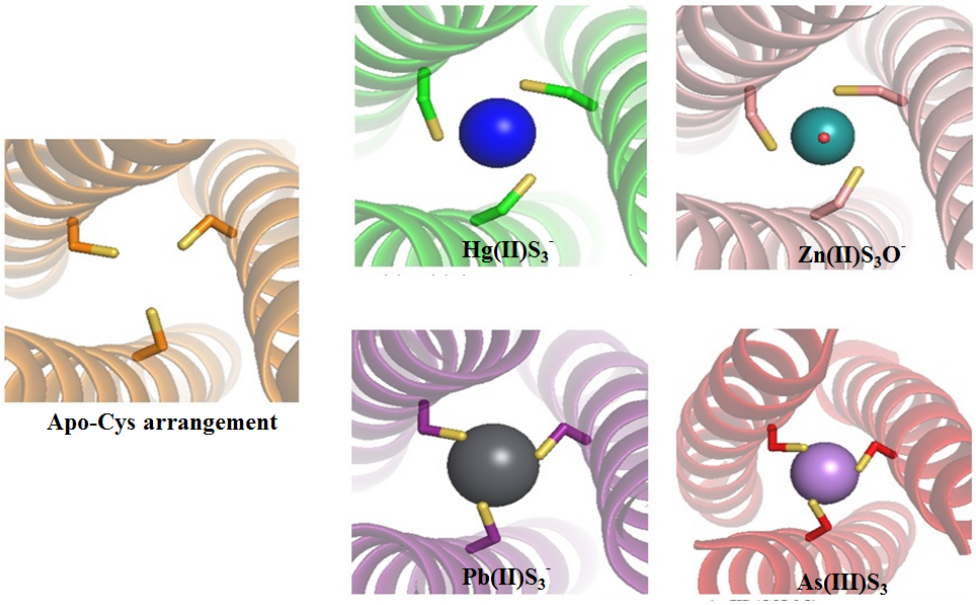

Figure 5-4. **Ligand organizations of the first coordination sphere of the designed metal sites.** In a) apo-coordination from apo-(**CS**L16C)$_3$, b) trigonal Hg(II)S_3^- from Hg(II)$_S$Zn(II)$_N$(**GRAND-CS**L16CL30H)$_3^+$ (The water observed in the structure is unbound to Hg(II).), c) 4-coodinate Zn(II)(Cys)$_3$(H_2O)$^-$ from Zn(II)(**GRAND-CS**L12AL16C)$_3^-$, d) trigonal pyramidal Pb(II)$(S)_3$ from Pb(II)$_S$Zn(II)$_N$(**GRAND-CS**L16CL30H)$_3^+$ and e) trigonal pyramidal As(III)$(S)_3$ from As(III)(**CS**L9C)$_3$ (PDB code: 2JGO)[20].

below the metal site. As a results, Cd(II)(**TRI**L2WL16CL19$_D$L)$_3^-$ shows to sequester Cd(II) with an equal contribution of 5-coordination Cd(II)$S_3O_2^-$ and 4-coordination Cd(II)S_3O^- species. Combined with the knowledge learned from the L12$_D$LL16C design, it suggests that the effect of steric modification in the second coordination by D-Leu shows to depend on its location around the metal binding site. Moreover, it is interesting that the contribution of 4-coordination Cd(II) shifts to 70% (while the other 30% species is Cd(II)S_3O^-) when D-Leu residues are incorporated at the twelfth and nineteenth positions simultaneously in Cd(II)(**GRAND-CS**L12$_D$LL16CL19$_D$L)$_3^-$. This emphasizes that while the D-Leu below the binding site opens a hole for water access, the steric hindrance generated by D-Leu above the metal site results in a water blockage. However, the ability to exclude the water at the twelfth position is not 100% achieved here possibly due to the close proximity of D-Leu residues in this design that drastically destabilizes the coiled coil of three helices. The peptide becomes less folded and the core hydrophobic residues may not pack tightly. As a consequence, water molecule can still get access to the cavity above the metal site. Moreover, the benefit of chirality to control the Cd(II) structure is not limited to the second coordination sphere modification. Described in Chapter 4, it is observed that when the metal ligand is altered to D-Cys, Cd(II)(**TRI**L16$_D$C)$_3^-$ could bind Cd(II) with a pure Cd(II)S_3O^- species. Based on the physical characterization results, the use of non-coded D-amino acids and Pen ligand in 3SCC system have led to a high degree of control in Cd(II) binding structures; however, an explanation of precisely how these sequence modifications influenced the obtained metal structures has been elusive in the absence of crystallographic data. Herein, a series of crystal structures are employed to understand the impact of changing the internal hydrophobic residues on Cd(II) structures (**Figure 5-5**).

Despite a lack of Cd(II)-bound designed peptide structures, a known Hg(II)S_3^- crystal structure obtained from Hg(II)$_S$Zn(II)$_N$(**GRAND-CS**L16CL30H)$_3^+$ was used to represent a possible structural model for a trigonal Cd(II)S_3^- in which the reason was as described in *Section IV* of Chapter 2. The structural analyses between the apo-(**CS**L16C)$_3$ and Hg(II)$_S$Zn(II)$_N$(**GRAND-CS**L16CL30H)$_3^+$ suggest possible Cd(II) binding behavior in Cd(II)(**CS**L16C)$_3^-$. The alignment of Cys layers indicates that the metal induces a high degree of S_γ rotation causing a significant lowering of the sulfur plane toward the C-termini. This situation expands the hydrophobic cavity above the sulfur plane sufficiently to accommodate a water molecule. The existing water in Hg(II)$_S$Zn(II)$_N$(**GRAND-CS**L16CL30H)$_3^+$, though uncoordinated

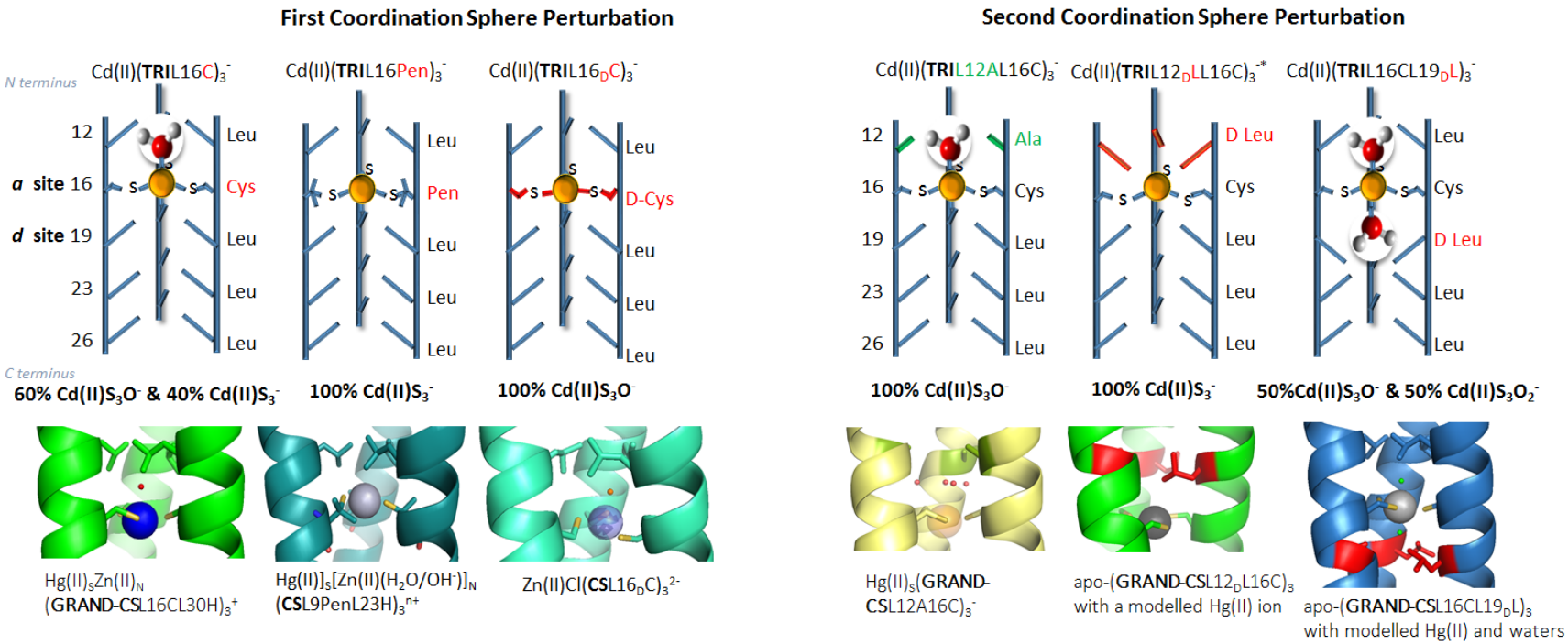

Figure 5-5. Schematic representation of the TRI-peptides designed to control Cd(II) structures and their supported crystallographic evidence using CoilSer or GRAND-CoilSer analogues.

to Hg(II), but could potentially form a coordinative ligand to Cd(II). This is because Cd(II) prefers the 4-coordinate geometry. However, a rational reason to support the evidence why only partial $Cd(II)S_3O^-$ can be formed in $Cd(II)(\mathbf{CS}L16C)_3^-$ is the hydrophobicity of leucine residues in the twelfth position can significantly destabilizes the water in the core of the 3SCC. Moreover, the complexation of $Cd(II)S_3O^-$ would cause the Cd(II) to move toward the water and require the three atom sulfur plane to expand significantly from the original apo-conformation, while less conformational rearrangement is required to bind the metal into the 3-coordinate structure. Therefore, a significant amount of $Cd(II)S_3^-$ is retained in $Cd(II)(\mathbf{CS}L16C)_3^-$. The $Hg(II)(\mathbf{GRAND\text{-}CS}L12A16C)_3^-$ is then used to assess how Ala can remove steric hindrance from Leu at the twelfth position by overlaying this structure with the $Hg(II)_SZn(II)_N(\mathbf{GRAND\text{-}CS}L16CL30H)_3^+$. As predicted, Ala design results in a larger space above the 16Cys that can allows for up to four unbound-to-Hg(II) waters to access the metal binding site confirming the proposed impact of the modification. This different number of waters molecules can explain the different degrees of solvation of Cd(II) in L12A16C and L16C designs. The metallated $Hg(II)_SZn(II)_N(\mathbf{GRAND\text{-}CS}L16CL30H)_3^+$ contains a small hydrophobic pocket that is able to house only a single water molecule at a relatively short Hg(II) to O distance of 2.79 Å, while the related distance determined from $Hg(II)(\mathbf{GRAND\text{-}CS}L12A16C)_3^-$ expands to 3.56 Å. These observations prove that the cavity for solvent does exist in L16C, but it may not allow for water access when Cd(II) is bound to the site resulting in only 60% $Cd(II)S_3O^-$ formation. On the other hand, in the L12AL16C design this steric restriction is no longer operative; therefore, only the favorable 4-coordinate CdS_3O species forms in $Cd(II)(\mathbf{TRI}L12AL16C)_3^-$.

Nonetheless, the absence of a water molecule in the interlayer spacing between 12Leu and 16Pen in the $Hg(II)(S_{Pen})_3^-$ of $[Hg(II)]_S[Zn(II)(H_2O/OH^-)]_N(\mathbf{CS}L9PenL23H)_3^{n+}$ [24] is the first indication implying that Pen ligand cannot generate enough space to accommodate a polar molecule within the hydrophobic core above the metal site. The overlay of $Hg(II)(S_{Pen})_3^-$ onto the $Hg(II)(S_{Cys})_3^-$ in $[Hg(II)_SZn(II)_N(\mathbf{GRAND\text{-}CS}L16CL30H)_3^+]$ confirms that the Pen plane is higher than the Cys due to the restriction of the bulky groups in Pen that prevent the thiols from rotating freely. Subsequently, the metal in $Hg(II)(S_{Pen})_3^-$ has to bind further toward the N-termini and closer to the 12Leu layer, thus generating less space that blocks the water. This explanation supports a fully $Cd(II)S_3^-$ formation in $Cd(II)(\mathbf{TRI}L16Pen)_3^-$.

The other way to generate $Cd(II)S_3^-$ formation is to use $L12_DL16C$ design. As discussed in

Chapter 3, the crystallographic apo-(**GRAND-CS**L12$_D$LL16C)$_3$ data affirms that reorientation of D-Leu twists the side chain lower toward the 16Cys site rather than the 12L-Leu residues in apo-(**CS**L16C)$_3$. The tighter-packing of 12D-Leu causes less interlayer space above the metal site compared to 12L-Leu. A preliminary result of the difference electron density map (F_o- F_c) obtained from the Hg(II)(**GRAND-CS**L12$_D$LL16C)$_3^-$ structure verifies that when the metal is present in the Cys plane there is no evidence of any positive difference density that could represent waters between the stacking of 12D-Leu and 16Cys layers. Thus, this steric encumbrance appears to be the basis for the water exclusion in Cd(II)(**TRI** L12$_D$LL16C)$_3^-$.

On the other hand, the apo-(**GRAND-CS**L16CL19$_D$L)$_3$ affirms that the replacement of D-Leu in the nineteenth position yields an opposite effect on the steric modification below the metal site. The 19D-Leu side chain deviates from the L-configuration by directing outward to the helical interface and toward the C-termini, generating less hydrophobic packing below the 16Cys site compared to the 19L-Leu in the apo-(**CS**L16C)$_3$. The presence of this larger cavity is further confirmed by the metallated-(**GRAND-CS**L16CL19$_D$L)$_3^-$. It is observed that when the metal is bound, the cavity below the metal site at the nineteenth position can allow for two water molecules, while only one water can be housed in the cavity above the metal site at the twelfth position [consistent with the result given from Hg(II)$_S$Zn(II)$_N$(**GRAND-CS**L16CL30H)$_3^+$]. The existence of two available pockets around the 16Cys site strongly support the spectroscopic evidence of Cd(II)(**TRI**L2WL16CL19$_D$L)$_3^-$ that both Cd(II)S$_3$O$_2^-$ (by one water occupying below and the other above the metal site at the same time) and Cd(II)S$_3$O$^-$ (at a time when only one water accessing to the site) can form into this design. The combined crystallographic results of Hg(II)$_S$Zn(II)$_N$(**GRAND-CS**L16CL30H)$_3^+$ and Hg(II)(**GRAND-CS**L16CL19$_D$L)$_3^-$ has led to the **GRAND-CS**L12$_D$LL16CL19$_D$L design to generate a higher control on Cd(II)S$_3$O$^-$ contribution; however, a full understanding of the double D-Leu mutation effect on the 3SCC peptide awaits for future structural characterizations.

The achievement of Cd(II)S$_3$O$^-$ in Cd(**TRI**L16$_D$C)$_3^-$ is structurally characterized using a combination analysis of apo-(**CS**L16$_D$C)$_3$ and Zn(II)(**CS**L16$_D$C)$_3$Cl^{2-} structures. Reported in Chapter 4, the effect of D-Cys ligand prior to metal binding is first determined by aligning the apo-(**CS**L16$_D$C)$_3$ onto apo-(**CS**L16C)$_3$. Due to the C$_\beta$ atom deviation, the D-Cys sulfur plane is highly distorted and positioned lower than the L-Cys plane with respect to the N-termini. This shift of sulfur planes downward to the C-termini indicates that the interlayer space above the metal site in

the apo-(**CS**L16$_D$C)$_3$ is larger than the apo-(**CS**L16C)$_3$. Upon Zn(II) binding, no significant ligand rotations is observed indicating that the apo-arrangement of D-Cys is *preorganized* for the 4-coordinate formation. Though the L-Cys ligands are predisposed and have to rotate to bind Zn(II), the layer of the metallated D-Cys plane is still found to be lower than the metallated L-Cys plane which could potentially generate a larger cavity above the metal site reflecting the impact of D-Cys on controlling 4-coordiante Cd(II). Based on these structural and spectroscopic characterizations, it has been observed that by changing amino acid ligand composition or altering the chirality of ligand either directly through the first or indirectly through the second coordination spheres, one can enforce Cd(II) coordination numbers ranging from an unfavorable three coordination to favorable and five coordinates.

To further investigate the properties of D-amino acids on controlling metal structures on other ion center, the crystallographic results in Chapter 4 demonstrates that D-Pen ligand shows the ability to alter coordination mode and the location of Hg(II) center from the L-Pen ligand. The incorporation of Pen results in a trigonal thiolate Hg(II) complex that forms internally within the hydrophobic core of the 3SCC at pH 8.5.[24] Surprisingly, the alternate configuration as well as the bulky effect causes D-Pen to form a linear Hg(II)S_2 complex on the edge of the metal plane nearby the helical interface (**Figure 5-6**). The studies suggest that in the absence of Hg(II) D-Pen ligands prefer to point the thiol out toward the helical interface while keeping the β-methyl groups in the core. Upon Hg(II) metal binding, even though the thermodynamically Hg(II)-thiolate bond formation is favorable, the energy penalty to cost the reorientation of D-Pen atoms is too high. This steric restriction prevents all three D-Pen thiols from moving freely through space, as a result Hg(II) could only bind on the surface where one thiol of the first D-Pen ligand is directed out to the helical interface and the second D-Pen ligand is from an adjacent chain where the Hg(II) induces some degree of this ligand rotation in order to achieve the linear complex. This observed behavior is totally opposed to the L-Pen where the L-configuration imposes all three thiols to point toward the interior, generating a *preorganized* tris-thiolate environment that can constrain Hg(II) to bind into a trigonal geometry.

Overall, my doctoral work has illustrated the opportunities afforded by *de novo* design to understand the fundamental principles of different metal geometries and how to achieve a high degree of control in coordinating the metal ion in the well-defined 3SCC peptides. The fundamental knowledge learned helps unravel the unappreciated features on defining metal

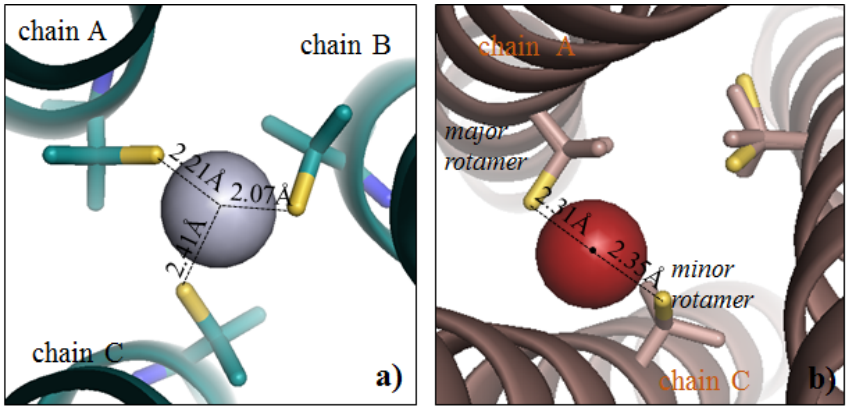

Figure 5-6. **PyMOL visualization representing different locations and different geometries of the bound Hg(II) center prepared from L-Pen versus D-Pen ligands obtained at pH 8.5.** Figures are a) a trigonal thiolate site, $Hg(II)(_{L}Pen)_3$ in the published structure $[Hg(II)]_S[Zn(II)(H_2O/OH^-)]_N(\mathbf{CS}L9PenL23H)_3^{n+}$ (PDB code: 3PBJ)[24] and b) a linear $Hg(II)(_{D}Pen)_2(H_{D}Pen)$. Main chain atoms of the helices are shown as ribbons, D-Pen at the sixteenth position as sticks. The trigonal Hg(II) is grey and the linear Hg(II) is red.

behaviors to understand the structural aspects of metal-proteins relationships in biology (e.g. metalloregulatory proteins in prokaryotic living organism). In the perspectives of protein design, the studies have shown that the geometry of 3SCC scaffold can serve as an excellent model to adopt a variety of different polyhedra of inorganic structures into the peptide based on the metal geometrical preferences. Most importantly, the premise of systematically correlating modifications with D-amino acids to engineer the steric environments and ligand organization of the metal center is believed to have a major impact on future metalloprotein design studies; i.e. developing *de novo* metalloenzymes that may catalyze biological reactions relevant to native systems. Therefore, broader applications of D-amino acids in protein design to generate novel bio-architectures essential for biophysical, industrial and pharmaceutical advantages is highly possible. In the following section, I suggest possible future works of the project.

Implications

The Use of D-amino acids in Future Structural Designs

One promising direction is to utilize D-amino acids to further establish preferred binding modes for other toxic metals in the thiol-rich environments. For example, engineering a protein-based trigonal planar Ag(I) binding site which has been observed in the BxmR that belongs to the ArsR/SmtB metalloregulary protein. To date, the structural detail of trigonal Ag(I) is unknown. By applying the knowledge gained from my project, the site could be prepared using D-amino acid ligands. Firstly, it is proposed that if the reorientation of D-Leu in **TRI**L12$_D$LL16C can completely block the water access of the Cd(II) binding site resulting in a 3-coordinate structure, the corresponding steric encumbrance in Ag(I)(**TRI**L12$_D$LL16C)$_3^{2-}$ could potentially do so. Moreover, this BxmR protein also sequesters Cu(I) into the same geometry as Ag(I). Therefore, one can also use the **TRI**L12$_D$LL16C to generate the Cu(I)(**TRI**L12$_D$LL16C)$_3^{2-}$ binding site. The spectroscopic characteristics of these new Cu(I)(**TRI**L12$_D$LL16C)$_3^{2-}$ and Ag(I)(**TRI**L12$_D$LL16C)$_3^{2-}$ as well as the previous results of Cd(II)(**TRI**L12$_D$LL16C)$_3^{-}$ will develop powerful spectral correlations for interrogating metal bound to proteins. Moreover, the crystallographic evidence will clarify a clearer understandings of how these two metals can selectively bind into the BxmR site with the same geometry.

Engineering D-amino acids into Future Metalloenzyme Designs

From a functional point of view, D-amino acids have been shown to have some well-known properties to make their incorporation in synthetic peptides and natural enzyme advantageous in medical and pharmaceutical advances.[55–57] The altered configuration of D-Ala introduced into a synthetic fragment was reported to enhance the degradative resistance of the commercial aminopeptidases and serum proteolytic enzymes. Miller *et al*. also demonstrated that the enantiomeric oligomer peptide containing solely D-amino acids (D-Ala, D-Phe, D-Arg) has significantly higher resistance to proteases compared to the L-oligomer.[58] Additionally, a non-natural D-Pandinin 2 showed to improve antibiotic activity.[59] With the necessary features learned from those synthetic peptide examples and the ability to control metal environments of D-amino acids from my current studies, these raise more challenging questions if one could exploit the D-isomers to engineer active sites in *de novo* metalloprotein enzymes that can perform metal-based biocatalytic activities that are applicable for pharmaceutical and industrial processes. This idea has led to the second future direction of my project.

Zastrow *et al*. designed an artificial metalloenzyme, $Hg(II)_SZn(II)_N$(**CS**L9CL23H)$_3$, containing two distinct metal sites within the 3SCC. The first $Hg(II)S_3^-$ site at the ninth position was designed for structural stabilization and a separated $Zn(II)His_3O$ at the twentieth positon was targeted for carbonic anhydrase activity.[24] The crystal structure revealed that the $ZnHis_3O$ site is formed within the interior of the coiled coil with a four-coordinate Zn(II) bound to three His residues and a water/hydroxyl ligand orienting to the N-termini. The first coordination sphere of this artificial site is structurally very similar to the CA II, the most active isoform of carbonic anhydrase found in nature. Undoubtedly, the designed peptide can catalyze the hydration of CO_2 with an efficiency faster than any other small molecule model and within ~300-fold of the native CAII.[24] One approach to further fine-tuning the catalytic efficiency of this *de novo* redox enzyme is to reorient the catalytic Zn(II) site away from the structural $Hg(II)S_3^-$ site allow for easier substrate access. This challenging task can be achieved when an inverted configuration of the metal histidine ligand is incorporated into the **GRAND-CS**L16CL23$_D$H (**GRAND-CoilSer** is considered in these proposed studies to improve the stability of the scaffold while containing a non-coded D-His in the sequence). It is proposed that the chirality of D-His would result in the reorientation of the imidazole ring which subsequently causes the hydroxylate ligand to direct

toward the frayed end of the C-termini when Zn(II) is bound to the site. This rearrangement of the Zn(II) site may possibly lead to catalytic CA efficiency.

Another interesting target is a binuclear type 3 (T3) copper center to mimic catechol oxidases/tyrosinase catalytic activities. These enzymes catalyze melanogenesis reactions, responsible for the formation of melanins, pigmentation, sclerotisation, primary immune response in living organisms.[60–66] The T3 type site is an oxygen carrier protein that contains a pair of two coupled copper ions named CuA and CuB in which each of them is co-ordinated by three His residues.[60] Designing a dinuclear center is possible in our peptide system. By exploiting the geometry of 3SCC, this copper-containing site can be engineered by introducing two tris-histidine layers into the construct. While the placement of L-His at the thirtieth position would point the imidazole ring to the N-termini making the base histidine layer upward, the only way to have the top histidine layer facing down toward the first later is to reorient the imidazole ring at the twenty-sixth position downward to the C-termini. This assumption can be achieved by the use of D-His ligand in the proposed **GRAND-CS**L26$_D$HL30H design. Crystal structures of the native enzymes show average distances between two copper centers around 4.2-4.3 Å.[60,64] Thus, the separation approximately by 4.3-4.8 Å between the two intervene hydrophobic layers of 3SCC should be sufficient to allow for metal-metal bridging interaction and dioxygen binding to the dinuclear site [Cu(II)–O_2–Cu(II)]. The proposed works will explore the feasibility of preparing metalloenzymes with D-amino acids at the active site and especially the impact of the reconfiguration of D-His side chains on the native catalytic activities. If activity is present, these studies will be a major breakthrough in protein design and will allow for more advanced applications of D-amino acids to the engineering of other functional metalloenzyme designs.

References

(1) Zastrow, M.; Pecoraro, V. L. *Coord. Chem. Rev.* **2013**, 2565-2588.

(2) Peacock, A. F. A.; Iranzo, O.; Pecoraro, V. L. *Dalton Trans.* **2009**, *9226*, 2271–2280.

(3) DeGrado, W. F.; Summa, C. M.; Pavone, V.; Nastri, F.; Lombardi, A. *Annu. Rev. Biochem.* **1999**, *68*, 779–819.

(4) Kaplan, J.; DeGrado, W. F. *Proc. Natl. Acad. Sci. U. S. A.* **2004**, *101*, 11566–11570.

(5) Matzapetakis, M.; Farrer, B. T.; Weng, T.-C.; Hemmingsen, L.; Penner-Hahn, J. E.; Pecoraro, V. L. *J. Am. Chem. Soc.* **2002**, *124*, 8042–8054.

(6) Lee, K.-H.; Matzapetakis, M.; Mitra, S.; Marsh, E. N. G.; Pecoraro, V. L. *J. Am. Chem. Soc.* **2004**, *126*, 9178–9179.

(7) Matzapetakis, M.; Ghosh, D.; Weng, T.-C.; Penner-Hahn, J. E.; Pecoraro, V. L. *J. Biol. Chem.* **2006**, *11*, 876–890.

(8) Matzapetakis, M.; Pecoraro, V. L. *J. Am. Chem. Soc.* **2005**, *127*, 18229–18233.

(9) Dieckmann, G. R. Ph.D. Dissertation, University of Michigan, 1995.

(10) Dieckmann, G. R.; McRorie, D. K.; Lear, J. D.; Sharp, K. a; DeGrado, W. F.; Pecoraro, V. L. *J. Mol. Biol.* **1998**, *280*, 897–912.

(11) Dieckmann, G. R.; Mcrorie, D. K.; Tierney, D. L.; Utschig, L. M.; Singer, C. P.; O'Halloran, T. V; Penner-hahn, J. E.; Degrado, W. F.; Pecoraro, V. L. *J. Am. Chem. Soc.* **1997**, *7863*, 6195–6196.

(12) Iranzo, O.; Thulstrup, P. W.; Ryu, S.-B.; Hemmingsen, L.; Pecoraro, V. L. *Chemistry* **2007**, *13*, 9178–9190.

(13) Iranzo, O.; Jakusch, T.; Lee, K.-H.; Hemmingsen, L.; Pecoraro, V. L. *Chemistry* **2009**, *15*, 3761–3772.

(14) Iranzo, O.; Chakraborty, S.; Hemmingsen, L.; Pecoraro, V. L. *J. Am. Chem. Soc.* **2011**, *133*, 239–251.

(15) Iranzo, O.; Ghosh, D.; Pecoraro, V. L. *Inorg. Chem.* **2006**, *45*, 9959–9973.

(16) Pecoraro, V. L.; Peacock, A. F. A.; Iranzo, O.; Marek, Ł. **2009**, 183–197.

(17) Peacock, A. F. A.; Hemmingsen, L.; Pecoraro, V. L. *Proc. Natl. Acad. Sci. U. S. A.* **2008**, *105*, 16566–16571.

(18) Łuczkowski, M.; Stachura, M.; Schirf, V.; Demeler, B.; Hemmingsen, L.; Pecoraro, V. L. *Inorg. Chem.* **2008**, *47*, 10875–10888.

(19) Chakraborty, S.; Touw, D. S.; Peacock, A. F. A.; Stuckey, J.; Pecoraro, V. L. *J. Am. Chem. Soc.* **2010**, *132*, 13240–13250.

(20) Touw, D. S.; Nordman, C. E.; Stuckey, J. a; Pecoraro, V. L. *Proc. Natl. Acad. Sci. U. S. A.* **2007**, *104*, 11969–11974.

(21) Touw, D. Ph.D. Thesis, Structural and Spectroscopic Studies of Heavy Metal Binding to *de Novo* Designed Coiled Coil Peptides, University of Michigan, **2007**.

(22) Ghosh, D.; Lee, K.-H.; Demeler, B.; Pecoraro, V. L. *Biochemistry* **2005**, *44*, 10732–10740.

(23) Ghosh, D.; Pecoraro, V. L. *Curr. Opin. Chem. Biol.* **2005**, *9*, 97–103.

(24) Zastrow, M. L.; Peacock, A. F. A.; Stuckey, J. A.; Pecoraro, V. L. *Nat. Chem.* **2012**, *4*, 118–123.

(25) Neupane, K. P.; Pecoraro, V. L. *Angew. Chem. Int. Ed. Engl.* **2010**, *49*, 8177–8180.

(26) Zampella, G.; Neupane, K. P.; De Gioia, L.; Pecoraro, V. L. *Eur. J. Inorg. Chem.* **2012**, *18*, 2040–2050.

(27) Lovejoy, B.; Choe, S.; Cascio, D.; Mcrorie, D. K.; William, F.; Eisenberg, D.; Degrado, W. F. *Science* **1993**, *259*, 1288–1293.

(28) Utschig, L. M.; Bryson, J. W.; Halloran, T. V. O. *Science* **1995**, *268*, 380–385.

(29) Zeng, Q.; Stålhandske, C.; Anderson, M. C.; Scott, R. A.; Summers, A. O. *Biochemistry* **1998**, *37*, 15885–15895.

(30) Brown, N. L.; Stoyanov, J. V; Kidd, S. P.; Hobman, J. L. *FEMS Microbiol. Rev.* **2003**, *27*, 145–163.

(31) Helmann, J. D.; Ballard, B. T.; Walsh, C. T. *Science* **1990**, *247*, 946–948.

(32) Chang, C. C.; Lin, L. Y.; Zou, X. W.; Huang, C. C.; Chan, N. L. *Nucleic Acids Res.* **2015**, *13*, 7612-7623.

(33) Utschig, L.M.; Wright J.G.; O'Halloran T. V. In *Methods Enzymology*, Academic Press: San Diego, 1993, 226, 71-97.

(34) Huffman, D.L.; Utschig, L.M.; O'Halloran, T.V. In *Metal Ions in Biological Systems*, Dekker, New York, 1997, 34, 503-527.

(35) Barkay, T.; Miller, S. M.; Summers, A. O. *FEMS Microbiol. Rev.* **2003**, *27*, 355–384.

(36) Busenlehner, L. S.; Pennella, M. a.; Giedroc, D. P. *FEMS Microbiol. Rev.* **2003**, *27*, 131–143.

(37) Ye, J.; Kandegedara, A.; Martin, P.; Rosen, B. P. *J. Bacteriol.* **2005**, *187*, 4214–4221.

(38) Silver, S. *J. Bacteriol.* **1995**, *177*, 4437–4441.

(39) Banci, L.; Bertini, I.; Cantini, F.; Ciofi-Baffoni, S.; Cavet, J. S.; Dennison, C.; Graham, A. I.; Harvie, D. R.; Robinson, N. J. *J. Biol. Chem.* **2007**, *282*, 30181–30188.

(40) Hobman, J. L.; Julian, D. J.; Brown, N. L. *BMC Microbiol.* **2012**, *12*, 109.

(41) Chen, P. R.; Wasinger, E. C.; Zhao, J.; Van der Lelie, D.; Chen, L. X.; He, C. *J. Am. Chem. Soc.* **2007**, *129*, 12350–12351.

(42) Erskine, P. T.; Newbold, R.; Brindley, a a; Wood, S. P.; Shoolingin-Jordan, P. M.; Warren, M. J.; Cooper, J. B. *J. Mol. Biol.* **2001**, *312*, 133–141.

(43) Erskine, P. T.; Duke, E. M. H.; Tickle, I. J.; Senior, N. M.; Cooper, J. B. *Acta Crystallogr. Sect. D Biol. Crystallogr.* **2000**, 421–430.

(44) Dean P.A.W.; Vittal, J.J.; Payne, N. C. *Inorg.Chem.* **1984**, *23*, 4232-4236.

(45) Christou, G.; Folting, K.; Huffman, J. C. *Polyhedron* **1984**, *3*, 1247-1253.

(46) Perez-Lourido, P.; Romero, J.; Garcia-Vazquez, J.A.; Sousa, A.; Zheng, Y.; Dilworth, J. R.; Trans, D. *J. Chem. Soc.* **2000**, 769.

(47) Ren, Z.-G.; Tang, X. -Y.; Li, L.; Liu, G.-F.; Li, H.-X.; Chen, Y.; Zhang, Y.;Lang, J. P. *Inorg.Chem.Commun.* **2007**, 1253.

(48) Rossini, A.J.; Macgregor, A.W.; Smith, A. S.; Schatte, G.; Schurko, R. W.; Briand, G. G. *Dalt. Trans.* **2013**, *42*, 9533-9546.

(49) Kandegedara, A.; Thiyagarajan, S.; Kondapalli, K. C.; Stemmler, T. L.; Rosen, B. P. *J. Biol. Chem.* **2009**, *284*, 14958–14965.

(50) Sun, Y.; Wong, M. D.; Rosen, B. P. *J. Biol. Chem.* **2001**, *276*, 14955–14960.

(51) Tebo, A. G.; Hemmingsen, L.; Pecoraro, V. L. *Metallomics* **2015**, 1–7.

(52) Borsari, M. *Inorg.Chem.* **2011**, 1–16.

(53) Lee, K.-H.; Cabello, C.; Hemmingsen, L.; Marsh, E. N. G.; Pecoraro, V. L. *Angew. Chem. Int. Ed. Engl.* **2006**, *45*, 2864–2868.

(54) Peacock, A. F. A.; Stuckey, J. A.; Pecoraro, V. L. *Angew. Chem. Int. Ed. Engl.* **2009**, *48*, 7371–7374.

(55) Mahalakshmi, R.; Balaram, P. In *A New Frontier in Amino Acid and Protein Research*; Nova Science Publishers, Inc., **2006**; 416–430.

(56) Aravinda, S.; Shamala, N.; Roy, R. S.; Balaram, P. *Proc Indian Acad Sci - Chem Sci* **2003**, *115*, 373–400.

(57) Durani, S. *Acc. Chem. Res.* **2008**, *41*, 1301–1308.

(58) Miller, S. M.; Simon, R. J.; Ng, S.; Zuxkermann, R. N.; Kerr, J. M.; Moos, W. H. *Drug Dev. Res.* **1995**, *35*, 20–32.

(59) Carmona, G.; Rodriguez, A.; Juarez, D.; Corzo, G.; Villegas, E. *Protein J.* **2013**, *32*, 456–466.

(60) Rolff, M.; Schottenheim, J.; Decker, H.; Tuczek, F. *Chem. Soc. Rev.* **2011**, *40*, 4077–4098.

(61) Rompel, A; Fischer, H.; Meiwes, D.; Büldt-Karentzopoulos, K.; Dillinger, R.; Tuczek, F.; Witzel, H.; Krebs, B. *J. Biol. Inorg. Chem.* **1999**, *4*, 56–63.

(62) Della Longa, S.; Ascone, I.; Bianconi, A; Bonfigli, A; Castellano, A. C.; Zarivi, O.; Miranda, M. *J. Biol. Chem.* **1996**, *271*, 21025–21030.

(63) Gasparetti, C.; Faccio, G.; Arvas, M.; Buchert, J.; Saloheimo, M.; Kruus, K. *Appl. Microbiol. Biotechnol.* **2010**, *86*, 213–226.

(64) Hakulinen, N.; Gasparetti, C.; Kaljunen, H.; Kruus, K.; Rouvinen, J. *J. Biol. Inorg. Chem.* **2013**, *18*, 917–929.

(65) Matoba, Y.; Kumagai, T.; Yamamoto, A.; Yoshitsu, H.; Sugiyama, M. *J. Biol. Chem.* **2006**, *281*, 8981–8990.

(66) Monzani, E.; Quinti, L.; Perotti, A.; Casella, L.; Gullotti, M.; Randaccio, L.; Geremia, S.; Nardin, G.; Faleschini, P.; Tabbì, G. *Inorg. Chem.* **1998**, *37*, 553–562.

Appendix

Appendix A

A. Crystallographic evidence of noncovalent interactions and external Zn(II) binding sites at the crystal packing interface observed in the crystal structures reported in Chapter 2

Non-covalent Interactions

*apo-(**CS**L16C)$_3$*

The peptide structure has both intra- and interhelical salt bridge interactions to help stabilize the orientation of the three-stranded coiled coil scaffold as shown in **Figure A-1**. The pairs of interactions are listed in **Table A-1**. Three of the intrahelical salt bridges are observed close to the N-termini of the 3SCC structure. There are six of the interhelical salt bridge interactions between Glu residues at the *e* positions and Lys residues at the *g* positions and also two unusual interhelical salt bridges present between *b* and *g* residues. The presence of the first water shells reveals that they mediate H-bonding interactions with the charged residues along the helical interface.

*Hg(II)$_S$Zn(II)$_N$(**GRAND-CS**L16CL30H)$_3^+$*

Several types of electrostatic interactions generated from the charged side chain residues lying on the 3SCC surface are present in this crystal structure as listed in **Table A-2**. Firstly, six of them are interhelical salt bridge interactions between *e* (Glu) and *g* (Lys) positions as shown in the helical diagram (**Figure A-2**). Three of which are found in the middle of the structure, where a Lys residue at the fifteenth position from one strand salt bridges with a Glu residue at the twentieth position from an adjacent strand. The other three occur at the far end of the structure between Lys (*g* position) and Glu (*e* position) residues of the fourth and fifth heptads. No intrahelical interactions between side chains are observed in this structure, but instead interactions

occur between some side chains and the helical backbone from their respective chain. For example, the carboxylate anion of 1Glu interacts with the amide nitrogen of 3Glu, 14Ser hydroxyl group to the carbonyl oxygen of 10Ala and the $N\varepsilon_2$ of 24Gln to the carbonyl backbone of 20Glu. Thirdly, polar water molecules form shells around the peptide helical interface by mediating the hydrogen bonds to the charged residue side chains (27Glu, 28Lys, 31Glu and 34Glu of every chain). Moreover, to promote appropriate folding and the three dimensional crystal packing, several charged residues along the surface are H-bonded to the side chains from adjacent trimers.

*Zn(II)(**GRAND-CS**L12A16C)$_3^-$*

Again H-bonding and salt bridge interactions are observed along the packing interfaces of Zn(II)(**GRAND-CS**L12A16C)$_3^-$. The helical diagram are shown in **Figure A-3**. It is found that nine interhelical salt bridges (between *e* and *g* residues) are contributed between the three helices. Six of the pairs are similar to that seen in Hg(II)$_S$Zn(II)$_N$(**GRAND-CS**L16CL30H)$_3^+$ and Pb(II)$_S$Zn(II)$_N$(**GRAND-CS**L16CL30H)$_3^+$ as listed in **Table A-3.** The other three interactions are observed in the same manner between 22Lys and 27Glu from two neighboring helices. The unusual salt bridge interactions between *b* (29Lys) and *g* (31Glu) residues of two adjacent strands are found close to the C-termini. Moreover, the first heptad of each chain is stabilized by an intrahelical side chain interaction and a H-bond between the 1Glu and amide backbone of 4Ala(same chain). The packing within a trimer is also facilitated by interactions of the polar O_γ atoms of 14Ser with amide backbones of their respective chain 10Ala and between 35His ($N\varepsilon_1$) atoms and the carbonyl groups of main chain 34Glu. Moreover, examination of the interfaces from the N→C termini reveals a number of charge-charge interactions between trimers and an H-bonding network formed by the first shell of waters and the helical interface side chains. The latter extends and is thought to generate a connection with the charged residues of nearby trimers.

*Hg(II)(**GRAND-CS**L12A16C)$_3^-$*

Nine salt bridges are determined along the Hg-bound (**GRAND-CS**L12A16C)$_3^-$ construct that resemble the Zn-bound structure. However, only six of the pairs are identical to the Zn(II)-bound structure in which three of them appear to be between 15Lys and 20Glu from two adjacent helices within a trimer and the other three pairs are between 29Lys and 34Glu. The remainder are found near the N-terminus of the structure using 8Lys of one strand to interact with 13Glu of

another. Other intrahelical salt bridge interactions are also observed as listed in **Table A-4**. The helical diagram of salt bridge interactions is shown in **Figure A-4**. Moreover, it is observed the the several charged residues point their chains outward to the solvent region form a decent H-bonding network with waters to mediate crystal packing.

*$Pb(II)_S Zn(II)_N$(**GRAND-CS**L16CL30H)$_3^+$*

Similar numbers and side chain positions of interhelical salt bridge pairs are observed between the $Pb(II)_S Zn(II)_N$(GRAND-CSL16CL30H)$_3^+$ and $Hg(II)_S Zn(II)_N$(GRAND-CSL16CL30H)$_3^+$ structures (**Figure A-5** and **Table A-5)**. Three intrahelical interactions are observed at the top part of the structures between 2Trp($N\varepsilon_1$) and the main chain 1Glu of its respective chain. The same types of interactions also happen between 1Glu($O\varepsilon_1$) and the main chain of 4Ala. Moreover, both of the ε-oxygen atoms of 1Glu form H-bonds diagonally with the amide backbone of 3Glu of an adjacent chain in the helices. In addition, many of charge-charge interactions from charged residues are observed along the crystal packing interfaces of symmetry related trimers.

External Metal Binding Sites

*apo-(**CS**L16C)$_3$*

The external Zn(II) binding sites are bound at the crystal packing interface and display a tetrahedral geometry. The four ligands coordinated to the first Zn(II) ion include 24GluA ($O\varepsilon_2$), 24GluB ($O\varepsilon_2$) and 28HisB ($N\varepsilon_2$) (both from another symmetry related molecule of peptide) and a solvent water. The second Zn(II) is bound to 28HisA ($N\varepsilon_2$), 20GluB ($O\varepsilon_1$) and 24GluB ($O\varepsilon_1$) from an adjacent symmetry related peptide and 3GluB ($O\varepsilon_1$) from another adjacent symmetry related molecule. The third external Zn(II) has its ligands as 28HisC ($N\varepsilon_2$), 6GluA ($O\varepsilon_1$) and 1GluC ($O\varepsilon_2$) from a symmetry related peptide molecule and an exogenous solvent water. The three dimensional packing of the helices is demonstrated in **Figure A-6**.

*$Hg(II)_S Zn(II)_N$(**GRAND-CS**L16CL30H)$_3^+$*

An external Zn(II) binding site is observed further down to the C-terminus of the single strand of peptide that is occupied per asymmetric unit. This Zn(II) displays tetrahedral geometry with two of the ligands being 31Glu ($O\varepsilon_1$) and 35His ($N\varepsilon_2$) from the fourth and fifth heptad,

respectively. The other two ligands are from 22Lys (N_z) and 27Glu ($O\varepsilon_1$) from another symmetry related molecule of peptide. When taken three adjacent asymmetric units that are imposed by the three fold axis in order to achieve a three stranded coiled coil packing **(Figure A-7)**. These three Zn(II) ion sites link the coiled coil together and are at the crystal-packing interfaces on the exterior of the 3SCC peptide.

*Zn(II)(**GRAND-CS**L12A16C)$_3^-$*

It seems that the crystallographic packing of the peptide in the R32 space group has an external Zn(II) binding site (per ASU) at the crystal packing interface as this observation is again found in Zn(II)(**GRAND-CS**L12A16C)$_3^-$. The site is in a tetrahedral geometry and located further down to the C-terminal end. Slightly different from the Hg(II)$_S$Zn(II)$_N$(**GRAND-CS**L16CL30H)$_3^+$ structure, three of the exterior amino acids from the fifth heptad in the same strand are required to coordinate to Zn(II) [31Glu ($O\varepsilon_1$), 34Glu ($O\varepsilon_2$) and 35His ($N\varepsilon_2$)]. The fourth heptad comes from 3Glu ($O\varepsilon_1$) of an adjacent symmetry related peptide. The three dimensional packing of the helices is demonstrated in **Figure A-8**.

*Hg(II)(**GRAND-CS**L12A16C)$_3^-$*

Likewise Zn(II)(**GRAND-CS**L12A16C)$_3^-$ has a full Zn(II) ion per ASU close to the C-terminal end. The site is again tetrahedral with all four bound ligands from the helical interface side chains. 31Glu ($O\varepsilon_1$), 34Glu ($O\varepsilon_2$) and 35His ($N\varepsilon_2$) are used as ligands to coordinate with the Zn(II) ion and the fourth ligand comes from 3Glu ($O\varepsilon_1$) of an adjacent symmetry related trimer. The coordination of the Zn(II) site at the crystal packing interface in this structure (**Figure A-8**) is identical to Zn(II)(**GRAND-CS**L12A16C)$_3^-$.

*Pb(II)$_S$Zn(II)$_N$(**GRAND-CS**L16CL30H)$_3^+$*

The external Zn(II) coordination at the crystal packing interfaces in the Pb(II)$_S$Zn(II)$_N$(**GRAND-CS**L16CL30H)$_3^+$ structure is similar to the observation of Hg(II)$_S$Zn(II)$_N$(**GRAND-CS**L16CL30H)$_3^+$ (**Figure A-7).**

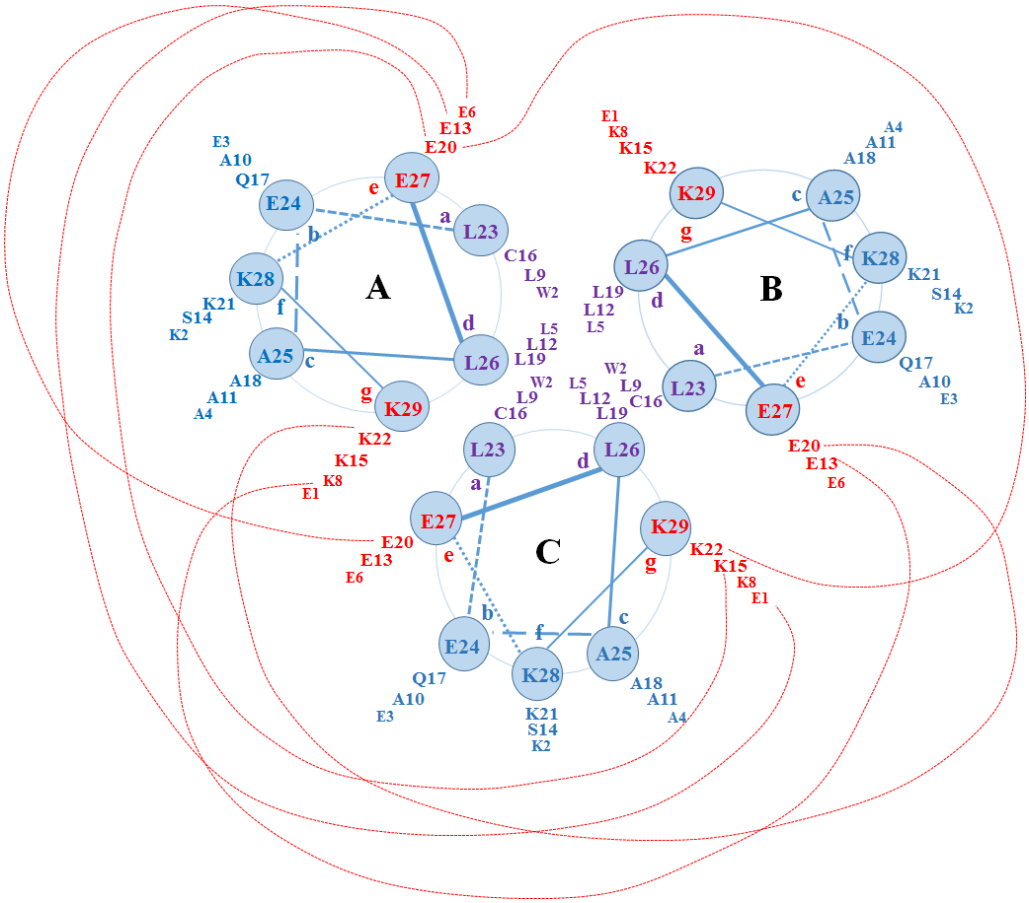

Figure A-1. Helical wheel diagram of apo-(CSL16C)$_3$. Red dash lines between different residues from helices A, B and C represent interhelical electrostatic interactions. Residues at *e* and *g* positions are labeled in red, *a* and *d* in purple and *b*,*f* and *g* in blue.

Table A-1: Non-covalent Interactions observed in apo-(**CS**L16C)$_3$

Molecule 1	**Molecule 2**
<u>Interhelical salt bridge interactions</u>	
20GluA ($O\varepsilon_1$, $O\varepsilon_2$)	15LysC (N_z)
20GluA ($O\varepsilon_1$)	22LysC (N_z)
13GluB ($O\varepsilon_1$)	8LysA (N_z)
20GluB ($O\varepsilon_1$)	22LysA (N_z)
20GluC ($O\varepsilon_1$, conformation B)	15LysA (N_z, conformation A)
24GluA ($O\varepsilon_1$)	22LysC (N_z)
20GluA ($O\varepsilon_2$)	22LysB (N_z)
1GluB ($O\varepsilon_2$)	21LysB (N_z)
<u>Intrahelical salt bridge interactions</u>	
3GluB ($O\varepsilon_1$)	7LysB(N_z)
2TrpC ($N\varepsilon_2$)	6GluC ($O\varepsilon_2$)
2TrpC ($N\varepsilon_2$)	1GluC ($O\varepsilon_1$)
<u>Charged residue-solvent interactions</u>	
13GluA ($O\varepsilon_1$, $O\varepsilon_2$),	water
17GlnA ($N\varepsilon_2$),	water
24GluA ($O\varepsilon_1$),	water
8LysB (N_z),	water
15LysB (N_z),	water
27GluB ($O\varepsilon_1$, $O\varepsilon_2$),	water
13GluC ($O\varepsilon_1$, $O\varepsilon_2$),	water
8LysC (N_z),	water
24GluC ($O\varepsilon_1$, $O\varepsilon_2$)	water
14SerA($O\gamma$)	water
14SerB($O\gamma$)	water
14SerC($O\gamma$)	water
	water

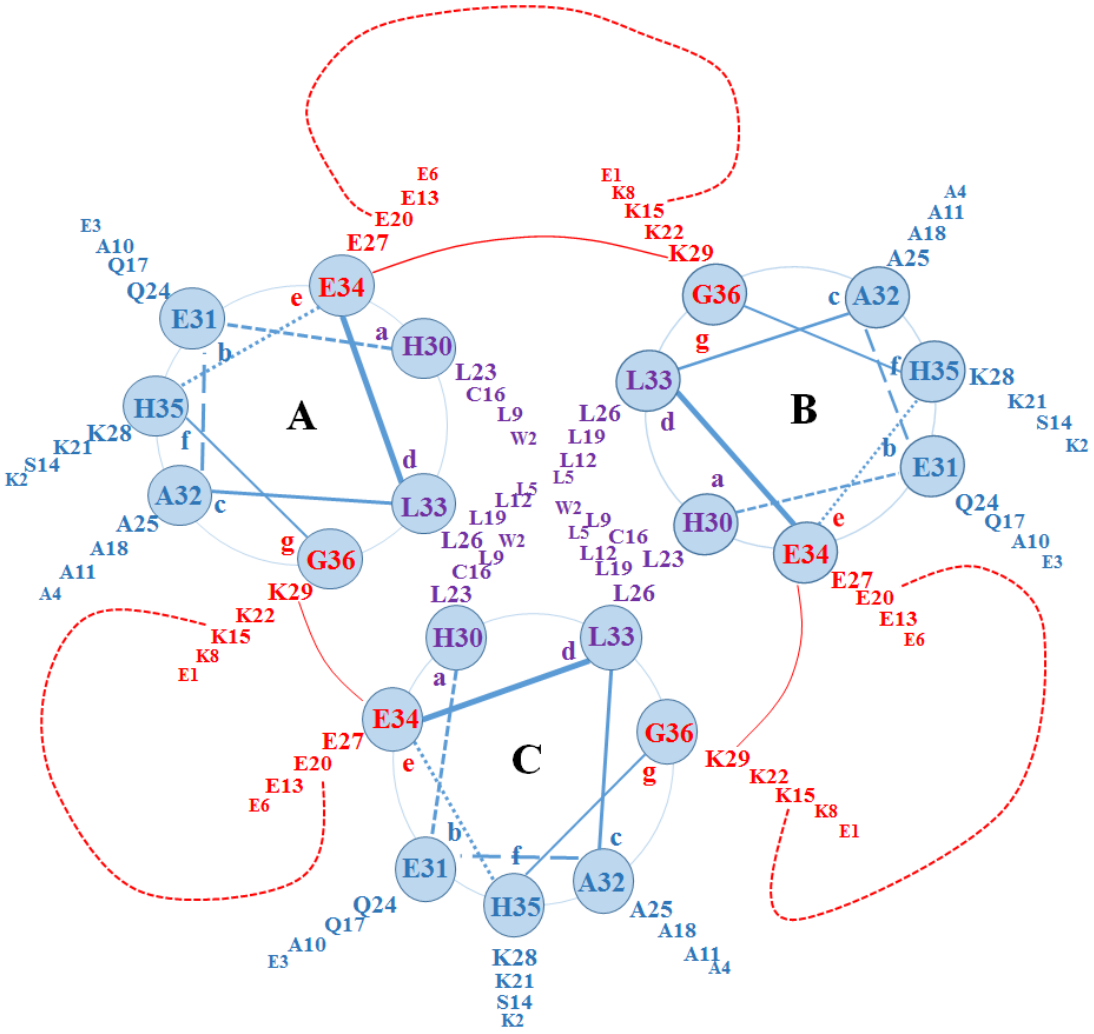

Figure A-2. Helical wheel diagram of $Hg(II)_5Zn(II)_N$(GRAND-CSL16CL30H)$_3^+$. Red lines between different residues from helices A, B and C represent interhelical electrostatic interactions; red dash lines (interactions between K15 and E20) and solid lines (interactions between K29 and E34). Residues at *e* and *g* positions are labeled in red, *a* and *d* in purple and *b*,*f* and *g* in blue.

Table A-2: Non-covalent interactions observed in $Hg(II)_S Zn(II)_N$(**GRAND-CS**L16CL30H)$_3^+$

Molecule 1	**Molecule 2**
<u>Interhelical salt bridge interactions</u>	
15LysB(N_z)	20GluA($O\varepsilon_1$)
15LysC(N_z)	20GluB($O\varepsilon_1$)
15LysA(N_z)	20GluC($O\varepsilon_1$)
29LysB(N_z)	34GluA($O\varepsilon 1$,$O\varepsilon_2$)
29LysC(N_z)	34GluB($O\varepsilon_1$,$O\varepsilon_2$)
29LysA(N_z)	34GluC($O\varepsilon_1$,$O\varepsilon_2$)
<u>Other interactions</u>	
carboxylate anion of 1GluA	amide nitrogen of 3GluA
carboxylate anion of 1GluB	amide nitrogen of 3GluB
carboxylate anion of 1GluC	amide nitrogen of 3GluC
hydroxyl group of 14SerA	carbonyl oxygen of 10AlaA
hydroxyl group of 14SerB	carbonyl oxygen of 10AlaB
hydroxyl group of 14SerC	carbonyl oxygen of 10AlaC
$N\varepsilon_2$ of 24GlnA	carbonyl backbone of 20GluA
$N\varepsilon_2$ of 24GlnB	carbonyl backbone of 20GluB
$N\varepsilon_2$ of 24GlnC	carbonyl backbone of 20GluC

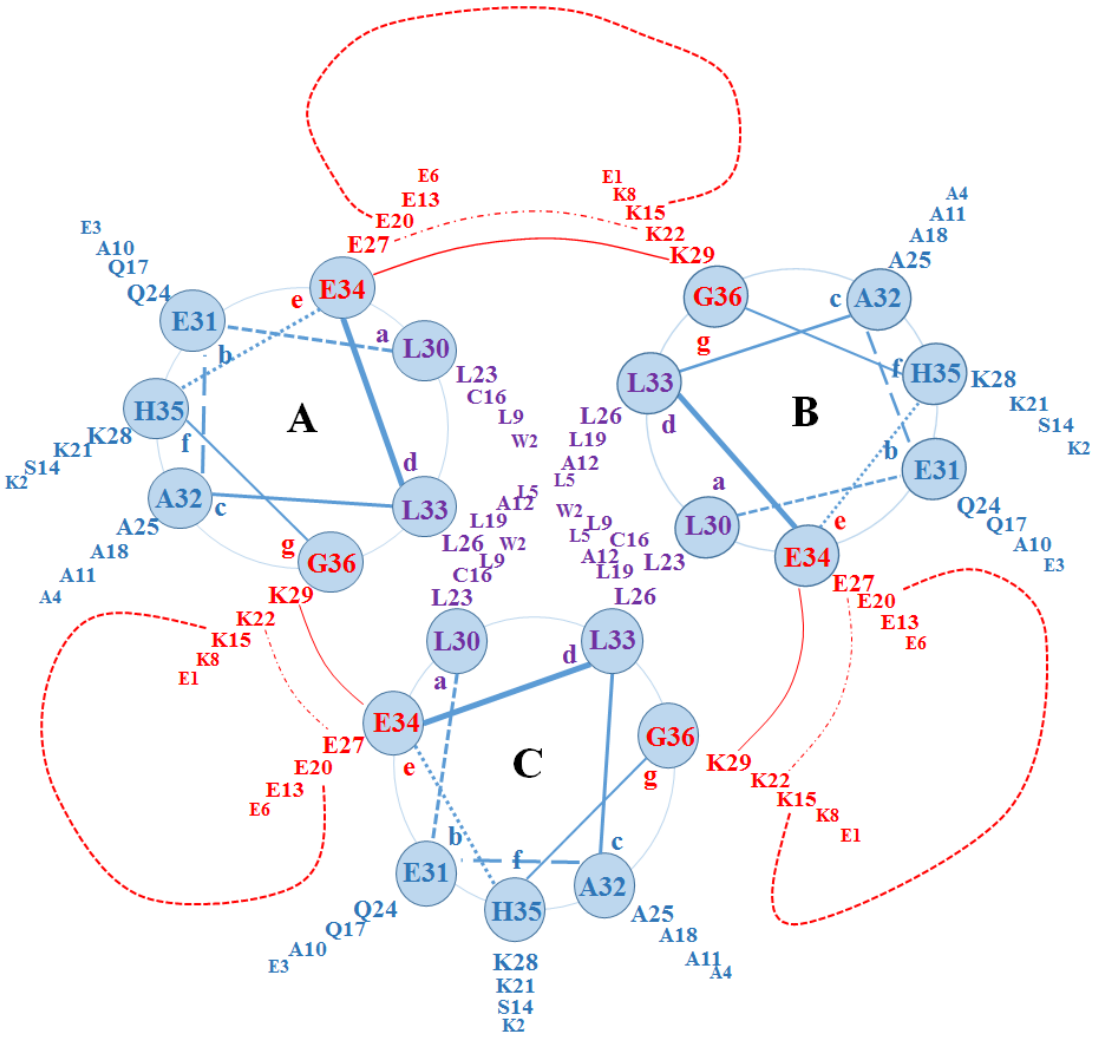

Figure A-3. Helical wheel diagram of Zn(II)(GRAND-CSL12AL16C)$_3^-$. Red lines between different residues from helices A, B and C represent interhelical electrostatic interactions; red dash lines (interactions between K15 and E20), red broken lines (interactions between K22 and E27) and solid lines (interactions between K29 and E34). Residues at *e* and *g* positions are labeled in red, *a* and *d* in purple and *b*,*f* and *g* in blue.

Table A-3: Non-covalent interactions observed in $Zn(II)_5$(**GRAND-CS**L12AL16C)$_3^-$

Molecule 1	**Molecule 2**
Interhelical salt bridge interactions	
15LysB(N_z)	20GluA($O\varepsilon_1$)
15LysC(N_z)	20GluB($O\varepsilon_1$)
15LysA(N_z)	20GluC($O\varepsilon_1$)
29LysB(N_z)	34GluA($O\varepsilon1$,$O\varepsilon_2$)
29LysC(N_z)	34GluB($O\varepsilon_1$,$O\varepsilon_2$)
29LysA(N_z)	34GluC($O\varepsilon_1$,$O\varepsilon_2$)
22LysA(N_z)	27GluC($O_{\varepsilon1}$,$O_{\varepsilon2}$)
22LysB(N_z)	27GluA($O_{\varepsilon1}$,$O_{\varepsilon2}$)
22LysC(N_z)	27GluB($O_{\varepsilon1}$,$O_{\varepsilon2}$)
29LysA(Nz)	31GluB
29LysB(Nz)	31GluC
29LysC(Nz)	31GluA
Intrahelical salt bridge interactions	
2TrpA($N\varepsilon_1$)	6GluA($O\varepsilon_2$)
2TrpB($N\varepsilon_1$)	6GluB($O\varepsilon_2$)
2TrpC($N\varepsilon_1$)	6GluC($O\varepsilon_2$)
Other interactions	
1GluA($O\varepsilon_2$)	amide backbone of 4AlaA
1GluB($O\varepsilon_2$)	amide backbone of 4AlaB
1GluC($O\varepsilon_2$)	amide backbone of 4AlaC

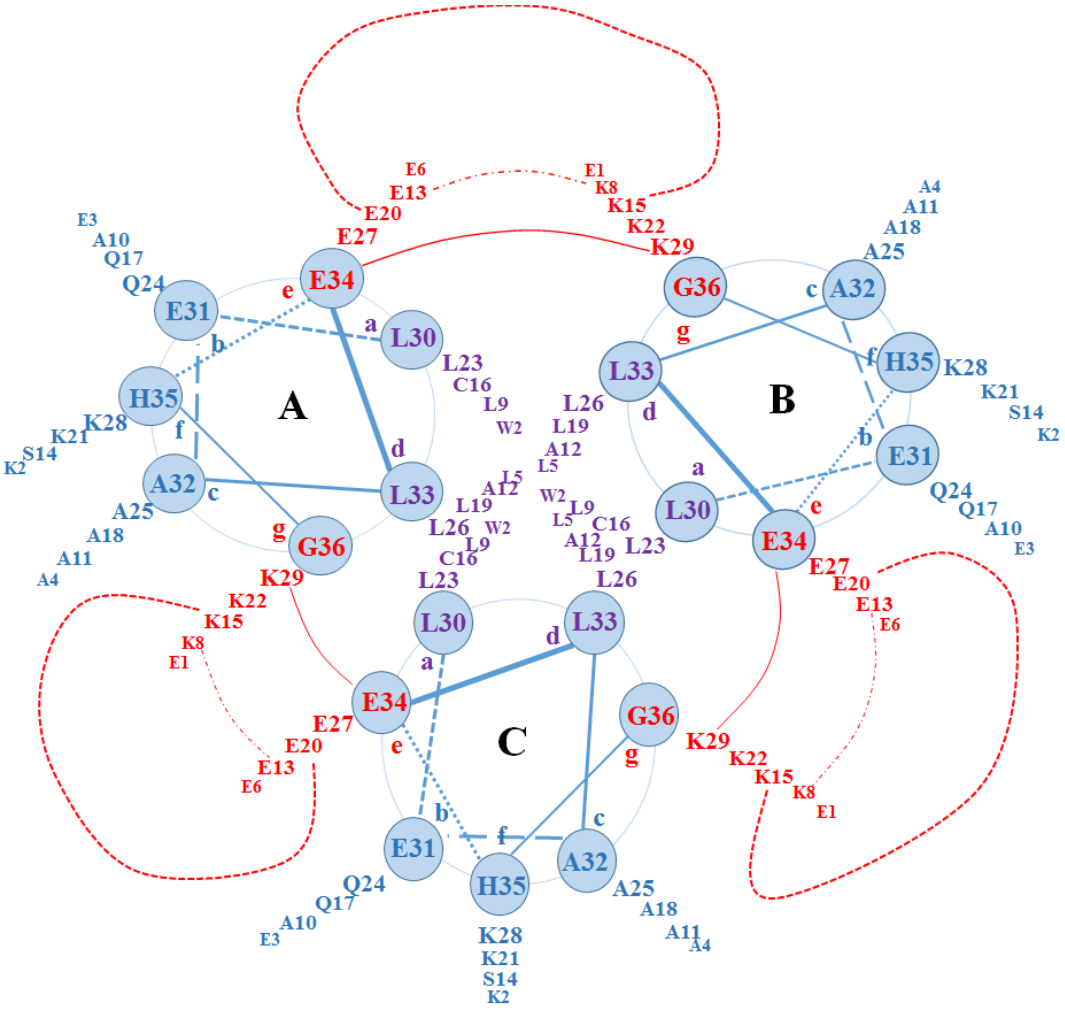

Figure A-4. Helical wheel diagram of Hg(II)(GRAND-CSL12AL16C)$_3^-$. Red lines between different residues from helices A, B and C represent interhelical electrostatic interactions; red dash lines (interactions between K15 and E20), red broken lines (interactions between K8 and E13) and solid lines (interactions between K29 and E34). Residues at *e* and *g* positions are labeled in red, *a* and *d* in purple and *b*,*f* and *g* in blue.

Table A-4: Non-covalent interactions observed in Hg(II)(**GRAND-CS**L12AL16C)$_3^-$

Molecule 1	**Molecule 2**
Interhelical salt bridge interactions	
15LysB(N_z)	20GluA($O\varepsilon_1$)
15LysC(N_z)	20GluB($O\varepsilon_1$)
15LysA(N_z)	20GluC($O\varepsilon_1$)
29LysB(N_z)	34GluA($O\varepsilon1$)
29LysC(N_z)	34GluB($O\varepsilon_1$)
29LysA(N_z)	34GluC($O\varepsilon_1$)
8LysA(N_z)	13GluB($O\varepsilon_1$)
8LysB(N_z)	13GluC($O\varepsilon_1$)
8LysC(N_z)	13GluA($O\varepsilon_1$)
Intrahelical salt bridge interactions	
2TrpA($N\varepsilon_1$)	6GluA($O\varepsilon_1$,$O\varepsilon_2$)
2TrpB($N\varepsilon_1$)	6GluB($O\varepsilon_1$,$O\varepsilon_2$)
2TrpC($N\varepsilon_1$)	6GluC($O\varepsilon_1$,$O\varepsilon_2$)
Other interactions	
14SerA($O\gamma$)	amide backbone of 10AlaA
14SerB($O\gamma$)	amide backbone of 10AlaB
14SerC($O\gamma$)	amide backbone of 10AlaC
22LysA(Nz)	carbonyl backbone of 18AlaC
22LysA(Nz)	carbonyl backbone of 18AlaC
22LysA(Nz)	carbonyl backbone of 18AlaC

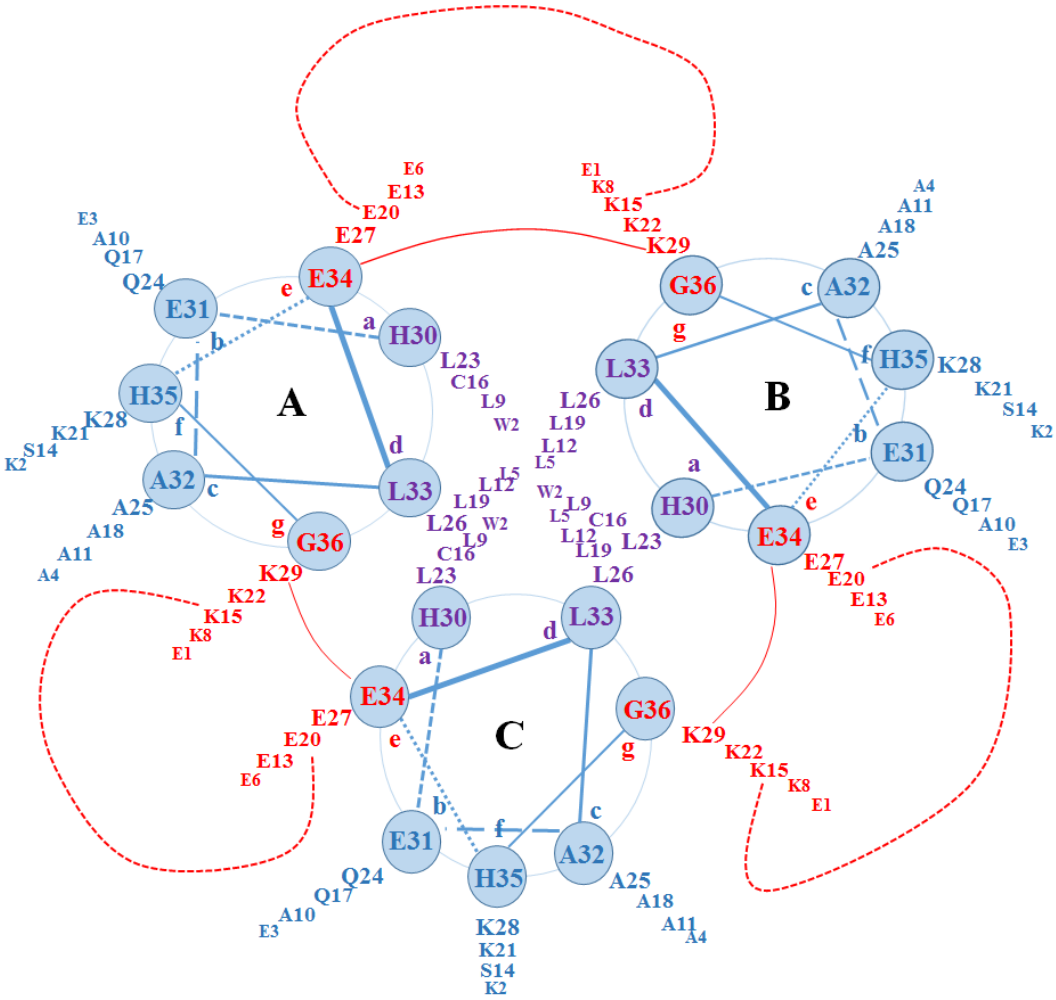

Figure A-5. Helical wheel diagram of Pb(II)$_S$Zn(II)$_N$(GRAND-CSL16CL30H)$_3^+$. Red lines between different residues from helices A, B and C represent interhelical electrostatic interactions; red dash lines (interactions between K15 and E20) and solid lines (interactions between K29 and E34). Residues at *e* and *g* positions are labeled in red, *a* and *d* in purple and *b*,*f* and *g* in blue.

Table A-5: Non-covalent interactions observed in $Pb(II)_S Zn(II)_N$(**GRAND-CS**L16CL30H)$_3^+$

Molecule 1	**Molecule 2**
Interhelical salt bridge interactions	
15LysB(N_z)	20GluA($O\varepsilon_1$)
15LysC(N_z)	20GluB($O\varepsilon_1$)
15LysA(N_z)	20GluC($O\varepsilon_1$)
29LysB(N_z)	34GluA($O\varepsilon1$,$O\varepsilon_2$)
29LysC(N_z)	34GluB($O\varepsilon_1$,$O\varepsilon_2$)
29LysA(N_z)	34GluC($O\varepsilon_1$,$O\varepsilon_2$)
Intrahelical salt bridge interactions	
2TrpA($N\varepsilon_1$)	1GluA($O\varepsilon_1$)
2TrpB($N\varepsilon_1$)	1GluB($O\varepsilon_1$)
2TrpC($N\varepsilon_1$)	1GluC($O\varepsilon_1$)
1GluA($O\varepsilon_1$)	amide backbone of 4Ala
1GluB($O\varepsilon_1$)	amide backbone of 4Ala
1GluC($O\varepsilon_1$)	amide backbone of 4Ala
1GluA($O\varepsilon_1$,$O\varepsilon_2$)	amide backbone of 3Glu
1GluB($O\varepsilon_1$,$O\varepsilon_2$)	amide backbone of 3Glu
1GluC($O\varepsilon_1$,$O\varepsilon_2$)	amide backbone of 3Glu

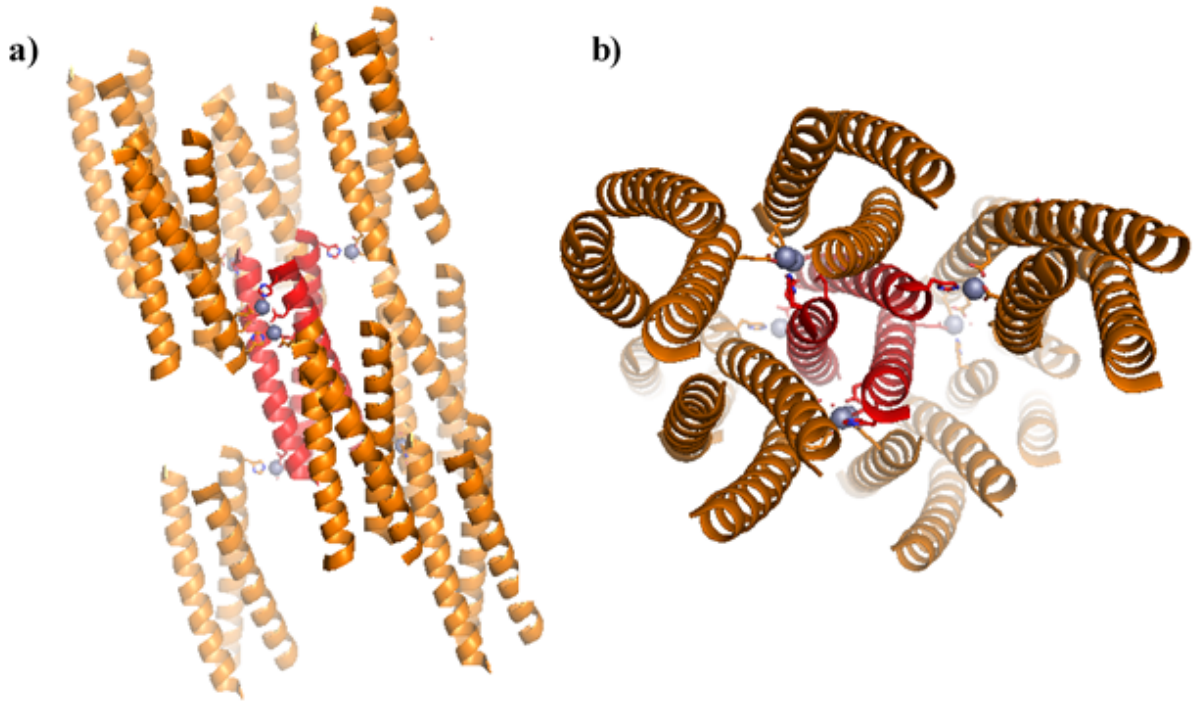

Figure A-6. PyMOL representation of the peptide packing at the crystal packing interfaces mediated by Zn(II) binding sites observed in the apo-$(CSL16C)_3$ peptide. Shown is a) Side view of the packing around the central coiled coil (red) with seven Zn(II) sites to hold eight other neighboring helices and b) Bottom-up view of the packing.

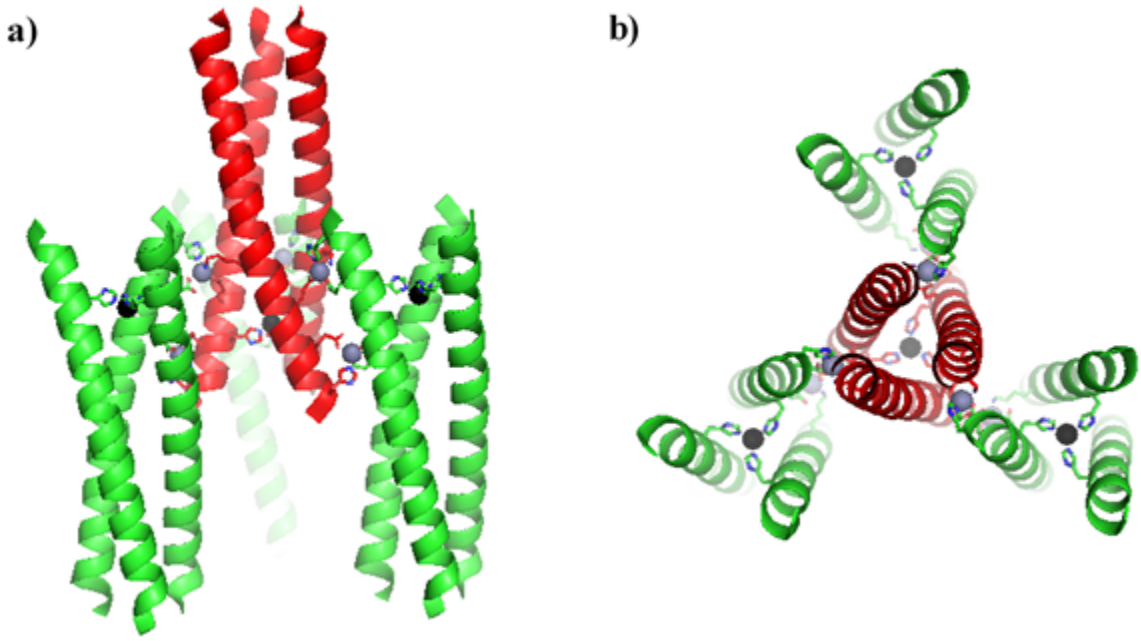

Figure A-7. PyMOL representation of the Zn(II)–mediated packing sites that are located along the packing interfaces linking trimeric coiled coils of Hg(II)$_S$Zn(II)$_N$(GRAND-CSL16CL30H)$_3^+$ together (same evidence also observed in Pb(II)$_S$Zn(II)$_N$(GRAND-CSL16CL30H)$_3^+$). Shown is a) Side view of the packing of a central coiled coil (red) with the six Zn(II) ions that are coordinated by side chains with neighboring helices (green) and b) Top down view of the packing. Zn(II) ions of the internal Zn(II)$(Cys)_3(H_2O)^-$ sites at the thirtieth position are labeled in black. External Zn(II) ions are grey. In both panels, only four symmetry related helices are included and the internal Hg(II)S_3^- at the sixteenth position are omitted for clarity.

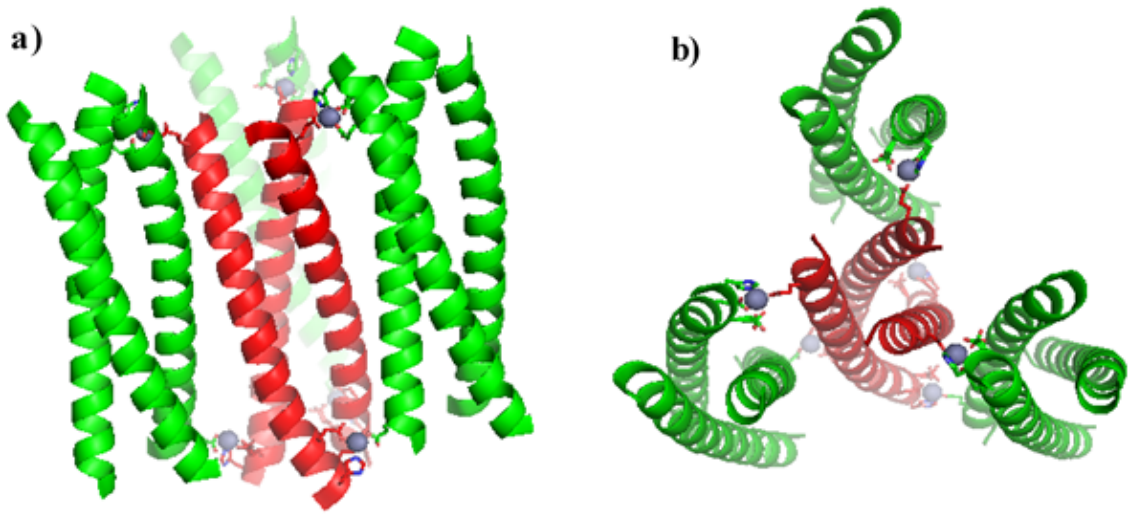

Figure A-8. PyMOL representation of the Zn(II)–mediated packing sites that are located along the packing interfaces linking trimeric coiled coils of Zn(II)(GRAND-CSL12AL16C)$_3^-$ together. Shown is a) Side view of the packing of a central coiled coil (red) with the six Zn(II) ions that are coordinated by side chains with neighboring helices (green) and b) Top down view of the packing. In both panels, the internal Zn(II)(Cys)$_3$(H$_2$O)$^-$ sites at the sixteenth position are omitted and only four symmetry related helices are included for clarity.

B. Discussion of the interactions observed at the lattice packing interfaces of the CoilSer and GRAND-CoilSer peptides

Unfortunately, the **TRI** peptide family has not formed high quality crystals suitable for x-ray diffraction studies. Therefore, **CoilSer** (a related 3SCC designed by DeGrado and coworkers) has been exploited to perform crystallization. CoilSer contains 29 amino acids formed with four heptad repeats. When mutated to include a cysteine residue, it has been shown to bind metals in an analogous manner to the **TRI** peptides. Non-polar leucine residues are placed in the *a* and *d* positions which influence the hydrophobic aggregation at the core of the coiled coil in **CoilSer**; however, the unique components that make it suitable for crystallization are modifications in the *b* and *f* positions. Importantly in **TRI**, only lysine and glutamate residues are used at the *b* and *f* positions, respectively; whereas **CoilSer** is modified to 3Glu, 10Ala, 17Gln and 24Glu in the *b* position, and to 7Glu, 14Ser, 21Lys and 28His in the *f* position. The 28His, in particular, is the highlighted residue that serves as a coordinating ligand to form external tetrahedral Zn(II) binding sites at the crystal packing interfaces as demonstrated in **Figure A-6**. These Zn(II) sites are usually bound with 28His and glutamate residues from the adjacent symmetry related molecules or sometimes with water, allowing for peptide packing in a three dimensional lattice form. The Cys substitution in **CoilSer** variants appear to crystalize into parallel three-stranded coiled coil structures.[1–4] Furthermore, in order to crystallize some peptide designs that contain several mutation along the sequence, an extra heptad of $L_aQ_bA_cL_dE_eK_fK_g$ is added in between the third and fourth heptads of **CoilSer** resulting in the longer sequence called **GRAND-CoilSer (GRAND-CS)**. As predicted, this longer peptide had significantly greater stability.

Crystallographically confirmed, all of the **GRAND-CoilSer** variants self-assemble into parallel triple-stranded α-helical coiled coils, with an average length of 53.86 Å and diameter of 3.46 Å. (The diameter of each layer is determined from an innercircle radius within an equatorial triangle in which the edge has a distance equal to C_α-C_α separation of residues in that particular layer. The average of the diameters is calculated by taking the diameters from *a* through *g* positions in each heptad into account.)The three helices consist of ten helical turns. However, the trimeric form of the shorter apo-(**CS**L16C)$_3$, containing only eight helical turns is only 43.14 Å in length with an average diameter of 3.38 Å. The features of this shorter construct correspond to the previously published crystal structures of **CoilSer** derivatives; apo-(**CS**L9C)$_3$, As(III)(**CS**L9C)$_3$, apo-(**CS**L16Pen)$_3$ and apo-(**CS**L16$_D$Pen)$_3$ [1–3,5]. The main chain dihedral angles, ψ and φ, for all of

the non-glycine residues of the **GRAND-CoilSer** variants and the apo-(**CS**L16C)$_3$ structure fall in the preferred Ramanchandran regions ranging from -50 to 50 and -50 to -120, respectively.

Several types of forces are found to stabilize the coiled coil constructs. The most important one being the hydrophobic stabilization energy provides the main driving forces for the coiled coil formation through Van Der Waal interactions between leucine layers at the core center. The hydrophobic collapse of the longer **GRAND-CoilSer** 3SCC constructs comes from ten hydrophobic leucine layers that are occupied alternatively at *a* and *d* positions along the sequence, while eight layers of leucine residues are observed in apo-(**CS**L16C)$_3$. Moreover, these coiled coil constructs are also stabilized by both intra- and interhelical salt bridge interactions between charged residues at the accessible solvent regions. Regarding the length difference between the **GRAND-CoilSer** versus **CoilSer**, the structures could reveal some variations of these interactions along the sequences. The shorter helices of apo-(**CS**L16C)$_3$ are overlaid onto the longer helices of the metallated Hg(II)$_S$Zn(II)$_N$(**GRAND-CS**L16CL30H)$_3^+$ in **Figure A-9** (because these two structures will be first used to understand Hg-binding in *Section I* in chapter 2). Both structures are folded in a parallel three-stranded coiled coil scaffold with the bound Hg(II) not affecting the secondary structure. The α-helical backbones of the two structures do not perfectly align with each other, which is probably because the ends of the coiled coils of both structures are fraying in different ways. In the apo-protein, the diameters of the first two amino acid layers (1Glu and 2Trp) are longer than in the Hg(II)$_S$Zn(II)$_N$(**GRAND-CS**L16CL30H)$_3^+$ (1Glu: 3.99 vs 2.91 Å and 2Trp: 2.72 vs 2.56Å for apo- vs metallated-structures, respectively) indicating that the N-termini of the apo-(**CS**L16C)$_3$ structure are slightly more frayed compared to Hg(II)$_S$Zn(II)$_N$(**GRAND-CS**L16CL30H)$_3^+$. However, the average diameters for the rest of the heptads in apo-(**CS**L16C)$_3$ are comparable to Hg(II)$_S$Zn(II)$_N$(**GRAND-CS**L16CL30H)$_3^+$ (second heptad: 3.26 vs 3.31 Å, third heptad: 3.24 vs 3.26 Å and fourth heptad: 3.33 vs 3.37 Å for apo- vs metallated-structures, respectively). When considered the average diameter of the last heptad of the longer helices (fifth heptad), it appears to be 4.50 Å. This significant increase in length of the coiled coil diameter compared to the first four repetitions in the sequence strongly indicates that the C-terminus region of Hg(II)$_S$Zn(II)$_N$(**GRAND-CS**L16CL30H)$_3^+$ is significantly frayed, whereas the C-termini of apo-(**CS**L16C)$_3$ structure are better folded based upon the average diameter of the last heptad (3.33 Å), which is still comparable in diameter to the well-packed region of both the longer and shorter scaffolds.

I hypothesize that the greatly frayed C-terminal end observed in $Hg(II)_SZn(II)_N$(**GRAND-CS**L16CL30H)$_3^+$ is due to the perturbation of the packing in the helix due to the Leu to His substitution at the thirtieth position (fifth heptad). This site was originally engineered for catalytic purposes that required three histidines to bind Zn(II) as a carbonic anhydrase model. Sterically, the imidazole ring of histidine is more demanding than the leucine side chain. The substitution occurs at an *a* position, so the His side chains are expected to orient toward the core of the structure. Thus, the pocket size has to be sufficiently large in order to accommodate three imidazole rings internally into the plane. The $C\alpha$-$C\alpha$ distance of this 30His layer is 9.93 Å (diameter = 2.87 Å), a somewhat shorter separation than seen in the preceding *a* layers. Undoubtedly the region close to the C-termini is affected once this buried site is perturbed by such a bulky residue, Apparently, this part of the 3SCC must expand to a subsequently longer average diameter at the fifth heptad. The $C\alpha$-$C\alpha$ separation of 26Leu is only 8.12 Å (diameter ≅ 2.34 Å); however, the $C\alpha$-$C\alpha$ of 33Leu layer that is placed at one hydrophobic layer below the 30His shows the longest $C\alpha$-$C\alpha$ separation among the hydrophobic Leu layers with 11.62 Å (diameter = 3.35 Å). Moreover, the 35His layer is drastically perturbed. The $C\alpha$-$C\alpha$ separation in this particular plane appears to be 20.54 Å corresponding to a 5.92 Å diameter. These numbers are the longest $C\alpha$-$C\alpha$ separation and longest diameter in the structure.

The effect of the internal 30His site on the folding of the fifth heptad is more pronounced when comparing the $Hg(II)_SZn(II)_N$(**GRAND-CS**L16CL30H)$_3^+$ structure with other **GRAND-CoilSer** structures that contain the less sterically demanding Leu residues at both the thirtieth and thirty-third positions. Two candidates are Zn(II)(**GRAND-CS**L12AL16C)$_3^-$ and Hg(II)(**GRAND-CS**L12AL16C)$_3^-$ structures. As predicted, the diameters of the two Leu layers in these **GRAND-CS**L12AL16C scaffolds are much less than observed in $Hg(II)_SZn(II)_N$(**GRAND-CS**L16CL30H)$_3^+$. They are found to be only 2.01(30Leu), 2.30(33Leu) Å for Zn(II)(**GRAND-CS**L12AL16C)$_3^-$, and 2.03(30Leu), 2.29(33Leu) Å for Hg(II)(**GRAND-CS**L12AL16C)$_3^-$. In addition to the diameters of these core layers being affected, the overall packing around the C-terminal region of these two structures are also purturbed. The average diameters of the fifth heptad in Zn(II)(**GRAND-CS**L12AL16C)$_3^-$ and Hg(II) (**GRAND-CS**L12AL16C)$_3^-$ diminish to 3.37 and 3.45 Å, respectively, while it is 4.50 Å in 30His-containing structure. These observations suggest

that in the absence of 30His layer, the last heptad of the **GRAND-CoilSer** becomes well-packed with tighter hydrophobic interactions by Leu residues (**Figure A-10**).

The similar effect of 30His toward the end of the **GRAND-CoilSer** structure is also observed in the $Pb(II)_SZn(II)_N$(**GRAND-CS**L16CL30H)$_3^+$. Similarly, the average diameter of last heptad is also about 4.52 Å, which is longer than the rest of the heptads (~3.35 Å) indicating that the C-termini of the helices are also frayed out. Each heptad of the Pb(II)-binding structure is comparable in size to the Hg(II)-binding structure. This evidence clarifies that upon binding to these different heavy metals into the 16Cys layer, the inner packing of the three stranded (**GRAND-CS**L16CL30H)$_3$ scaffolds remain the same, which clearly supports that the bound metals do not perturb the secondary structure of the coiled coils.

Moreover, the frayed end of the $Hg(II)_SZn(II)_N$(**GRAND-CS**L16CL30H)$_3^+$ and $Pb(II)_SZn(II)_N$(**GRAND-CS**L16CL30H)$_3^+$ helices is also found to affect the 3D crystal packing at the helical interfaces of the lattice form. The fact that the replacement of His in lieu of Leu residues causes the average diameter of this layer to lengthen by 0.5-0.8 Å, therefore, in order to prevent the end of the helices from fraying this much to accommodate the imidazole rings and still retain the native fold of 3SCC packing, the 30His-containing **GRAND-CoilSer** peptides are also found to be stabilized through external Zn(II) coordination and interhelical salt bridge interactions between charged residues at the helical interface in a different manner from the **GRAND-CS**L12AL16C structures.

The discussion of this part will categorize the **GRAND-CoilSer** peptides reported in chapter 2 into two groups. The first group is $Hg(II)_SZn(II)_N$(**GRAND-CS**L16CL30H)$_3^+$ and $Pb(II)_SZn(II)_N$(**GRAND-CS**L16CL30H)$_3^+$ that contain His residue at the thirtieth position. The second group is Zn(II)(**GRAND-CS**L12AL16C)$_3^-$ and Hg(II)(**GRAND-CS**L12AL16C)$_3^-$ that have normal Leu residue at the thirtieth position. Similarly, both groups of the peptides require external Zn(II) binding sites to link the trimeric coiled coil together. When considering only one ASU (one strand occupied), it is shown that the Zn(II) ion is observed far to the end of the helix. As a consequence, a trimer is an inclusion of three ASUs that are threefold symmetry related. In the 30His-structures, Zn(II) sites display a pseudotetrahedral geometry with four ligands solely from the charged residues on the exterior. Each Zn(II) is bound to 33His and 31Glu (that come from the same helix in an ASU of the R32 space group), 22Lys and 27Glu from two adjacent helices of an adjacent trimer that is symmetry related to the first trimer with a rotoinversion right-

handed threefold screw axis ($\bar{3}_2$). As a consequence, one can realize that each exterior Zn(II) site requires 3 ASUs from two neighboring trimers to form at the three-fold related crystal packing interfaces. The external Zn(II) coordination, thus, mediates the packing of the coiled coils in 3D layers which strongly facilitates the crystallization. Shown in **Figure A-7**, the overall packing of both $Hg(II)_S Zn(II)_N$(**GRAND-CS**L16CL30H)$_3^+$ and Pb(II)(**GRAND-CS**L16CL30H)$_3^-$, respectively is achieved when each helical strand in an ASU contributes four amino acid ligands to bind three different Zn(II) ions (two of them are on the same interhelical interface and the other is on the opposite face) in order to hold three different trimers together. The first Zn(II) is far to the C-terminus bound to 33His and 31Glu residues. The second Zn(II), which is located close to the middle of the sequence, uses 27Glu. These residues 27Glu, 31Glus and 33His are relatively to one side of the strand while 22Lys is on the other side coordinating to the third Zn(II). Looking from this particular perspective, each strand of the trimer is bound with two Zn(II) ions (a total of six Zn(II) binding sites per trimer); one is far below to the C-terminal end at the fifth heptad and the other is located in between the third and fourth heptads. This latter type of Zn(II) site, near the middle of the sequence, is thought to help maintain the packing of three helices from fraying apart when the internal Zn(II)$(His)_3(H_2O)$ site at the thirtieth position is present. This assumption is supported from the evidence of different locations of the exterior Zn(II) ions that are found in the crystal packing interfaces of the **GRAND-CS**L12AL16C peptides where there is no 30His. Though these two groups of peptides crystallized in the same space group (R32), the different amino acid substitutions in this particular position affects the Zn(II) binding on the boundaries between ASUs. **Figure A-8** shows the 3D packing of Zn(II)(**GRAND-CS**L12AL16C)$_3^-$ and Hg(II)(**GRAND-CS**L12AL16C)$_3^-$. Again, all outer Zn(II) are 4-coordinate using four amino acid ligands and are located at the terminal ends of the helices. Each Zn(II) is bound to three ligands of the last heptad [31Glu ($O\varepsilon_1$), 34Glu ($O\varepsilon_2$) and 35His ($N\varepsilon_2$)] from one single helix in an ASU of a trimer. The fourth ligand is 3Glu ($O\varepsilon_1$) from one of the helices of an adjacent trimer that is associated with the first trimer through ($\bar{3}_2$) symmetry operation. In this type of lattice packing, an external Zn(II) ion requires interface residues from 2ASUs of two symmetry related trimers to assess the binding. When considering a single strand in an ASU, it is found that it utilizes those respective four ligands to bind to two Zn(II) ions. The first one at the C-terminus lying on one face, linking with a helix of a neighboring trimer. The second is located at the other tail and faces oppositely, linking to another trimer. With this arrangement, when taking three helices into

account, a trimer actually interacts to six external Zn(II) sites in order to achieve the packing with three symmetry related trimers nearby. Based on the non-requirement of 22Lys and 27Glu residues to achieve a Zn(II) binding at the packing interfaces, the unique packing observations strongly emphasize that the **GRAND-CS**L12AL16C derivatives do not require any Zn(II) to bind in the middle of the sequence like in the 30His-containg peptides. This is potentially due to the greater efficiency of the internal hydrophobic folding around the C-terminal region of the **GRAND-CS**L12AL16C peptides. (compact size with overall shortened diameter). A rational reason to support this idea comes from the fact that the two core layers (30His and 33Leu) of the last heptad in Zn(II)(**GRAND-CS**L12AL16C)$_3^-$ and Hg(II)(**GRAND-CS**L12AL16C)$_3^-$ have the diameters significantly shorter than in Hg(II)$_S$Zn(II)$_N$(**GRAND-CS**L16CL30H)$_3^+$ and Pb(II)(**GRAND-CS**L16CL30H)$_3^-$. This implies that apart from the terminal Zn(II) sites observed at the accessible surface areas, the buried hydrophobic aggregation of the 31Leu and 33Leu layers of **GRAND-CS**L12AL16C variants provides some extent of the hydrophobic driving force that is strong enough to hold the helices together without any requirement of additional external Zn(II) site situated between the heptads in the middle of the structure to help stabilize the scaffold. However, this sort of requirement is needed for the 30His-containing constructs where a drastic frayed end is observed. To efficiently retain the three stranded packing, the energy penalty from placing the interior His residues can be compensated by constraining some charged interface residues close to the thirtieth position to interact with Zn(II). In these cases, 22Lys and 27Glu of each strand are selected to achieve the task. This specific location of the external binding site is located above the internal 30His layer with respect to the N-termini, while the other site at the fifth heptad is down below. The close-up view of both internal and external Zn(II) binding sites is shown in **Figure A-7**, **a**.

Apart from the distinct lattice packing behavior, the two groups of **GRAND-CoilSer** peptides also show different amounts of salt bridge interactions between interhelical strands within a trimer. Both of the 30His-containing constructs, regardless of which heavy metal is bound into the 16Cys layer, have six interhelical electrostatic contacts between *e* and *g* positions required to help stabilize the orientation of the 3SCC scaffold. Three pairs take place quite close to the N-termini between the second heptad [15Lys (N_z), *g* position] of one strand and the third heptad [20Glu ($O_{\varepsilon 1}$), *e* position] of an adjacent monomer. The other three are found almost to the other end of the structure close to the C-termini from the interaction between 29Lys (N_z, *g* position,

fourth heptad) and 34Glu ($O_{\varepsilon 1}$ and $O_{\varepsilon 2}$, *e* position, fifth heptad) of two adjacent strands, respectively. Apart from the main driving force of the hydrophobic collapse to generate the coiled coil formation following "a knob into a hole" theory[6] these salt bridge interactions are shown to provide an additional stabilization in order to help orient the three strands as parallel 3SCCs. As shown in **Figure A-11(a)**, these interactions occur only from the middle to bottom part of the 3SCC structure. When taking these types of interactions into consideration with the external Zn(II)-mediating packing sites along the ASU interfaces, it is obvious that one trimer arranging from N → C termini requires the diagonal interactions between 15Lys and 20Glu to take place above the Zn(II) sites that are coordinated to 22Lys and 27Glu from two neighboring strands of that trimer. Far below exists the interactions between the 29Lys and 34Glu. Lastly to this end, another type of Zn(II) binding sites that uses the 31Glu and 35His as coordinating ligands are situated at the lowest position. From these crystallographic observations, it is obvious that in order to achieve the three stranded coiled coil stabilization, each heptad of the nearby helices have to link with each other either through salt bridge interactions and Zn(II) coordination. Firstly, the second and the third heptads of a trimer are diagonally linked with electrostatic salt bridges. The third and the fourth repetitions are holding through a Zn(II)-binding site. Next, another electrostatic interaction occurs between the fourth and fifth repetitions and finally the last heptad(fifth) uses two of its residues to bind another Zn(II). These two types of interactions happening alternatively between the heptads from the bottom half of the structure strongly emphasize that the frayed end of the 30His-containing constructs also needs additional forces apart from the electrostatic interactions between the depronated Glu (*e* position) and Lys (*g* position) to retain the folding of tertiary structure of each individual 3SCC. The top part of the structures are stabilized through H-bonding interactions between charged side chains and the amide backbone of a closeby amino acid backbone in their respective chain. For examples, 1Glu ($O_{\varepsilon 1}$, $O_{\varepsilon 2}$) with the main chain of 3Glu and 14Ser (O_{γ}) with the main chain of 10Ala (found in both structures). In $Pb(II)_S Zn(II)_N$(**GRAND-CS**L16CL30H)$_3^+$, 1Glu also interacts with the main chain of 4Ala, while in $Hg(II)_S Zn(II)_N$(**GRAND-CS**L16CL30H)$_3^+$ the observations were found between 24Gln (N_{ε}) with the main chain of 20Glu. In the lattice packing of trimers, the high symmetry of R32 with 18 symmetry operators, results in a closed-packing between helices in the unit cell. This causes a trimer to have greater amount of intermolecular contacts between its charged residues with other symmetry related trimers which are found mostly at the first two heptads. These interactions are

reasoned to facilitate the 3SCC orientations at the top part of the structure. Moreover, several waters are also found to mediate H-bonding interactions with the polar side chains from the last two heptads. The resulting H-bonding network of this first shell solvent water is also thought to facilitate the packing between trimers.

Unlike the first group of the peptides, Zn(II)(**GRAND-CS**L12AL16C)$_3^-$ and Hg(II)(**GRAND-CS**L12AL16C)$_3^-$ are 3SCC-oriented with nine salt bridge stabilization. In Zn(II)(**GRAND-CS**L12AL16C)$_3^-$, six interactions(3 pairs of 15Lys and 20Glu, 3 pairs of 29Lys and 34Glu) are similar to what was observed in those 30-His containing constructs. These confirm that the second and third heptads of two adjacent strands in this structure are linked with an electrostatic interaction and so is the connection between the fourth and fifth heptads. The other three interactions are observed in between 22Lys (N_z) and 27Glu ($O_{\varepsilon 1}$, $O_{\varepsilon 2}$) stabilizing the third and fourth heptads together. These particular electrostatic pairs become interesting when one realizes that Zn(II)(**GRAND-CS**L12AL16C)$_3^-$ exploit the charged difference of these two side chains through non-covalent interaction; however, in those 30His-constructing structures the electron pair of N_z (22Lys) and $O_{\varepsilon 1}$ (27Glu) atoms are utilized as ligands to a Zn(II) binding site via coordinative interaction at the crystal packing interface. Referred to the different external Zn(II) locations between these two types of structures because of the drastic frayed end observed in the 30His-constructs, these observations suggest that when Zn(II) is not required to bind in the middle of the sequence to stabilize the high level of fraying caused by the internal 30His site, both 22Lys and 27Glu residues, in turn, interact with each other to help maintain the 3SCC scaffold. As the electrostatic interaction is quite weaker compared to metal coordination, this evidence additionally emphasizes that the combination of these charged pairs and the internal hydrophobic aggregation around that region is efficient enough to hold the three helices of Zn(II)(**GRAND-CS**L12AL16C)$_3^-$ together. Moreover, there are also some unusual interhelical electrostatic interactions between *b* and *g* positions of two neighboring chains [31Glu ($O_{\varepsilon 2}$) and 29Lys (N_z)]. Apparently from a viewpoint of a standalone trimer, all of these electrostatic interactions that influences the three strand packing (**Figure A-11, b**) are found only from the bottom half of the structure resemble to what was observed in the 30His-constructs. The first heptad is stabilized through intrahelical interactions between 2Trp ($N_{\varepsilon 1}$) and 6Glu ($O_{\varepsilon 2}$). Some side chains interact with an amide backbone of an amino acid within its respective chain. For examples, 14Ser (O_γ) with the main chain of

10Ala and 35His ($N_{\delta 1}$) with 34Glu. Interestingly, in this Zn(II)(**GRAND-CS**L12AL16C)$_3^-$ structure the intermolecular charged-charged interactions between symmetry related trimers are in greater amount from N→ C termini (even more than the 30His-constructs) and also hundreds of water molecules form the first solvent shell with charged residues at the crystal packing interfaces. The observations declare when the external Zn(II) sites are located at both end termini with a Zn(II)-Zn(II) separation of 44.3 Å, an appropriate amount of intermolecular contacts are required to help facilitate the 3D packing. Conversely, in the 30His-constructs where Zn(II) ions at the crystal packing interfaces are close to each other with only 11.5 Å in separation, there are not many intermolecular contacts observed along the interfaces. Some are found at the top part of the structure and barely is observed at the bottom half. This evidence suggests that when Zn(II) sites are located in a close distance, the metal coordination is powerful and efficiently able to hold adjacent trimers together. However, once such sites are much longer separated in distance as observed in the Zn(II)(**GRAND-CS**L12AL16C)$_3^-$ structure other charged interactions in the solvent face are required to facilitate the 3D packing.

Hg(II)(**GRAND-CS**L12AL16C)$_3^-$ also declares nine interhelical salt bridges within the 3SCC scaffold. The first six pairs are similar to those observed in the previous three structures (15Lys and 20Glu, 29Lys and 34Glu). Unlike the Zn(II)(**GRAND-CS**L12AL16C)$_3^-$, the other three pairs are found around the top part of the structure diagonally linking the first (8Lys, N_z) and second (13Glu, $O_{\varepsilon 1}$) heptads together instead of the interactions between 22Lys and 27Glu residues. It seems that each heptad is diagonally linked with the next heptad down below from the neighboring chain through salt bridge connections except between the third (22Lys) and fourth (27Glu) heptads (**Figure A-11, c**). Instead, both 22Lys and 27Glu residues are H-bonded with waters. It is interesting that when salt bridges are spreading from top to bottom of the 3SCC scaffold, the amount of intermolecular interactions directly from side chain to side chain between two adjacent trimers is diminished. The packing of trimeric neighbors in Hg(II)(**GRAND-CS**L12AL16C)$_3^-$ are greatly mediated by the interactions between the charged side chains and the first shell water molecules that form the H-bonding networks along the outer interfaces of neighboring trimers. Likewise, these observations correspond to the previous assumption that such interactions happening along the interhelical faces are thought to help the external Zn(II) binding sites to stabilize the 3D packing especially when Zn(II) ions are greater apart, 44.2 Å. Moreover, three pairs of intrahelical contacts are found in the first heptad [2Trp ($N_{\varepsilon 1}$) and 6Glu ($O_{\varepsilon 2}$)] and

again some residues use their charged side chains to interact with the peptide backbone of an adjacent amino acid in its respective chain [14Ser (O_γ) with the main chain of 10Ala and 22Lys (N_z) with 18Ala to help retain the secondary structure.

Though crystallized in a different space group from the longer **GRAND-CoilSer** peptides (R32), the crystal packing interfaces of the apo-(**CS**L16C)$_3$ (C2) also require external Zn(II) binding sites to link the coiled coil together. All three Zn(II) ions are observed per asymmetric unit and display a tetrahedral geometry exploiting helical interface His and Glu residues from joint asymmetric units of neighboring trimers. The first Zn(II) is bound to 24GluA from its respective ASU, 28HisB and 24GluB($O_{\varepsilon1}$) from an adjacent trimer in another ASU (2_1 symmetry related) and the last ligand is an exogenous water. The second Zn(II) is located at a distance of 4.96 Å close to the first site because 24GluB ($O_{\varepsilon2}$) is used as a bridging ligand between the two sites. The other three ligands are 28HisA in its ASU, 20GluB from the same trimer of 24GluB (that is related to the first trimer with 2_1 symmetry operation) and 3GluB of another trimer (which is related by the twofold axis with the first trimer). Apparently, these external Zn(II) sites hold three adjacent trimers together. The third Zn(II) site utilizes 28HisC($N_{\varepsilon2}$) in its ASU, 6GluA($O_{\varepsilon1}$) and 1GluC($O_{\varepsilon2}$) from another 2_1-symmetry related to the first trimer(different from the ones linked by the previous Zn(II) sites) and the fourth ligand is water. This particular site holds two trimers together. Thus, from a perspective of a trimer, the three helices use their charged ligands to bind to seven Zn(II)ions holding seven neighboring trimers altogether in order to achieved the packing in 3D. The overall crystal packing of apo-(**CS**L16C)$_3$ is shown in **Figure A-6**.

Seven interhelical electrostatic interactions between *e* and *g* positions are observed along the helical interfaces of apo-(**CS**L16C)$_3$ structure. Between chain A and C exists two interactions. The first pair is found almost on top of the structure between 1GluA ($O_{\varepsilon2}$) and 8Lys (N_z) stabilizing the first heptad of those corresponding two chains. The second stabilization is in the middle of the structure taking place between the second heptad of chain C [15Lys (N_z)] and the third heptad of chain A [20GluA ($O_{\varepsilon1}$, $O_{\varepsilon2}$)]. More two salt bridges are observed between chain A and B [8LysA (N_z) and 13GluB ($O_{\varepsilon1}$), 20GluB ($O_{\varepsilon1}$) and 22LysA (N_z)]. Lastly, 15LysB (N_z) interacts with 20GluC ($O_{\varepsilon1}$, $O_{\varepsilon2}$) and 22LysB (N_z) interacts with 20GluC ($O_{\varepsilon2}$) linking chain B and C. It is found that not only the electrostatic interactions occur between normal *e* and *g* positions, there are also unusual interhelical pairs happening between *b* and *g* residues. One interaction is observed further down to the C-termini linking the fourth heptad, 24GluA ($O_{\varepsilon1}$) (where $O_{\varepsilon2}$ is used as a Zn(II)-

binding ligand) and the third heptad, 22LysC (N_z) together. Similar to the longer structures, 14Ser (O_γ) residues are found to interact with the amide backbone of 10Ala of its respective chain. Moreover, there are three possible intrahelical interactions [2TrpB and 6GluB; 3GluB and 7LysB; 2TrpB and 6GluB] stabilizing the top part of the structure. The packing of three helices itself are also greatly influenced by H-bonding interactions between the interface charged residues and water molecules or ethylene glycols (crystal precipitation reagent). Different from the **GRAND-CoilSer** packing, the lower symmetry of C2 space group seems to affect the salt bridge interactions between interhelical chains of symmetry related trimers as only three pairs are observed. This strongly suggests that when the shorter helices is packed in monoclinic cell with 4 symmetry operations (The threefold symmetry of the helices in a trimer is not allowed.), the intermolecular connections between neighboring trimers become less. Subsequently the trimers in apo-(**CS**L16C)$_3$ is less-packed compared to the longer helices that each helix is constrained by the higher rhombohedral R32 symmetry with 18 operations. Such constraint causes high exposure of charged residues along the accessible solvent surface areas between ASUs which encourages much greater contacts of polar interactions between residues that eventually influences the packing of the **GRAND-CoilSer** peptides. This rare observation of salt bridge contacts between trimers also implies that the external Zn(II) sites provide strong stabilization that may be sufficient enough to hold the 29-amino acid 3SCC together compared to the 36-residue in length of the **GRAND-CoilSer** peptides that needs high amount of other forces. In summary, the **GRAND-CoilSer** and **CoilSer** structures are different in amino acid length and apparently stabilized through those respective forces in different manner; however, they all perfectly show that they are able to fold into a well-defined parallel three-stranded coiled coil. The α-helical alignment of structures declares that the overall scaffolds of the designed peptides looks reasonable to provide insight of structural details that are useful to learn the metal binding studies.

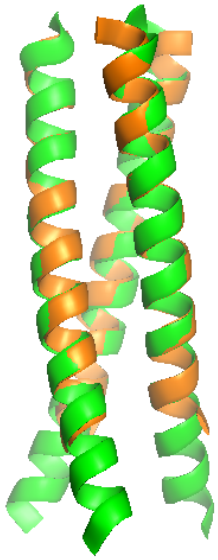

Figure A-9. Side view of an overlay between the apo-(CSL16C**)$_3$ and Hg(II)$_S$Zn(II)$_N$(GRAND-CSL16CL30H)$_3^+$ structures indicating that there is no change in the overall secondary structures of GRAND-CoilSer and CoilSer derivatives.** Shown in green is the Hg(II)$_S$Zn(II)$_N$(**GRAND-CS**L16CL30H)$_3^+$ and in orange is apo-(**CS**L16C)$_3$.

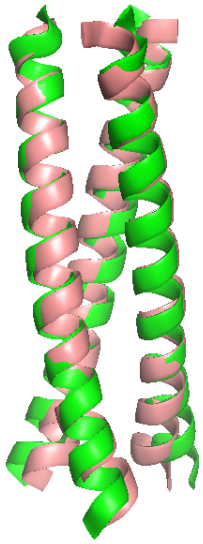

Figure A-10. An alignment of the helical backbones between $Hg(II)_SZn(II)_N$(GRAND-CSL16CL30H)$_3^+$ (green) and Zn(II)(GRAND-CSL12AL16C)$_3^-$ (pink) demonstrates the frayed end caused by the internal 30His site in the $Hg(II)_SZn(II)_N$(GRAND-CSL16CL30H)$_3^+$ structure. The residue side chains and bound metals are omitted for clarity.

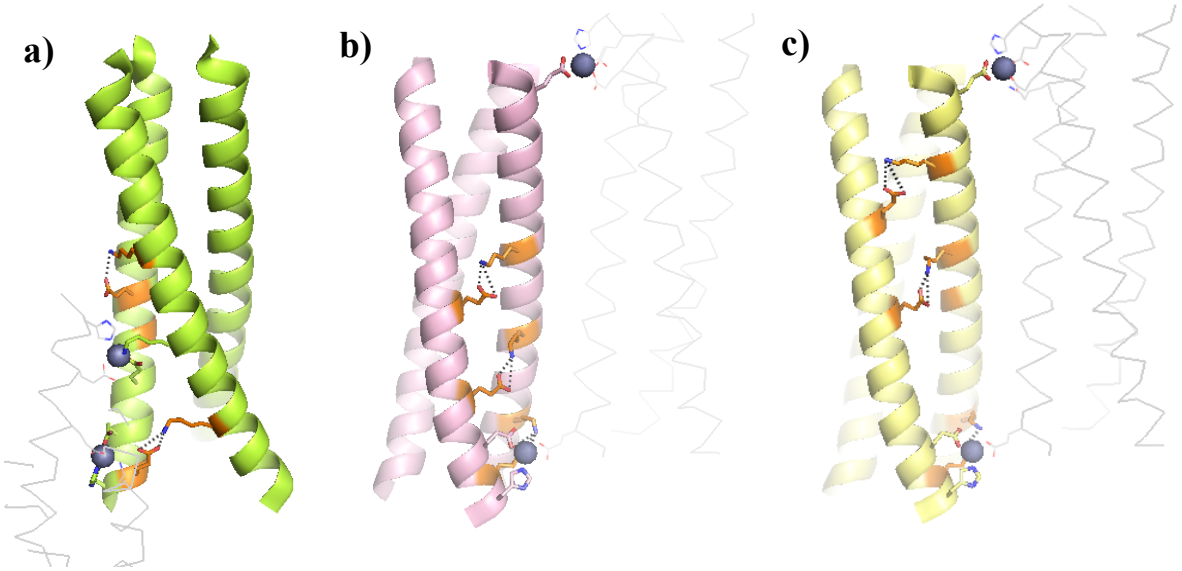

Figure A-11. Side view representation of the salt bridge interactions along the helical interface of the GRAND-CoilSer derivatives. Due to the threefold symmetry along the scaffold, only interactions happening on one face between the two adjacent strands are included for clarity. Shown in a) representing the pairs of interactions in $Hg(II)_SZn(II)_N$(**GRAND-CS**L16CL30H)$_3^+$ and $Pb(II)_SZn(II)_N$(**GRAND-CS**L16CL30H)$_3^+$, b) Zn(II)(**GRAND-CS**L12AL16C)$_3^-$ and c) Hg(II)(**GRAND-CS**L12AL16C)$_3^-$. Backbones of the peptides are shown as ribbon diagrams. Lys and Glu side chains that form salt bridges are as orange sticks. Zn(II) ions are grey spheres. Side chains that are bound to the external Zn(II) ions are as sticks. The salt bridge pairs are labeled as dash lines. The symmetry related molecule of the peptide is shown as lines.

References

(1) Chakraborty, S.; Touw, D. S.; Peacock, A. F. A.; Stuckey, J.; Pecoraro, V. L. *J. Am. Chem. Soc.* **2010**, *132*, 13240–13250.

(2) Touw, D. S.; Nordman, C. E.; Stuckey, J. a; Pecoraro, V. L. *Proc. Natl. Acad. Sci. U. S. A.* **2007**, *104*, 11969–11974.

(3) Peacock, A. F. A.; Stuckey, J. A.; Pecoraro, V. L. *Angew. Chem. Int. Ed. Engl.* **2009**, *48*, 7371–7374.

(4) Zastrow, M.; Pecoraro, V. L. *Coord. Chem. Rev.* **2013**, 2565-2588.

(5) Touw, D. Ph.D. Thesis, Structural and Spectroscopic Studies of Heavy Metal Binding to de Novo Designed Coiled Coil Peptides, University of Michigan, **2007**.

(6) Crick, F. H. C. *Acta Crystallogr.* **1953**, *6*, 689–697.